

THE UNIVERSITY OF CALGARY

MULTIRESOLUTION APPROXIMATION IN GRAVITY FIELD MODELING

by

ZUOFA LI

A DISSERTATION

SUBMITTED TO THE FACULTY OF GRADUATE STUDIES

IN PARTIAL FULFILLMENT OF THE REQUIREMENTS FOR THE

DEGREE OF DOCTOR OF PHILOSOPHY

DEPARTMENT OF GEOMATICS ENGINEERING

CALGARY, ALBERTA

NOVEMBER, 1996

© Zuofa Li 1996



**National Library  
of Canada**

**Acquisitions and  
Bibliographic Services**

**395 Wellington Street  
Ottawa ON K1A 0N4  
Canada**

**Bibliothèque nationale  
du Canada**

**Acquisitions et  
services bibliographiques**

**395, rue Wellington  
Ottawa ON K1A 0N4  
Canada**

*Your file Votre référence*

*Our file Notre référence*

**The author has granted a non-exclusive licence allowing the National Library of Canada to reproduce, loan, distribute or sell copies of his/her thesis by any means and in any form or format, making this thesis available to interested persons.**

**The author retains ownership of the copyright in his/her thesis. Neither the thesis nor substantial extracts from it may be printed or otherwise reproduced with the author's permission.**

**L'auteur a accordé une licence non exclusive permettant à la Bibliothèque nationale du Canada de reproduire, prêter, distribuer ou vendre des copies de sa thèse de quelque manière et sous quelque forme que ce soit pour mettre des exemplaires de cette thèse à la disposition des personnes intéressées.**

**L'auteur conserve la propriété du droit d'auteur qui protège sa thèse. Ni la thèse ni des extraits substantiels de celle-ci ne doivent être imprimés ou autrement reproduits sans son autorisation.**

0-612-20749-8

## ABSTRACT

There are various types of data available for gravity field modeling, such as terrestrial or marine mean gravity anomalies, airborne gravity disturbances and geoidal heights computed from satellite altimetry. One common feature of these data types is that they have different resolutions and accuracies. To combine these data, a multiresolution problem has to be solved. The objective of this dissertation is therefore the development of a framework for multiresolution approximation in gravity field modeling. First, multiresolution approximation problems are formulated, and four classes of multiresolution approximation problems are given to demonstrate the necessity of introducing the idea of multiresolution approximation in gravity field modeling. Next, a general methodology of combining different methods for solving multiresolution approximation problems are presented. Both signal domain and measurement domain approaches are considered. Two signal domain approaches, i.e. the fine-to-coarse estimation scheme and the coarse-to-fine estimation scheme, are derived by combining a discrete wavelet transform and least-squares collocation as two special tools. A measurement domain approach is also proposed by using a multirate system and a multiple-input single-output system as two special tools. A detailed comparison between the proposed approach and stepwise least-squares collocation is conducted. Finally, the application of the proposed framework to gravity field modeling is demonstrated through numerical examples. The effect of using different wavelets is investigated. A numerical comparison between the signal domain approach, combining a wavelet transform and least-squares collocation, and the measurement domain approach, using a multirate system and a multiple-input single-output system, is performed. The main advantage of the proposed

framework is that it allows both estimation of signals at multiple scales and fusion of measurements at different scales.

## **ACKNOWLEDGMENTS**

I wish to express my deepest gratitude to my supervisor, Dr. K.P. Schwarz, for his continuous support, encouragement and guidance throughout the course of my graduate studies. I could not have achieved whatever I have without his support. He believed in my abilities even when I felt discouraged.

Dr. E.J. Krakiwsky, Dr. M.G. Sideris, Dr. L.T. Bruton, and Dr. F. Sanso are thanked for their advice on the dissertation, as members of the supervisory committee and/or the examination committee. The constructive criticism they offered during the examination has led to substantial changes in the thesis and has improved its quality. Dr. J.A.R. Blais is acknowledged for the his time and knowledge in discussing topics related to wavelet theory.

Special thanks are extended to my teachers and colleagues at Wuhan Technical University of Surveying and Mapping, P. R. China, particularly to Prof. Zelin Guan, the supervisor of my M.Sc. program for his inspiration and encouragement. I also wish to thank Dr. M. Wei, Mr. Y. Li, Mr. L. Wu, Mr. J. Li, Mr. H. Sun and Mr. W. Qiu for valuable discussions. The many other graduate students, faculty members and support staff who have made my graduate studies both fruitful and enjoyable through the discussions and fellowship are sincerely appreciated. I extend my gratitude to Dr. I. Daubechies at Princeton University and Dr. A.S. Willsky at MIT for responding to my request for technical papers.

Financial support for my Ph.D. studies was provided by the Natural Science and Engineering Research Council of Canada, the Helmut Moritz Scholarship, two Graduate Teaching Assistantships of the University of Calgary and research support by Canagrav Research Ltd. This is gratefully acknowledged.

Finally, thanks go to my wife, Ling, for her understanding, support and patience.

## TABLE OF CONTENTS

	Page
ABSTRACT.....	iii
ACKNOWLEDGMENTS.....	v
TABLE OF CONTENTS .....	vii
LIST OF TABLES .....	xi
LIST OF FIGURES .....	xii
NOTATION .....	xiv
CHAPTER	
<b>1. INTRODUCTION</b>	
1.1 BACKGROUND AND OBJECTIVES.....	1
1.2 DISSERTATION OVERVIEW .....	7
1.2.1 Outline.....	7
1.2.1 Contributions.....	9
<b>2. GRAVITY FIELD DETERMINATION .....</b>	<b>12</b>
2.1 BASIC TERMINOLOGY IN THE GRAVITY FIELD .....	12
2.2 GEOPOTENTIAL MODELS .....	14
2.3 INTEGRAL FORMULAS.....	18
2.3.1 Stokes' Solution versus Molodensky's Solution.....	18

2.3.2 Modification of Stokes' Formula.....	21
2.4 LEAST-SQUARES COLLOCATION.....	24
2.4.1 The Fundamental Equations for the Lease-Squares Collocation.....	25
2.4.2 Stepwise Collocation.....	29
2.4.3 The Covariance Functions.....	31
2.5 MULTIPLE-INPUT SINGLE-OUTPUT-SYSTEMS.....	34
2.6 FORMULATION OF MULTIREOLUTION APPROXIMATION PROBLEMS FOR GRAVITY FIELD MODELING.....	37
<b>3. AN INTRODUCTION TO WAVELETS AND MULTIRATE SYSTEMS .....</b>	<b>45</b>
3.1 WAVELET TRANSFORMS VERSUS WINDOWED FOURIER TRANSFORMS	45
3.2 MULTIREOLUTION ANALYSIS.....	48
3.2.1 One-Dimensional Multiresolution Analysis.....	49
3.2.2 Two-Dimensional Multiresolution Analysis.....	54
3.3 COMPACTLY SUPPORTED ORTHONORMAL WAVELETS.....	57
3.4 DISCRETE WAVELET TRANSFORMS USING ORTHONORMAL WAVELET TRANSFORMS.....	63
3.4.1 One-Dimensional Discrete Wavelet Transform.....	63
3.4.2 Two-Dimensional Discrete Wavelet Transform.....	67
3.5 THE CHOICE OF WAVELETS .....	71
3.6 MULTIRATE SYSTEMS.....	75
3.6.1 Fundamentals of Multirate Systems.....	75
3.6.2 Polyphase Structure.....	78

3.6.3 Window Techniques for the Design of a Multirate Lowpass FIR Filter.....	80
3.6.4 Two-Dimensional Decimation and Interpolation Filters.....	81
3.6.5 Multirate Filter Banks.....	83
<b>4. SOLUTIONS TO THE MULTIREOLUTION APPROXIMATION PROBLEM FOR GRAVITY FIELD MODELING .....</b>	<b>88</b>
4.1 GENERAL METHODOLOGY.....	88
4.2.1 Signal Domain Approaches.....	91
4.2.2 Measurement Domain Approaches.....	93
4.2 SIGNAL DOMAIN APPROACHES COMBINING WAVELET TRANSFORMS AND LEAST-SQUARES COLLOCATION.....	99
4.2.1 Fine-to-Coarse Estimation Scheme.....	99
4.2.2 Coarse-to-Fine Estimation Scheme.....	107
4.3 A MEASUREMENT DOMAIN APPROACHES COMBINING A MULTIRATE SYSTEM AND A MISO SYSTEM.....	114
4.4 COMPARISON BETWEEN THE PROPOSED ALGORITHMS AND STEPWISE LEAST-SQUARES COLLOCATION.....	120
<b>5. NUMERICAL RESULTS AND ANALYSIS.....</b>	<b>129</b>
5.1 TEST DATA AND SOFTWARE.....	129
5.1.1 Multiresolution Data.....	129
5.1.2 Software Overview.....	137
5.2 TWO EXAMPLES.....	138

5.2.1 Geoidal Height Determination from Fine-Scale Airborne Gravity Disturbance Data and Coarse-Scale Geoidal Height Data.....	138
5.5.2. Fusion of Fine-scale Airborne Gravity Disturbance Measurements with Coarse- Scale Terrestrial Gravity Disturbance Measurements.....	145
5.3 EFFECTS OF USING DIFFERENT WAVELETS.....	151
5.4 NUMERICAL COMPARISON BETWEEN A SIGNAL DOMAIN APPROACH AND A MEASUREMENT DOMAIN APPROACH.....	156
<b>6. CONCLUSIONS AND RECOMMENDATIONS.....</b>	<b>169</b>
6.1 CONCLUSIONS.....	169
6.2 RECOMMENDATIONS.....	171
<b>REFERENCES.....</b>	<b>174</b>

## LIST OF TABLES

1.1 Resolution of different measurements and different gravity field signals.....	4
2.1 $n_{\max}$ and $r_{\text{model}}$ for some geopotential models.....	17
2.2 Characteristics of different classes of multiresolution approximation problems.....	43
3.1 Coefficients $h(n)$ for the compactly supported wavelets with different $N$ .....	60
4.1 Capabilities of different methods for solving multiresolution problems.....	91
4.2 Combination of different methods for solving the multiresolution approximation problems.....	98
4.3 Summaries of the fine-to-coarse estimation scheme and the stepwise LSC.....	122
5.1 Statistics of measurements noise.....	133
5.2 Statistics of geoidal height estimation before and after data fusion.....	140
5.3 Statistics for the fusion of airborne gravity disturbances and terrestrial gravity disturbance using the two estimation schemes .....	146
5.4 Statistics of geoidal height error at fine-scale using different wavelets.....	152
5.5 Geoidal height error due to inaccurate representation using different wavelets.....	153
5.6 The statistics of the geoidal height errors using both methods (I).....	161
5.7 The statistics of the terrestrial gravity disturbance errors using both methods.(I).....	161
5.8 The statistics of the geoidal height errors using both methods (II).....	164
5.9 The statistics of the terrestrial gravity disturbance errors using both methods (II).....	164
5.10 The gravity disturbance error due to the aliasing effect.....	166

## TABLE OF FIGURES

2.1 A MISO system.....	34
2.2 Formulation of multiresolution approximation problem.....	39
3.1 Time-Frequency resolution of the windowed Fourier transforms.....	46
3.2 Time-Frequency resolution of the wavelet transforms.....	48
3.3 Three examples of orthonormal wavelets (Daubechies, 1992).....	53
3.4 Examples of Daubechies wavelets (Daubechies, 1992) .....	62
3.5 Decomposition and reconstruction of 1D signal .....	65
3.6 Decomposition and reconstruction of 2D signal .....	69
3.7 Visualization of 2D discrete wavelet transform .....	69
3.8 Lena image before and after a wavelet transform.....	70
3.9 Ideal half-band frequency response.....	72
3.10 Frequency response of different Daubechies wavelet FIR filter.....	74
3.11 Multirate system building blocks.....	76
3.12 Decimation and interpolation filters.....	76
3.13 Sampling rate conversion by a rational number.....	78
3.14 Decimation and interpolation filters in a polyphase form.....	79
3.15 Analysis and synthesis filter bank.....	84
3.16 Multirate filter bank.....	85
3.17 Frequency response of an octave analysis filter bank.....	85
3.18 Octave analysis filter bank.....	86
3.19 Octave synthesis filter bank.....	87

4.1 Block diagram for a fine-to-coarse estimation procedure.....	94
4.2 Block diagram for a coarse-to-fine estimation procedure.....	95
4.3 Block diagram for a measurement domain approach.....	97
5.1 3D plot of gravity anomalies.....	130
5.2 The fine-scale airborne gravity disturbance.....	134
5.3 The coarse-scale geoidal height.....	135
5.4 The coarse-scale terrestrial gravity disturbance.....	136
5.5 Basic structure of the programs.....	137
5.6 The errors of geoidal height at fine-scale before and after data fusion.....	141
5.7 Normalized power spectral density of the geoidal height errors before and after data fusion.....	144
5.8 Errors of the terrestrial gravity disturbance estimates at fine scale before and after data fusion.....	148
5.9 Normalized power spectral density of the gravity disturbance errors before and after data fusion .....	150
5.10 External geoidal height errors using different wavelets.....	155
5.11 Relative energy distribution of the geoidal height and terrestrial gravity disturbance..	155
5.12 Frequency response of Daubechies lowpass filter (N=40).....	159
5.13 Frequency response of lowpass FIR Daubechies and Kaiser filters.....	160
5.14 Geoidal height errors using both methods.....	162
5.15 Terrestrial gravity disturbance errors using both methods.....	163

## NOTATIONS

$r$	radial distance
$\phi$	latitude
$\lambda$	longitude
$G$	gravitational constant
$M$	mass of the earth
$a$	equatorial radius of the reference ellipsoid
$\bar{C}_{lm}, \bar{S}_{lm}$	set of fully normalized harmonic coefficients
$\bar{P}_{lm}$	fully normalized Legendre functions
$n_{\max}$	maximum degree of the geopotential model
$r_{\max}$	maximum resolution of the gravity field from a geopotential model
$N$	geoidal height
$R$	mean Earth radius,
$\gamma$	mean gravity of the earth
$S(\psi)$	Stokes function
$r$	spherical distance
$\Delta g$	gravity anomaly
$\delta g$	gravity disturbance
$\sigma$	unit sphere.
$\Sigma$	plane

$(x, y)$	computation point in a plane
$(x', y')$	moving point in a plane
$K(x, y)$	planar Stokes' function
$N^{GM}$	geoidal height computed from a geopotential model
$\delta \bar{C}_{lm}, \delta \bar{S}_{lm}$	spherical harmonic coefficients for the differences of the Earth's gravity potential and the normal gravity potential
$N^S$	geoidal height computed from Stokes' integration
$\Delta g_{GM}$	gravity calculated from a geopotential model,
$\Delta g_r$	reduced gravity disturbance, i.e. $\Delta g - \Delta g_{GM}$
*	convolution or conjugate operator
T	disturbing potential
l	vector of measurements
$L_i$	linear functional operator
B	vector of linear functionals
n	vector of measurement noise
t	vector of signals
$C_{tt}$	covariances of signals
$C_{nn}$	covariances of measurement noise
$C_{ll}$	covariances of measurements
$C_{st}$	covariance matrix relating the observed quantities to the quantities being predicted

$\hat{s}$	vector of predicted quantities
$E_{\hat{s}\hat{s}}$	the error covariance of $\hat{s}$
$K(P, Q)$	covariance function of the disturbing potential
$C(P, Q)$	covariance function of the gravity anomaly
$X_{WF}(\omega, \tau)$	windowed Fourier transform
$X_W(a, b)$	wavelet transform
$h_{a,b}(t)$	basis function generated from a single prototype wavelet by translation and dilation
$\mathbb{R}$	set of real number
$L^2(\mathbb{R})$	square integrable function space
$V_i$	subspace of a multiresolution analysis
$W_i$	the orthogonal complement of $V_i$
$\phi(x)$	scale function
$\psi(x)$	wavelet function
$h(n), g(n)$	filtering coefficients
$C^\infty$	infinite differentiable function space
$C^k$	k order differentiable function space
$\otimes$	Kronecker product
$m$	level of resolution or scale
$y_m$	measurements at scale $m$

$x_m$	signal at scale $m$
$x(m)$	estimate of signal $x$ at scale $m$ based on all measurements with resolution higher (lower) or equal to $m$
$x(m+)$	estimate of signal $x$ at scale $m$ based on all measurements with resolution higher than $m$
$x(m-)$	estimate of signal $x$ at scale $m$ based on all measurements with resolution lower than $m$
$x_o(m)$	optimal estimate of $x$ at scale $m$ based on all available measurements.
$H(z)$	transfer function
$\omega$	curcular frequency
$H(\omega)$	frequency response
$P(\omega)$	power spectral density

## **CHAPTER 1**

### **INTRODUCTION**

#### **1.1 BACKGROUND AND OBJECTIVES**

Mapping of the earth's gravity field is considered a primary goal in geodesy, geophysics and geodynamics (Colombo, 1991). There are two conceptual approaches to the approximation of the Earth's gravity field, the model approach and the operational approach (Moritz, 1980). The model approach essentially consists of formulating a mathematical model in the form of a geodetic boundary value problem (BVP), employing an analytical point of view, and applying it via a discretization process (Sanso, 1987). A number of techniques for solving geodetic boundary problems have been developed, e.g., spherical harmonic expansion and integration techniques, such as Stokes' formula and Molodensky's solution (Heiskanen and Moritz, 1967). The operational approach starts from the real measurements, with as few modifications and corrections as possible, and sets up a general estimation principle, which uses the smallest possible mathematical information on the unknowns, but knowledge on their statistical behaviour (Sanso, 1987). This approach leads to least-squares collocation, which is a technique for combining observational data of different types for an optimal estimation of the gravity field signal and other parameters. This method is not dependent on data distribution, although it is numerically advantageous to create a regular data distribution.

In general, these two methods don't consider multiresolution data. In practice, there are various types of data available for gravity field modeling, such as terrestrial or marine mean gravity anomalies, airborne gravity disturbances and geoidal heights computed from satellite altimetry. One feature of these data types is that they have different resolutions either because they represent different functionals of the gravity field or because they have been sampled. Here resolution refers to the minimum wavelength which can be resolved from the data. For example, resolution of data from airborne gravimetry and satellite altimetry are different both in minimum wavelength resolution and area coverage. The second feature of these data is that they are obtained at different altitudes. For example, airborne gravimetric data are at flight height, while terrestrial gravity data are on the ground. Due to the attenuation of the gravity field with increasing altitude, these data correspond to different spectrums of the gravity field. The third feature is that these data have different noise levels due to different measurement procedures and different technologies. Finally, the gravity field signal to be estimated from one or more of these data may be different from the gravity functionals observed. To combine data of different observables with different resolutions, different altitudes and different noise levels for estimation of gravity field signals at different resolutions, the following multiresolution problem has to be solved:

*Given measurements of various functionals of the anomalous gravity field at different resolution levels and at different altitudes, estimate gravity field signals at multiple resolutions.*

The need for the formulation of a multiresolution problem in physical geodesy was realized some time ago, although the term multiresolution was not used. For example, Schwarz (1984) classified gravity field information in four categories: the low frequency part, the medium frequency part, the high frequency part, and the very high frequency part. In terms of resolution, the first part corresponds to low resolution, while the combination of the first two, the first three and all four parts corresponds to medium resolution, high resolution and very high resolution, respectively. This classification also suggests the data type to be used for the resolution of each frequency part. Table 1.1 summarizes measurement types, signal attenuation due to altitude and gravity field signals determined.

From Table 1.1, it can easily be seen that measurements at different resolutions should be combined to achieve better estimation of the gravity field signal at different resolution scales. As is indicated in Table 1.1, there are at least three reasons why a multiresolution approach is of interest in gravity field modeling. First, different functionals of the anomalous potential are used which are sensitive to different bands of the anomalous gravity spectrum. Second, data at different elevations are used - e.g. ground, aircraft heights, satellite heights - which, due to the attenuation of the gravity with distance from the disturbing masses, display a different spectral behaviour dependent on altitude. Finally, as already mentioned, data sampling is also responsible for different resolution levels.

Resolution	Measurements at different resolution	Attenuation due to altitude	Gravity field signals determined
Low	Orbit perturbation	strong 300 km -800km ( satellite altitude)	Geoidal height Gravity anomaly
Medium	Altimeter data Mean gravity anomalies (1° × 1°) and (20' × 20') Satellite gradiometer data Satellite to satellite tracking	no no strong strong	Geoidal height Gravity anomaly Deflection of vertical Second derivatives of disturbing potential
High	(5' × 5') mean gravity anomalies Deflections of the vertical Airborne gravimetric data Airborne gradiometric data	no no medium Strong	Gravity anomaly Gravity disturbance Deflection of vertical Second derivative of disturbing potential
Very high	Dense height data, at least (1 km x 1 km) Airborne gradiometric data	no Strong	Gravity anomaly Deflection of the vertical Second derivatives of disturbing potential

Table 1.1 Resolutions of different measurements and different gravity field signals

Sanso (1987) was the first to make mention of the multiresolution problem in physical geodesy when he investigated the relation between the discrete ( operational ) and the continuous formulation (model) from a resolution point of view with the purpose of

providing the reciprocal consistency of the two approaches. In his paper, he wrote that “when describing a physical object, we may find an even radically different behaviour, depending on the scale at which we look at it or more precisely from the resolution of our description, i.e. from the dimensions of the smallest particular we want to be able to distinguish in our object. Coming back to our example of a set of gravity measurements, the question is should we treat it as a continuum or as a discrete set? The answer is: it depends on the resolution with which we want to describe the field.”

The conventional method to deal with multiresolution data is least-squares collocation, which combines all data with different resolutions simultaneously. The problem of using least-squares collocation in this case is that it does not take the multiresolution data structure into account. In other words, it only considers the spatial correlation not the resolution correlation of multiresolution data. For example, when estimating a signal at one resolution from measurements at another resolution, least-squares collocation only considers the distance between two points at two different resolutions. Information regarding resolution is not used. Therefore, from a theoretical point of view, it cannot be directly used to deal with data of different resolutions. One way of avoiding this problem is to upsample or downsample measurements at different resolution levels to the same resolution level by using either a multirate system or a wavelet transform before applying least-squares collocation.

A general way to solve the above problem is to use multirate digital signal processing

systems (multirate systems). A multirate system is a system which allows to change from a sampling rate to another sampling rate within the system. Therefore it can be used to link different resolution scales by using a decimation or an interpolation filter or a multirate filter bank. It cannot solve, however, the problems of combining different observables of the gravity field, different data attenuation and different noise levels.

A wavelet transform also provides a mathematical tool to investigate multiresolution problems. It is closely related to the multirate system since a discrete wavelet transform can be viewed as a special case of tree structured multirate filter banks. The fundamental idea behind wavelets is to decompose data into different frequency components, and then study each component with a resolution matched to its scale (Daubechies, 1992). Roughly speaking, the aim of wavelets is to obtain base functions (called wavelets) as localized as possible, both in time (or space) and frequency (spectral domain). These functions are generated from a single “generating wavelet” or “mother wavelet” by translations and dilations. The wavelet transform has a form similar to that of a windowed Fourier transform. However, the basic function possesses windows of variable size, which make adaptation to spatial phenomena at different scales possible (Daubechies, 1992). Therefore wavelet transforms have advantages over Fourier transforms and windowed Fourier transforms because they allow the analysis or processing of data at different scales or resolutions. It is this feature that makes wavelets interesting and useful for solving gravity field problems. However it cannot totally solve the multiresolution

problems in gravity field approximation for the same reason mentioned in the context of multirate systems.

The objective of this dissertation is to introduce and develop a framework for multiresolution approximation in gravity field modeling. Instead of combining all available measurements at the same time, the gravity field signal at each resolution level will be estimated by using the measurements from either a fine-to-coarse scale or a coarse-to-fine scale one by one. A discrete wavelet transform or a multirate system is used as a tool to link different resolution levels.

## **1.2 DISSERTATION OVERVIEW**

### **1.2.1 Outline**

The dissertation is organized as follows. Chapter 2 provides the background theory of the approximation of the Earth's gravity field and a new formulation of multiresolution approximation problems in gravity field modeling. Four methods for modeling the Earth's gravity field, i.e., the geopotential model approach, the integration approach, the least-squares collocation approach, and the multiple-input single-output system approach, are briefly reviewed from a multiresolution point of view. Multiresolution approximation problems are formulated, and four classes of multiresolution approximation problems are given to demonstrate the necessity of introducing the idea of multiresolution approximation in gravity field modeling.

In Chapter 3, concepts of wavelet theory are introduced which are fundamental of the development of the subsequent chapter. Also, a brief review of multirate systems is given for the same purpose. Multiresolution analysis is formulated, the criteria for generating an orthonormal wavelet, especially a compact support Daubachies's wavelet, from a multiresolution analysis are described and discrete wavelet transforms using orthonormal wavelets are given. The choice of wavelets is discussed. The basic concepts of multirate systems is also described including decimator and interpolator, decimation and interpolation filter, polyphase decomposition, lowpass FIR filter design by the windowing technique, and multirate filter banks.

The primary theoretical contribution of this dissertation is presented in Chapter 4, in which a general methodology and specific algorithms for solving multiresolution approximation problems are developed. Both signal domain and measurement domain approaches are considered. Two signal domain approaches, i.e. the fine-to-coarse estimation scheme and the coarse-to-fine estimation scheme, are derived by using a discrete wavelet transform and least-squares collocation as two special tools for this development. A measurement domain approach is also proposed by using a multirate system and a multiple-input single-output system as two special tools. A comparison between the proposed approaches and stepwise least-squares collocation is conducted.

In Chapter 5, the procedure for generating multiresolution data is described first. Then, numerical tests are presented to demonstrate the applicability of the proposed framework

to gravity field modeling. Two numerical tests are conducted by using the signal domain approaches. First, geoidal height determination is done by using fine-scale airborne gravity disturbance data and coarse-scale geoidal height data. Then, downward continuation is studied by using a combination of fine-scale airborne gravity disturbance data with coarse-scale terrestrial gravity disturbance data. The effect of using different wavelet bases for the estimated gravity field signal is also studied. A numerical comparison between the signal domain approach and the measurement domain approach is performed to assess the performance of both methods.

Conclusions formed throughout this dissertation and recommendations for further investigations are presented in Chapter 6.

### **1.2.2 Contributions**

Specific contributions of this dissertation include:

- *Formulation of gravity field approximation in terms of a multiresolution problem.*

Although the problem of gravity field modeling has been studied extensively for years, the existence of a multiresolution problem in this field has not received attention. In Section 1.1, the need for solving a multiresolution problem in gravity field modeling has been stated. In Chapter 2, it will be shown that the classical approaches to gravity field approximation cannot be used to solve this problem. In Section 2.6, a general

mathematical formulation of the problem will be given and four classes of multiresolution problems related to gravity field modeling will be introduced.

- *Theoretical development of a framework for multiresolution approximation in gravity field modeling.* A general methodology for solving multiresolution approximation problems is introduced in Section 4.1. Two signal domain approaches, a fine-to-coarse estimation and a coarse-to-fine estimation, are presented using a discrete wavelet transform and least-squares collocation as two specific tools in Section 4.2. In Section 4.3, a measurement domain approach using a multirate system and a multiple-input single-output system as two specific tools is proposed as an alternative. A detailed comparison of the first method with stepwise least-squares collocation is given in Section 4.4.

- *Numerical investigation of the potential applications of the proposed framework to gravity field modeling.* In Chapter 5, the proposed framework is applied to the solution of the multiresolution approximation problem in gravity field. In Section 5.3, two numerical tests are performed to show the applicability of the proposed framework. The effect of using different wavelets is investigated in Section 5.4. A numerical comparison between the signal domain approach combining a wavelet transform and least-squares collocation and the measurement domain approach using a multirate system and a multiple-input single-output system is performed in Section 5.5, where the estimation results of the two

methods are analyzed in terms of dependence on the signal to be estimated, the resolution difference between different scales and the choice of lowpass filters.

## **CHAPTER 2**

### **GRAVITY FIELD DETERMINATION**

In this chapter, some basic definitions in the gravity field are given first, and four methods of modeling the Earth's gravity field, the geopotential model approach, the integration approach, the least-squares collocation approach and multiple-input single-output system solution, are then briefly reviewed from a multiresolution point of view. Finally multiresolution approximation problems are formulated and four different classes of problems are identified.

#### **2.1 BASIC TERMINOLOGY IN THE GRAVITY FIELD**

The gravity potential of the Earth  $W$  is equal to the sum of the gravity potential  $V$ , produced by the attraction of the density distribution of the Earth, and the centrifugal potential  $\Phi$ , i.e.

$$W = V + \Phi, \tag{2.1}$$

The main objective of physical geodesy is to determine the physical Earth's surface  $S$  and the gravity potential  $w$ . The surface of the earth is usually approximated by an ellipsoid of revolution which is an equipotential surface of a normal gravity field of the Earth as defined in Heiskanen and Moritz (1967). The normal gravity potential is denoted by  $U$

and the normal gravity by  $\gamma$ . The disturbing potential  $T$  is then defined as the difference between the actual gravity potential  $W$  and the normal gravity potential  $U$  at the same point  $P$ , i.e.

$$T_p = W_p - U_p, \quad (2.2)$$

which satisfies Laplace equation outside the Earth's surface, i.e.

$$\Delta T = \frac{\partial^2 T}{\partial x^2} + \frac{\partial^2 T}{\partial y^2} + \frac{\partial^2 T}{\partial z^2} = 0 \quad (2.3)$$

where  $(x, y, z)$  is a coordinate in an earth-fixed rectangular coordinate system.

The gravity anomaly  $\Delta g$  is defined as the difference between the measured gravity made on the earth surface point  $P$  and the normal gravity  $\gamma$  on the ellipsoid point  $Q$  corresponding to  $P$ , i.e.

$$\Delta g_p = g_p - \gamma_Q, \quad (2.4)$$

The gravity disturbance  $\delta g$  is defined as the difference between the measured and the normal gravity  $\gamma$  at same point  $P$ , i.e.

$$\delta g_p = g_p - \gamma_p, \quad (2.5)$$

The geoidal height  $N$  is defined as the difference between the geoid, the equipotential surface which best approximates mean sea level, and the ellipsoid.

The fundamental equations describing the relationship between the disturbing potential  $T$  and the gravity anomaly  $\Delta g$ , the gravity disturbance  $\delta g$  and the geoidal height  $N$  are

$$\Delta g_p = -\frac{\partial T_p}{\partial r} - \frac{2}{R} T_p, \quad (2.6)$$

$$\delta g_p = -\frac{\partial T_p}{\partial r}, \quad (2.7)$$

$$N_p = \frac{T_p}{\gamma}, \quad (2.8)$$

In planar approximation, (2.7) and (2.8) become

$$\Delta g_p = -\frac{\partial T_p}{\partial z}, \quad (2.9)$$

$$\delta g_p = -\frac{\partial T_p}{\partial z}, \quad (2.10)$$

## 2.2 GEOPOTENTIAL MODELS

The gravitational potential of the Earth can be expressed in an Earth-fixed and Earth-

centered coordinate system by the well-known harmonic series:

$$V(r, \phi, \lambda) = \frac{GM}{r} \left[ 1 + \sum_{l=2}^{\infty} \sum_{m=0}^l \left( \frac{a}{r} \right)^l \left( \bar{C}_{lm} \cos m\lambda + \bar{S}_{lm} \sin m\lambda \right) \cdot \bar{P}_{lm}(\sin \phi) \right], \quad (2.11)$$

where  $r$ ,  $\phi$  and  $\lambda$  are the geocentric coordinates of a point,  $GM$  is the product of the gravitational constant  $G$  and the mass of the earth  $M$ ,  $a$  is the equatorial radius of the reference ellipsoid,  $\bar{C}_{lm}$  and  $\bar{S}_{lm}$  are a set of fully normalized harmonic coefficients, and  $\bar{P}_{lm}$  are fully normalized Legendre functions.

A geopotential model for the anomalous potential  $T$  can then be written as follows:

$$T(r, \phi, \lambda) = \frac{GM}{r} \left[ 1 + \sum_{l=2}^{n_{\max}} \sum_{m=0}^l \left( \frac{a}{r} \right)^l \left( \delta \bar{C}_{lm} \cos m\lambda + \delta \bar{S}_{lm} \sin m\lambda \right) \cdot \bar{P}_{lm}(\sin \phi) \right], \quad (2.12)$$

where  $n_{\max}$  is maximum degree of the geopotential model (integer),  $\delta \bar{C}_{lm}$  and  $\delta \bar{S}_{lm}$  are the harmonic coefficients difference between the true gravity potential and the normal gravity potential. Gravity anomalies, geoidal height, and other functionals of  $T$  can be obtained by using formulas (2.6), (2.8), etc.

The coefficients  $\delta \bar{C}_{lm}$  and  $\delta \bar{S}_{lm}$  in formula (2.12) can be determined from the analysis of satellite orbit perturbations with or without combination with surface gravity data.

$n_{\max}$  can be determined using the following the rule of thumb:

$$n_{\max} = \frac{180^\circ}{d}, \quad (2.13)$$

where  $d$  is the grid spacing, in degree, or resolution of the data used in the determination of the geopotential coefficients.

On the other hand, the resolution of the gravity field  $r_{\text{model}}$ , which can be resolved from a given geopotential model, can be calculated using the following formula:

$$r_{\text{model}} = \frac{180^\circ}{n_{\max}}. \quad (2.14)$$

There are a number of geopotential models available. Table 2.1 lists  $n_{\max}$  and  $r_{\text{model}}$  for some geopotential models. For more detailed information regarding these geopotential models, references are made to Lerch et al. (1979, 1981 and 1982), Rapp (1978, 1981), Rapp et al. (1991) and Reigber et al. (1983a and 1983b).

Geopotential model	$n_{\max}$	$r_{\text{model}}$ (deg)
GEM 9	22	8.12
GEM10	30	6
GEM10B	36	5
GEM10C	180	1
GEM L-2	20	9
GEMT1	36	5
GEMT2	36	5
GRIM 3 Model	36	5
GRIM 3B Model	36	5
Rapp 1978 Model	180	1
Rapp 1981 Model	180	1
Rapp 1991A Model	360	0.5

Table 2.1  $n_{\max}$  and  $r_{\text{model}}$  for some geopotential models.

From Table 2.1, it is easy to see that the maximum degree of the geopotential models is between 20 and 360, corresponding to a resolution of the gravity field between  $9^\circ$  and  $0.5^\circ$ . This means that geopotential models contain the low and medium frequency parts of the spectrum, but have very little information on high and very high frequencies because the data types used do not contain this information. Therefore, it is necessary to combine the model with other data types containing higher frequencies in order to obtain

resolution of the gravity field better than  $0.5^\circ$ , especially in the determination of local and regional gravity fields. It should also be mentioned that the accuracy of the geopotential coefficients becomes poorer and poorer with increasing degree and order. Thus, resolution to degree and order 360, or any degree and order, does not mean that the model coefficients are perfect.

## 2.3 INTEGRAL FORMULAS

### 2.3.1 Stokes' solution versus Molodensky's solution

The integration approach is based on the geodetic boundary value problem (BVP), which attempts to find the potential on and outside a boundary from measurements made on the surface. Two most often used BVPs are Stokes' BVP and Molodensky's BVP.

Stokes' BVP can be described as follows: *Given gravity everywhere on the geoid, the geoid and the anomalous gravity potential is to be determined.*

After applying a linearization procedure and assuming spherical approximation, the above problem can be formulated as:

$$\begin{cases} \Delta T = 0, & \text{outside } S \\ \Delta g = -\frac{\partial T}{\partial r} - \frac{2}{R}T, & \text{on } S \end{cases} \quad (2.15)$$

where  $S$  is the sphere with mean Earth radius  $R$  and  $r = \sqrt{x^2 + y^2 + z^2}$ .

The solution to Stokes' BVP can be represented by integral formulas. Other gravity field quantities such as the geoidal height  $N$  and the deflections of the vertical ( $\xi$   $\eta$ ), can also be represented by integral formulas. The solution for  $N$  given by Stokes' integral formula is

$$N = \frac{R}{4\pi\gamma} \int \Delta g S(\psi) d\sigma, \quad (2.16)$$

where  $\gamma$  is the mean gravity of the Earth,  $S(\psi)$  is Stokes' function, i.e.

$$S(\psi) = \frac{1}{\sin \frac{\psi}{2}} - 6 \sin \frac{\psi}{2} + 1 - 5 \cos \psi - 3 \cos \psi \ln \left( \sin \frac{\psi}{2} + \sin^2 \frac{\psi}{2} \right), \quad (2.17)$$

$\psi$  is the spherical distance,  $\Delta g$  is the gravity anomaly, and  $\sigma$  is the unit sphere.

In the case of local or regional gravity field determination, Stokes' formula may be simplified by using a planar approximation:

$$N(x, y) = \frac{1}{2\pi\gamma} \int_{\Sigma} \Delta g(x', y') K(x - x', y - y') dx' dy', \quad (2.18)$$

where  $(x, y)$  and  $(x', y')$  are the computation point and the moving point in a plane  $\Sigma$ , and  $K(x, y)$  is the planar Stokes' function, i.e.

$$K(x, y) = \frac{1}{\sqrt{x^2 + y^2}}, \quad (2.19)$$

Equation (2.19) is referred to as the planar Stokes' formula.

The main limitation of Stokes' BVP is that a gravity reduction is necessary in order to reduce the measured gravity from the Earth's surface to the geoid. This is the reason why Molodensky's BVP was introduced.

Molodensky's BVP is the determination of the physical surface  $S$  and of the external gravity field of the earth from the gravity potential  $W$  and the gravity vector  $\vec{g}$  given everywhere on  $S$  (Molodensky et al., 1962). It theoretically overcomes the problems of gravity reduction and mass-shifting which are strictly due to the formulation of Stokes' BVP. The solution to Molodensky's BVP is given as a series for  $T$  with integral terms involving gravity anomalies and topographic heights (Molodensky et al., 1962; Moritz, 1980). The lower order terms of the series provide sufficiently accurate results for

practical application (Moritz, 1980; Sideris 1987). Moreover, the first term of Molodensky series for the geoid is nothing else but Stokes' integral. The sum of the first term and the second term, i.e. the  $g_1$  term, is approximately equal to Stokes' integration with Faye gravity anomalies. On the other hand, what is obtained by Molodensky's solution is the height anomaly and not the geoidal height, which is one of the reasons why Stokes' integration is much more widely used in practical applications ( Li, 1993).

### 3.2.2 Modification of Stokes' formula

Theoretically, the integration in Stokes' and Molodensky's formulas should be extended over the whole earth and the gravity anomaly should be known at every point. Practically, these conditions cannot be satisfied. Measurements are usually available only in a limited area and are often given in the form of grids corresponding to mean gravity anomalies. Therefore, modification of the integration is necessary to accommodate their practical application. The basic idea of the modification is to remove a long wavelength reference field from the gravity anomalies by using a geopotential model and then apply Stokes' integral to compute the geoidal height from the reduced gravity anomalies; see Forsberg and Tscherning (1981), Rauhut (1992) and Li (1993).

Stokes' formula after this modification can be expressed as

$$N = N^{GM} + N^S, \quad (2.20)$$

where  $N^{\text{GM}}$  is the geoidal height computed from a geopotential model, i.e.

$$N^{\text{GM}} = \frac{GM}{\gamma r} \sum_{l=2}^{n_{\text{max}}} \sum_{m=0}^l \left(\frac{a}{r}\right)^l \left( \delta \bar{C}_{lm} \cos m\lambda + \delta \bar{S}_{lm} \sin m\lambda \right) \cdot \bar{P}_{lm}(\sin \phi)], \quad (2.21)$$

$\delta \bar{C}_{lm}$  and  $\delta \bar{S}_{lm}$  are the spherical harmonic coefficients for the differences of the Earth's gravity potential and the normal gravity potential.  $N^{\text{S}}$  is the contribution of the reduced gravity anomaly,  $\Delta g_r = \Delta g - \Delta g_{\text{GM}}$ , computed from Stokes' integration from either (2.16) or (2.18).  $\Delta g_{\text{GM}}$  can be calculated from a geopotential model, i.e.,

$$\Delta g^{\text{GM}} = \frac{GM}{r^2} \sum_{l=2}^{n_{\text{max}}} (l-1) \sum_{m=0}^l \left(\frac{a}{r}\right)^l \left( \delta \bar{C}_{lm} \cos m\lambda + \delta \bar{S}_{lm} \sin m\lambda \right) \cdot \bar{P}_{lm}(\sin \phi)]. \quad (2.22)$$

Since the gravity anomalies are usually given in the form of grids corresponding to mean gravity anomalies,  $N^{\text{S}}$  can be replaced by the following summation

$$N^{\text{S}}(x, y) = \frac{\Delta x \Delta y}{2\pi\gamma} \sum_{i=0}^{N-1} \sum_{j=0}^{M-1} \Delta g_r(x_i', y_j') K(x - x_i', y - y_j') \quad (2.23)$$

in the case of the planar approximation, where  $x$  and  $y$  are the grid spacing along the  $x$ -axis and  $y$ -axis, respectively,  $N$  and  $M$  are the data numbers along each row and column, respectively, and  $\Delta g_r$  is the reduced gravity anomaly.

Equation (2.23) can also be expressed as a discrete convolution

$$N^S(x, y) = \Delta g_r * K_1, \quad (2.24)$$

where  $*$  is the convolution operator, and

$$K_1(x, y) = \frac{\Delta x \Delta y}{2\pi\gamma} K(x, y). \quad (2.25)$$

As can be seen from equation (2.24), the maximum resolution of  $N^S$  will be the same as that of  $\Delta g_r$ . This means that the maximum resolution of the gravity field depends on the measurements  $\Delta g$ . On the other hand, if the measurements are only given in an area of  $\Sigma^\circ \times \Sigma^\circ$ , the minimum resolution of the gravity field which can be resolved from local data is  $\Sigma^\circ$ , corresponding to the minimum degree and order of the harmonic expansion  $\frac{180^\circ}{\Sigma^\circ}$ . Therefore, the lowest degree and order of the geopotential model have to be larger than or equal to  $\frac{180^\circ}{\Sigma^\circ}$ . That means the minimum resolution in this solution is usually provided by the geopotential model. From the above discussion, it can be concluded that

equation (2.20) can be viewed as a direct fusion of different types of data with different resolutions, i.e. a lower resolution geopotential model and a higher resolution gravity anomaly, for geoidal height determination.

In this dissertation, new approaches for fusing different data types with different resolutions will be developed based on wavelet theory or multirate systems theory. They can not only handle the above situation but also other situations where integral approaches are not available.

## **2.4 LEAST-SQUARES COLLOCATION**

Integral formulas, such as Stokes' and Molodensky's formulas, use one type of data for the approximation of other functions of the gravity field. Different types of data are frequently available, containing useful information regarding the gravity field. Least-square collocation is one method capable of using different types of data, homogeneous or heterogeneous, to predict other gravity field quantities.

In the following, the basic principles of least-squares collocation are reviewed. Readers are referred to Krarup (1969), Moritz (1980), Sanso and Tscherning (1980), and Tscherning (1984) for a more detailed description regarding least-squares collocation theory.

### 2.4.1 The Fundamental Equations of Least-Squares Collocation

Any measurement of the anomalous gravity field can be represented as a linear functional of the disturbing potential  $T$  plus measurement noise, which can be written as follows:

$$l_i = L_i T + n_i, \quad (2.26)$$

( $i = 1, 2, \dots, q$ )

or

$$l = BT + n, \quad (2.27)$$

where the vector  $l$ , the  $B$  and the vector  $n$  comprise  $q$  measurements  $l_i$ ,  $q$  linear functionals  $L_i$ , and  $q$  measurement noises  $n_i$  ( $i = 1, 2, \dots, q$ ), respectively, i.e.

$$l = [l_1, l_2, \dots, l_q]^T,$$

$$B = [L_1, L_2, \dots, L_q]^T,$$

$$n = [n_1, n_2, \dots, n_q]^T,$$

Let

$$t = BT,$$

then

$$l = t + n. \quad (2.28)$$

In this way, the measurements can be explained as the synthesis of a “signal”  $t$ , which is a function of  $T$ , and a “noise”  $n$ .

Equation (2.28) is the mathematical model for least-squares collocation without considering systematic parameters. In this dissertation, all discussions on least-squares collocation will be based on this model and multiresolution approximation will refer to signals only. A more general mathematical model for least-squares collocation can be found in, e.g., Moritz (1980) and Krakiwsky (1990).

It is assumed that the mathematical expectation of the measurement  $l$  and the measurement noise  $n$  are zero, i.e.

$$E(l)=0, \quad E(n)=0. \quad (2.29)$$

When two types of measurements with different resolution are used, equation (2.29) can be split into two parts:

$$l_1 = t_1 + n_1, \quad (2.30a)$$

$$l_2 = t_2 + n_2, \quad (2.30b)$$

where  $l_1$  and  $l_2$  are the measurement vectors corresponding to the lower and higher resolution, respectively,  $t_1 = B_1 T$  and  $t_2 = B_2 T$  are the “signal” vectors, and  $n_1$  and  $n_2$  are the measurement noise vectors in this case.

The fundamental solution of equation (2.29) is based on the following minimum principle:

$$s^T C_{ss}^{-1} s^T + n^T C_{nn}^{-1} n = \text{minimum}, \quad (3.31)$$

which results in the following solution

$$\hat{s} = C_{st} C_{ll}^{-1} l, \quad (2.32)$$

with the error covariance matrix

$$E_{\hat{s}\hat{s}} = C_{ss} + C_{st} C_{ll}^{-1} C_{st}^T, \quad (2.33)$$

where  $C_{ll} = (C_{tt} + C_{nn})$  is the sum of the covariance matrices of the signals and the measurement noise,  $C_{st}$  is the cross-covariance matrix relating the quantities being predicted to the observed quantities,  $\hat{s}$  is vector of predicted quantities, and  $E_{\hat{s}\hat{s}}$  is the error covariance matrix of  $\hat{s}$ . The derivation of equations (2.32) and (2.33) can be found

in Moritz (1980).

One aspect that makes collocation a desirable technique is the combination of various functionals to improve estimates of the quantities desired. Another feature of least-squares collocation is that it allows for an estimate of the inherent error covariance matrix associated with the estimates  $\hat{s}$ .

When applied to equation (2.30), equation (2.32) becomes

$$\hat{S} = [C_1 \ C_2] \begin{bmatrix} C_{11} & C_{12} \\ C_{21} & C_{22} \end{bmatrix}^{-1} \begin{bmatrix} l_1 \\ l_2 \end{bmatrix}, \quad (2.34)$$

where

$$C_1 = C_{st_1}, \quad (2.35a)$$

$$C_2 = C_{st_2}, \quad (2.35b)$$

$$C_{11} = C_{t_1 t_1} + C_{n_1 n_1}, \quad (2.35c)$$

$$C_{22} = C_{t_2 t_2} + C_{n_2 n_2}, \quad (2.35d)$$

$$C_{12} = C_{t_1 t_2}, \quad (2.35e)$$

$$C_{21} = C_{21}^T, \quad (2.35f)$$

One problem associated with equation (2.34) is that the cross-covariance matrix  $C_{t_1 t_2}$  between two "signals"  $t_1$  and  $t_2$  at two different resolutions cannot be handled by

the conventional covariance function approach. The definition of the covariance function takes only the spatial correlation into account, but does not address the resolution problem. Therefore, from a theoretical point of view, it cannot be used to compute the correlation between signals with different resolution. The approaches developed in this dissertation will circumvent this problem by using wavelet transforms or multirate systems as links between different resolution levels.

#### 2.4.2 Stepwise Collocation

The main drawback of the least-squares collocation methods is that the inversion of a large matrix is needed in order to estimate the predicted signals. The inversion of a large matrix is a very time consuming process. To solve this problem, Moritz (1973) proposed a stepwise procedure. The basic idea is to partition the matrices  $C_{11}$  and  $C_{st}$  into two blocks corresponding to a partition of the measurements in two groups as was done for the two types of data with different resolution above.

The fundamental equations of stepwise collocation are

$$\hat{s}_1 = C_1 C_{11}^{-1} l_1, \quad (2.36a)$$

$$\hat{s} = \hat{s}_1 + K(l_2 - Al_1), \quad (2.36b)$$

with error covariance matrixes

$$E_{ss,1} = C_{ss} - C_1 C_{11}^{-1} C_1^T, \quad (2.37a)$$

$$E_{ss} = E_{ss,1} - \bar{C}_2 \bar{C}_{22}^{-1} \bar{C}_2^T, \quad (2.37b)$$

where

$$K = (C_2 + C_1 C_{11}^{-1} C_{12}) \bar{C}_{22}^{-1}, \quad (2.38a)$$

$$A = C_{21} C_{11}^{-1}, \quad (2.38b)$$

$$\bar{C}_{22} = C_{22} - C_{21} C_{11}^{-1} C_{12}, \quad (2.38c)$$

$$\bar{C}_2 = C_2 - C_1 C_{11}^{-1} C_{12}, \quad (2.38d)$$

If  $s(1)$  and  $s(2)$ , the signal at two different resolutions, are to be estimated from measurements at these two resolutions, Equation (3.6) can be written as follows, i.e.

$$\hat{s}_1(1) = C_1(1) C_{11}^{-1} l_1, \quad (2.39a)$$

$$\hat{s}_1(2) = C_1(2) C_{11}^{-1} l_1, \quad (2.39b)$$

$$\hat{s}(1) = \hat{s}_1(1) + K_1 (l_2 - A_1 l_1), \quad (2.39c)$$

$$\hat{s}(2) = \hat{s}_1(2) + K_2 (l_2 - A_1 l_1), \quad (2.39d)$$

where

$$K_1 = (C_2(1) + C_1(1) C_{11}^{-1} C_{12}) \bar{C}_{22}^{-1}, \quad (2.40a)$$

$$A_1 = C_{21} C_{11}^{-1}, \quad (2.40b)$$

$$K_2 = (C_2(2) + C_1(2)C_{11}^{-1}C_{12})\bar{C}_{22}^{-1}. \quad (2.40c)$$

The more detailed description of stepwise collocation can be found in Moritz (1980).

### 2.4.3 The Covariance Functions

It is easy to see from equations (2.32) and (2.34) that covariance matrices are essential to least-squares collocation. Theoretically, all covariances in the anomalous gravitational field may be derived from the basic covariance function  $K(P, Q)$  of the disturbing potential  $T$ . Since all quantities in the anomalous gravitational field can be expressed as linear functionals of  $T$ , all covariance functions required in equations (2.31) and (2.33) can be derived by covariance propagation, i.e.

$$(C_{tt})_{ij} = L_i L_j K(P, Q), \quad (2.41a)$$

$$(C_{st})_{ij} = S_i L_j K(P, Q), \quad (2.41b)$$

On the other hand, from a practical point of view, the covariance function  $C(P, Q)$  of the gravity anomaly  $\Delta g$ , has a more fundamental character because gravity anomalies form the main empirical material for the practical determination of the signal covariances (Moritz, 1980). In this case, an analytical expression is usually used for determining  $K(P, Q)$  from  $C(P, Q)$ .

In general, the covariance functions can be classified as either global or local, depending on the dimension of the area of interest (Jordan, 1972). In the development of global covariance functions, the usual techniques of spherical harmonic series expansion can be used. Such a model was developed by Tscherning and Rapp using  $1^\circ \times 1^\circ$  mean gravity anomalies and the degree variances  $c_3$  to  $c_{20}$ , computed from a geopotential model (Tscherning and Rapp, 1974). Local covariance functions are mainly computed by subtracting from a global covariance function a number of low degree terms and fitting the three essential parameters, i.e. the variance  $C_0$ , the correlation length  $\xi$  and the gradient variance  $G_0$ , estimated from local data, to an analytical expression for the local covariance function, which is used as an empirical covariance function.

One problem of using empirical covariance functions is that there is no common empirical covariance function for the whole Earth. This means, empirical covariance functions determined in different areas will vary from one sample to the next (Schwarz and Lachapelle, 1980), and the ones derived have to be adapted to the local situations. This makes least-square collocation unreliable, especially when estimating one functional from another. Furthermore, even if the covariance function would be consistent from one sample area to the next, it could not be used to deal with data at multiple resolution scales if it is determined from the data at only one resolution.

If the data in the area of interest are available and evenly distributed, the above problems may be overcome if covariance functions are estimated directly from the data instead of

being derived from an analytical covariance function. Estimation of the empirical covariance function directly from the data can be done from space domain or spectral domain. The formula for estimating the empirical covariance from space domain is

$$C(k,l) = \frac{1}{M} \frac{1}{N} \sum_{i=0}^{M-1-k} \sum_{j=0}^{N-1-l} f(i,j) f(i+k, j+l), \quad (2.42)$$

where the discrete data  $f(i, j)$  are given in a rectangular area in grid format,  $M$  and  $N$  is the data numbers along  $x$  and  $y$  directions, respectively. Since the covariance function and the power spectral density are a pair of forward and inverse Fourier transform, Equation (2.42) can also be computed from the spectral domain, i.e.

$$C(x, y) = \int_{-\infty}^{\infty} \int_{-\infty}^{\infty} P(u, v) e^{2\pi(ux+vy)} du dv \quad (2.43)$$

where  $P(u, v)$  is the power spectral density of the data  $f(x, y)$ .  $u$  and  $v$  are the circular frequency along  $x$  and  $y$  directions

When multiresolution data are involved, covariance functions can be computed at each resolution level using either Equation (2.42) or (2.43) as long as they are used at their corresponding resolutions.

References are made to Jordan (1972), Tscherning and Rapp (1974), Rapp (1976), Moritz (1980) and Tscherning (1984) for detailed discussions regarding covariance functions.

## 2.5 MULTIPLE-INPUT SINGLE-OUTPUT (MISO) SYSTEM SOLUTION

MISO systems have been used in physical geodesy for a number of years (Vassiliou, 1986; Wu and Sideris, 1995; Sideris, 1996; Wu, 1996; Li, 1996). A MISO system in the space domain can be illustrated by the diagram, shown in Figure 2.1.

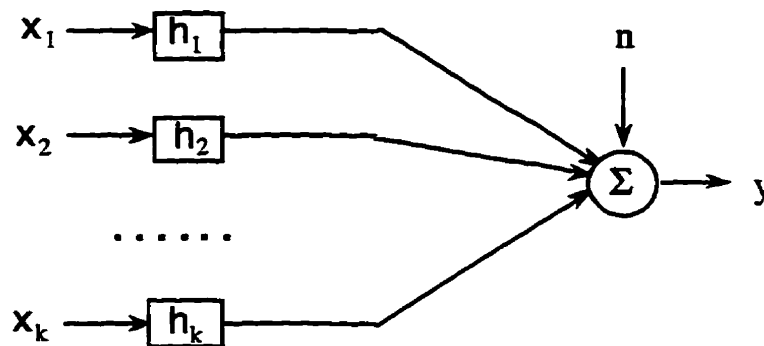


Figure 2.1 A MISO system

Mathematically, the system can be written as

$$y = \sum_{i=1}^k x_i * h_i + n, \quad (2.44)$$

where  $x_i$  ( $i = 1, 2, \dots, k$ ) is the input signal,  $y$  is the system output,  $n$  is the system noise,  $h_i$  is the impulse response, and  $*$  denotes the convolution operator.

Equation (2.44) can also be written in the frequency domain:

$$Y(\omega) = \sum_{i=1}^k X_i(\omega) H_i(\omega) + N(\omega), \quad (2.45)$$

where  $\omega$  is the circular frequency.  $X_i(\omega)$  ( $i = 1, 2, \dots, k$ ) are the Fourier transforms of  $x_i$  ( $i = 1, 2, \dots, k$ ),  $H_i(\omega)$  ( $i = 1, 2, \dots, k$ ) are the corresponding frequency responses of  $h_i$  ( $i = 1, 2, \dots, k$ ),  $Y(\omega)$  is the Fourier transform of  $y$ , and  $N(\omega)$  is the system noise expressed in the frequency domain.

In order to implement such a system, the  $H_i(\omega)$  ( $i = 1, 2, \dots, k$ ) have to be determined.

The following minimum criterion

$$P_{nn}(\omega) = |Y(\omega) - \sum_{i=1}^k X_i(\omega) H_i(\omega)|^2 = \text{minimum} \quad (2.46)$$

is used for this purpose, where  $P_{nn}(\omega)$  is the power spectral density of the output noise.

Since MISO systems can be implemented using double-input single-output system recursively (Wu and Sideris, 1995), only the following formula for determining  $H_i(\omega)$  ( $i = 1, 2$ ) is given (Sideris, 1996):

$$\hat{H}_1(\omega) = \frac{P_{y1}(\omega)}{P_{11}(\omega)} \frac{1}{1 + \frac{N_{11}(\omega) P_{22}(\omega) + N_{22}(\omega)}{P_{11}(\omega) N_{22}(\omega)}}, \quad (2.47a)$$

$$\hat{H}_2(\omega) = \frac{P_{y2}(\omega)}{P_{22}(\omega)} \frac{1}{1 + \frac{N_{22}(\omega) P_{11}(\omega) + N_{11}(\omega)}{P_{22}(\omega) N_{11}(\omega)}}, \quad (2.47b)$$

where  $P_{11}(\omega)$  and  $P_{22}(\omega)$  are power spectral densities of  $x_1$  and  $x_2$ ,  $P_{y1}(\omega)$  is the cross-spectral density of  $x_1$  and  $y$ , and  $P_{y2}(\omega)$  is the cross spectral density  $x_2$  and  $y$ , and  $N_{11}(\omega)$  and  $N_{22}(\omega)$  are the power spectral densities of the noise in  $x_1$  and  $x_2$ , respectively.

Therefore the estimate of the output signal in the frequency domain can be expressed as

$$\hat{Y}(\omega) = X_1(\omega) \hat{H}_1(\omega) + X_2(\omega) \hat{H}_2(\omega) \quad (2.48)$$

with the following power spectral density of the system output noise

$$P_{nn}(\omega) = P_{yy}(\omega) - |\hat{H}_1(\omega)|^2 P_{11}(\omega) - 2 \hat{H}_1^*(\omega) H_2(\omega) P_{12}(\omega) - |\hat{H}_2(\omega)|^2 P_{22}(\omega). \quad (2.49)$$

It should be noted that the above solution can be used when the input signals have the same sampling rates. In cases where the input signals have different sampling rates, it cannot be applied directly. This is the case when the input signals are measurements at multiple resolutions. In order to apply the MISO solution to this case, it is necessary to do upsampling or downsampling. One way of doing this is to use a multirate system, which will be discussed in Chapter 4.

## 2.6 FORMULATION OF MULTIREOLUTION APPROXIMATION PROBLEMS FOR GRAVITY FIELD MODELING

The discussion of available methods for gravity field modeling in the proceeding has shown that these methods are not suitable for estimating a gravity signal at multiple resolution levels based on multiresolution measurements. Therefore, it is necessary to develop a framework to solve such multiresolution approximation problems. To do this, multiresolution approximation problems have to be formulated. There are at least three situations in which such a formulation would be of advantage. First, it will allow for the approximation of the Earth's gravity field by a combination of data at different altitudes. Next, such a formulation will provide a way of combining different types of measurements at different resolution levels for estimation of a gravity field signal at multiple resolution. Finally, fusion of the same type of gravity field measurements at different resolutions from different sources will be feasible through such a formulation.

Multiresolution approximation problems of the gravity field can be described as follows:

*Given measurements of various functionals of the anomalous gravity field at different resolution levels and at different altitudes, estimate gravity field signal at multiple resolutions.*

The mathematical model for this problem can be formulated as

$$y_m = L_m(x_m) + v_m, \quad (2.50)$$

(  $m = 0, 1, \dots, M$  )

where  $y_m$  are measurements from  $M+1$  sensors or computed measurements at different resolution levels  $m$  ( $m=0, 1, 2, \dots, M$ ), e.g.  $y_0$  could be coarse-scale geoidal height measurements derived from satellite altimetry and  $y_1$  could be fine-scale airborne gravity disturbance measurements.  $x_m$  ( $m=0, 1, 2, \dots, M$ ) are the signals to be estimated at different resolutions, e.g. geoidal heights at two different resolution. The scale  $M$  corresponds to the highest resolution, while the scale 0 corresponds to the lowest resolution. For example, scale 0 corresponds to a resolution of 8 km, and scale  $M=4$  corresponds to a resolution of 1 km.  $L_m$  is the linear functional which relates the measurements  $y_m$  to the signal  $x_m$ , e.g. the gravity anomaly measurement can be related to the geoidal height signal through the following linear functional

$$L = -\gamma \left( \frac{\partial}{\partial r} + \frac{2}{r} \right) \quad (2.51)$$

In Equation (2.50),  $v_m$  ( $m=0, 1, 2, \dots, M$ ) is the measurement noise whose first and second moments are assumed to be known, i.e.

$$E(v_m) = 0, \quad (2.52a)$$

$$E(v_m v_m^T) = C_{vv}(m), \quad (2.52b)$$

It is also assumed that the measurement noise at different scales is uncorrelated, i.e.

$$E(v_i v_j^T) = 0, \quad i \neq j. \quad (2.52c)$$

Figure 2.2 illustrates this formulation of multiresolution approximation.

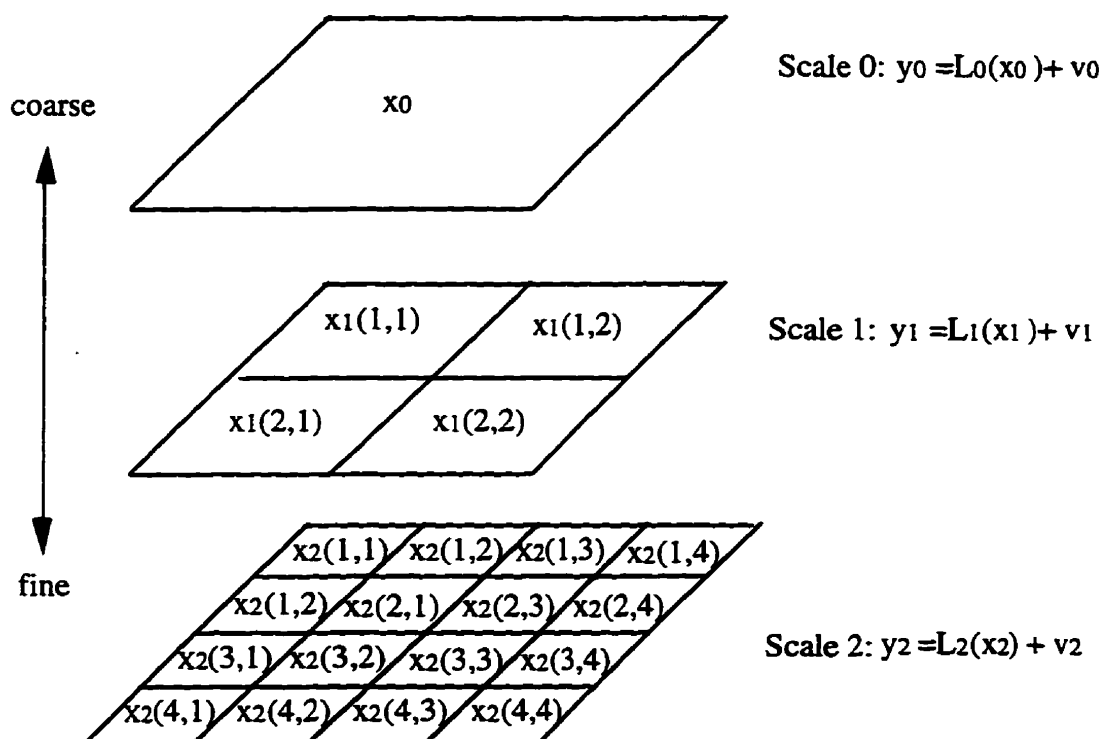


Figure 2.2 Formulation of multiresolution approximation problem

In the following, four classes of multiresolution approximation problems in gravity field modeling are identified, and some practical examples are given to demonstrate the

necessity of introducing the idea of multiresolution approximation in gravity field modeling.

**Class I: Multiresolution estimation of a gravity field signal using different types of measurements at different resolutions**

**Example 2.1:** Determination of geoidal heights in ocean area by using fine-scale shipborne gravity disturbance data and coarse-scale geoidal height data derived from satellite altimetry

This problem can be mathematically formulated as

$$\delta g_{\text{shipborne1}} = -\gamma \cdot \frac{\partial N_1}{\partial z} \Big|_{z=0} + v_1, \quad (2.53a)$$

$$N_{\text{altimeter0}} = N_0 \Big|_{z=0} + v_0, \quad (2.53b)$$

where  $\delta g_{\text{shipborne1}}$  and  $N_{\text{altimeter0}}$  are the fine-scale shipborne gravity disturbance measurements and the coarse-scale geoidal height measurements derived from satellite altimetry, respectively.  $N_1$  and  $N_0$  are the geoidal height at fine-scale and coarse-scale to be estimated.

**Class II: Multiresolution estimation of a gravity field signal using the same type of measurement at different resolutions and at different altitudes**

**Example 2.2:** Determination of the gravity disturbance on the Earth's surface using fine-scale airborne gravity disturbance data at flight height and coarse-scale terrestrial gravity disturbance data.

This problem can be mathematically written as follows:

$$\delta g_{\text{airborne}1} = L_1(\delta g_1) + v_1, \quad (2.54a)$$

$$\delta g_{\text{ground}0} = \delta g_0|_{z=0} + v_0, \quad (2.54b)$$

where  $\delta g_{\text{airborne}1}$  and  $\delta g_{\text{ground}0}$  are the fine-scale gravity disturbance measurements at flight level and ground.  $L_1$  is the Poisson operator. In planar approximation, which is defined as:

$$L_1(\delta g_1) = \iint_{\Sigma} K_1(x-x', y-y') \delta g_1(x', y') d\Sigma' = \iint_{\Sigma} \frac{1}{[(x-x')^2 + (y-y')^2]^{3/2}} \delta g_1(x', y') d\Sigma', \quad (2.55)$$

$\delta g_1$  and  $\delta g_0$  are the fine-scale and coarse-scale terrestrial gravity disturbances, respectively.

**Class III: Multiresolution estimation of a gravity field signal using different types of measurements at different resolutions and different altitudes**

**Example 2.3:** Determination of geoidal heights using fine-scale airborne gravity disturbance data and coarse-scale geoidal height data from satellite altimetry.

The problem can mathematically be formulated as follows:

$$\delta g_{\text{airborne}1} = -\gamma \cdot \frac{\partial N_1}{\partial z} \Big|_{z=H} + v_1, \quad (2.56a)$$

$$N_{\text{altimeter}0} = N_0 \Big|_{z=0} + v_0, \quad (2.56b)$$

where  $\delta g_{\text{airborne}1}$  and  $N_{\text{altimeter}0}$  are the fine-scale airborne gravity disturbance measurements at flight height  $H$  and the coarse-scale geoidal height measurements on a ocean area derived from satellite altimetry, respectively.  $N_1$  and  $N_0$  are the geoidal heights at fine-scale and coarse-scale to be estimated.

**Class IV: Fusion of the same of measurement type at different resolutions**

**Example 2.4:** Fusion of fine-scale and coarse-scale gravity disturbance data

This measurement fusion problem can be formulated as:

$$\delta g_{\text{source1}} = \delta g_1 + v_1, \quad (2.57a)$$

$$\delta g_{\text{source0}} = \delta g_0 + v_0, \quad (2.57b)$$

where  $\delta g_{\text{source1}}$  and  $\delta g_{\text{source0}}$  are the fine-scale and coarse-scale airborne gravity disturbances from two different sources, respectively.  $\delta g_1$  and  $\delta g_0$  are the estimates of gravity disturbances at fine-scale and coarse-scale, respectively.

Table 2.2 summarizes the characteristics of these four classes of multiresolution approximation problems.

Class	Measurement type at different resolutions	Altitude	Signal to be estimated at different resolutions
Class I	Different	Same	Same or different
Class II	Same	Different	Same or different
Class III	Different	Different	Same or different
Class IV	Same	Same	Same

Table 2.2 Characteristics of different classes of multiresolution approximation problems

After multiresolution approximation problems are formulated, the solutions to these problems must be developed. To do this, the concepts of wavelets and multirate systems are needed, which will be the topic of the next chapter.

## **CHAPTER 3**

### **AN INTRODUCTION TO WAVELETS AND MULTIRATE SYSTEMS**

In this chapter, some basic principles of wavelet theory and multirate systems will be reviewed, which will provide the basis for the development in the next chapter. Readers not familiar with the theories of wavelets and multirate systems are referred to Meyer (1992), Daubechies (1992), Vaidyanathan (1993) and Fliege (1994) for a more detailed description.

#### **3.1 WAVELET TRANSFORMS VERSUS WINDOWED FOURIER TRANSFORMS**

Wavelet theory is a relatively recent development in applied mathematics; see, e.g., Mallat (1989a), Meyer (1992) and Daubechies (1992). The concepts can be viewed as a synthesis of ideas originating during the last twenty or thirty years in pure mathematics (study of Calderon-Zygmund operator), physics (coherent states, renormalization group), and engineering (subband filtering ). Wavelets and wavelet transforms were first proposed by Grossman and Morlet (1984) as an alternative way to Fourier transforms for modeling seismic data. Later, Meyer (1990) recognized this work to be part of the field of harmonic analysis, and came up with a family of wavelets. His work was further developed specifically by Mallat (1989a, 1989b) and Daubechies (1988, 1992).

In order to introduce wavelet transforms, let us look at windowed or short-time Fourier transforms, which are often used in time-frequency analysis. The windowed Fourier transforms take the following form:

$$X_{\text{WFF}}(\omega, \tau) = \int_{-\infty}^{\infty} e^{-j\omega t} w(t - \tau) x(t) dt, \quad (3.1)$$

where  $w(\cdot)$  is an appropriate window, for instance a Gaussian window. That is,  $X_{\text{WFF}}(\omega, \tau)$  is the Fourier transform of  $x(t)$  windowed with  $w(\cdot)$  shifted by  $\tau$ .

The limitation of the windowed Fourier transform is that, because a single window is used for all frequencies, the resolution is the same at all locations in the time-frequency plane, as shown in Figure 3.1.

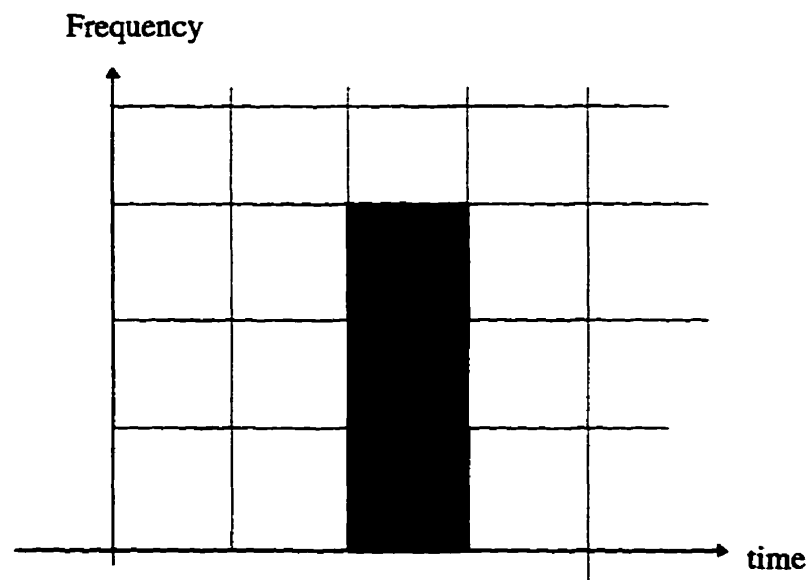


Figure 3.1 Time-frequency resolution of the windowed Fourier transforms

Of course, an arbitrarily high resolution in both time and frequency cannot be obtained at the same time. However, by varying the window used, one can trade resolution in time for resolution in frequency. In order to isolate the discontinuities in signals, one would like to have base functions which are very short, and to identify the slow changes in signals, one would like to use base functions which are very long. An intuitive way to achieve this is to have a short high-frequency basis, and a long low-frequency basis. That is exactly what is achieved with the wavelet transform (Vetterli and Herley, 1992).

The wavelet transform is defined as

$$X_W(a, b) = \int_{-\infty}^{\infty} h_{a,b}(t)x(t)dt, \quad (3.2)$$

where the base functions  $h_{a,b}(t)$  are generated from a single prototype wavelet by translation and dilation, i.e.

$$h_{a,b}(t) = \frac{1}{\sqrt{a}} h\left(\frac{t-b}{a}\right). \quad (3.3)$$

The variable  $b$  is the translation in time so that a varying  $b$  represents the “sliding” of the wavelet over  $x(t)$ . The variable  $a$  is the dilation/contraction factor that determines the characteristic frequency so that a varying ‘ $a$ ’ gives rise to a “spectrum”. Since ‘ $a$ ’ corresponds to frequency but is not frequency itself, it is often referred to as resolution or

scale. For a large 'a', the base function becomes a stretched version of the wavelet, corresponding to a low-frequency function, while for a small 'a', the base function becomes a contracted version of the wavelet, corresponding to a short high-frequency function. Therefore, for higher frequencies, the time resolution becomes better; for lower frequencies, the spectral resolution becomes better, as illustrated in Figure 3.2.

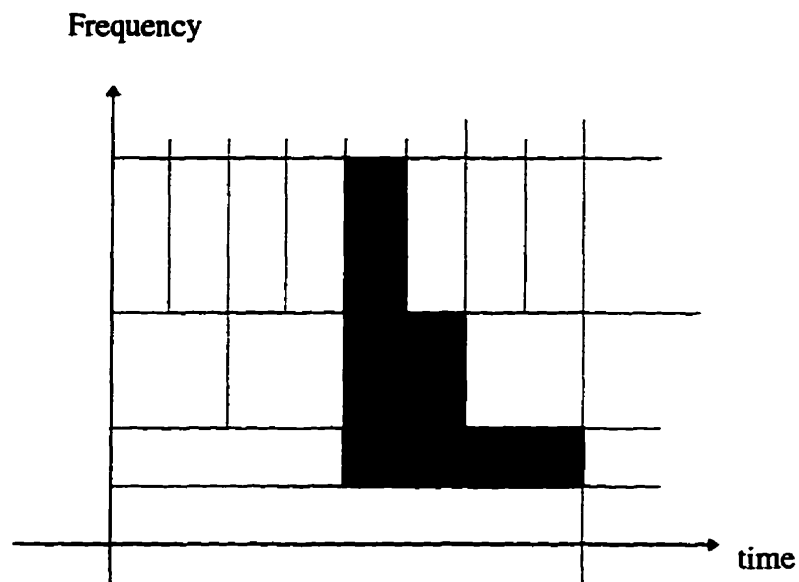


Figure 3.2 Time-Frequency resolution of the wavelet transforms

### 3.2 MULTIREOLUTION ANALYSIS

In the following, only orthonormal wavelets are described since orthogonality ensures that the coarse-scale approximation are the best approximations in a least-squares sense to the finer function. Orthonormal wavelets have only been studied during the last few years. It was difficult to construct an orthonormal wavelet base until a more systematic

approach, i.e. multiresolution analysis, was found by Mallat (1989a, 1989b) and Meyer (1990). Daubechies constructed compactly supported orthonormal wavelets based on this approach.

### 3.2.1 One-Dimensional Multiresolution Analysis

Multiresolution analysis can be interpreted as a successive approximation procedure (Vetterli and Herley, 1992). To understand what multiresolution analysis is, let us start with the following simple but intuitive example: Call  $V_0$  the space of all band-limited functions with frequencies in the interval  $(-\pi, \pi)$ . Then the set of functions

$$\phi(x - k) = \text{sinc}(x - k) = \frac{\sin(\pi(x - k))}{\pi(x - k)} \quad k \in \mathbb{Z} \quad (3.4)$$

forms an orthonormal basis for  $V_0$ , where  $\mathbb{Z}$  is the set of all integers. It is easy to see that if  $f(x) \in V_0$ , then  $f(x - n) \in V_1$ ,  $n \in \mathbb{Z}$ . Similarly, call  $V_1$  the space of all band-limited functions with frequencies in the interval  $(-2\pi, 2\pi)$ . Clearly, the set  $\{ \phi(2x - k), k \in \mathbb{Z} \}$  is an orthonormal basis for  $V_1$ , and  $V_0 \subset V_1$ . In particular, if  $f(x) \in V_0$ , then  $f(2x) \in V_1$ . Now, call  $W_0$  the space of bandpass functions with frequencies in the interval  $(-\pi, -\pi) \cup (\pi, 2\pi)$ . Then

$$V_1 = V_0 \oplus W_0 \quad (3.5)$$

That is,  $W_0$  is the orthogonal complement in  $V_1$  of  $V_0$ . In other words,  $V_1$  is equivalent to  $V_0$  plus some added detail corresponding to  $W_0$ .

From the above, it is clear, by scaling, that if  $V_i$  is the space of band-limited functions with frequencies in the interval  $(-2^i \pi, 2^i \pi)$  ( $i \in \mathbb{Z}$ ), the following relations hold:

$$V_i \subset V_{i+1},$$

$$V_{i+1} = V_i \oplus W_i.$$

The generalization of the above example leads to the following more general definition of multiresolution analysis: A multiresolution analysis is a sequence of subspaces  $\{V_i, i \in \mathbb{Z}\}$  of the square-integrable function space  $L^2(\mathbb{R})$  which has the following properties:

- 1)  $V_i \subset V_{i+1}, i \in \mathbb{Z}$ ;
- 2)  $\bigcap_{i \in \mathbb{Z}} V_i = \{0\}$  and  $\bigcup_{i \in \mathbb{Z}} V_i = L^2(\mathbb{R})$ ;
- 3)  $f(x) \in V_i \Leftrightarrow f(2x) \in V_{i+1}$ ;
- 4)  $f(x) \in V_0 \Leftrightarrow f(x-n) \in V_0, n \in \mathbb{Z}$ ;
- 5)  $\exists \phi(x) \in V_0$  such that  $\{\phi(x-n), n \in \mathbb{Z}\}$  is an orthonormal basis of  $V_0$ .

Since  $\{ \phi(x-n), n \in \mathbb{Z} \}$  forms the basis of the space  $V_0$ ,  $\{ 2^{i/2} \phi(2^i x - n), n \in \mathbb{Z} \}$  forms the basis of the space  $V_i$ . Therefore, any function in  $V_0 \subset V_1$  can be expressed in terms of the base functions of  $V_1$ . In particular,

$$\phi(x) = \sqrt{2} \sum_{n=-\infty}^{\infty} h(n) \phi(2x - n) \quad (3.6)$$

$$\text{with } h(n) = \int_{-\infty}^{\infty} \phi(x) \phi(2x - n) dx \text{ and } \sum_{n=-\infty}^{\infty} h^2(n) = 1.$$

Equation (3.6) is often referred to as the scaling function or the dilation function, which forms the basic function for generating wavelets. The constant coefficients  $h(n)$  are called low-pass filter coefficients since  $\phi(x)$  derives an approximation in  $V_0$  of signals in  $V_1$ .

The basic conclusion from multiresolution analysis is that whenever a collection of closed subspaces satisfies the above five properties, then there exists an orthonormal wavelet basis  $\{ \psi_{i,n}, i, n \in \mathbb{Z} \mid \psi_{i,n}(x) = 2^{i/2} \psi(2^i x - n) \}$  of the orthogonal complement  $W_i$  of  $V_i$  in  $V_{i+1}$ , i.e.

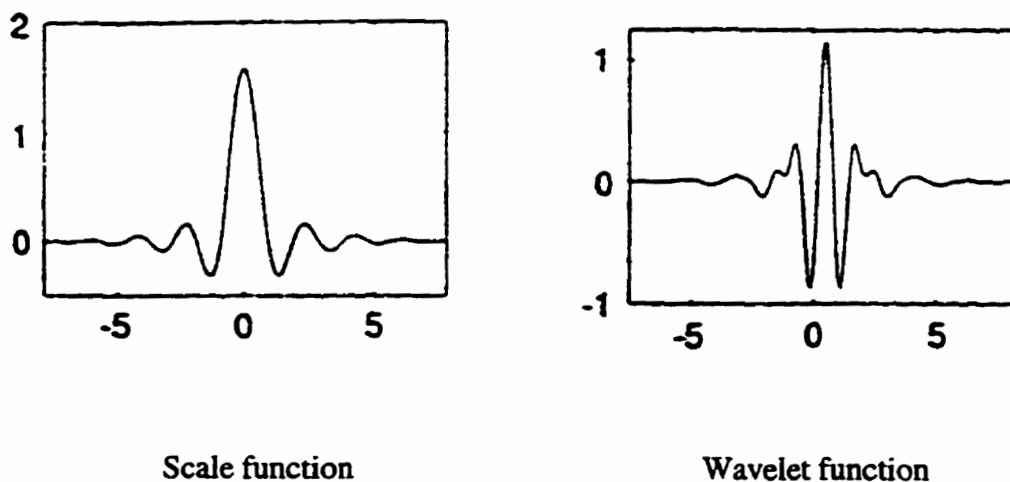
$$V_{i+1} = V_i \oplus W_i. \quad (3.7)$$

This implies  $V_{n+1} = W_n \oplus W_{n-1} \oplus W_{n-2} \oplus \dots$ . Moreover, the wavelet function  $\psi(x)$  corresponding to the scale function  $\phi(x)$  can be constructed explicitly as follows:

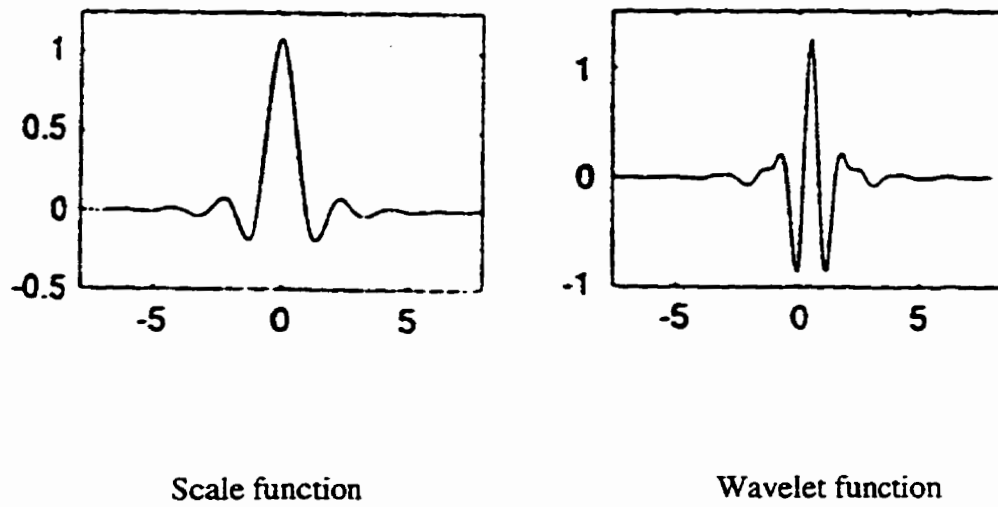
$$\psi(x) = \sqrt{2} \sum_{n=-\infty}^{\infty} g(n) \phi(2x - n), \quad (3.8)$$

where  $g(n) = (-1)^n h(-n+1)$ . The constant coefficients  $g(n)$  are called highpass filter coefficients since the orthonormal complement  $W_0$  to  $V_0$  is given by half-band highpass signals in  $V_1$ .

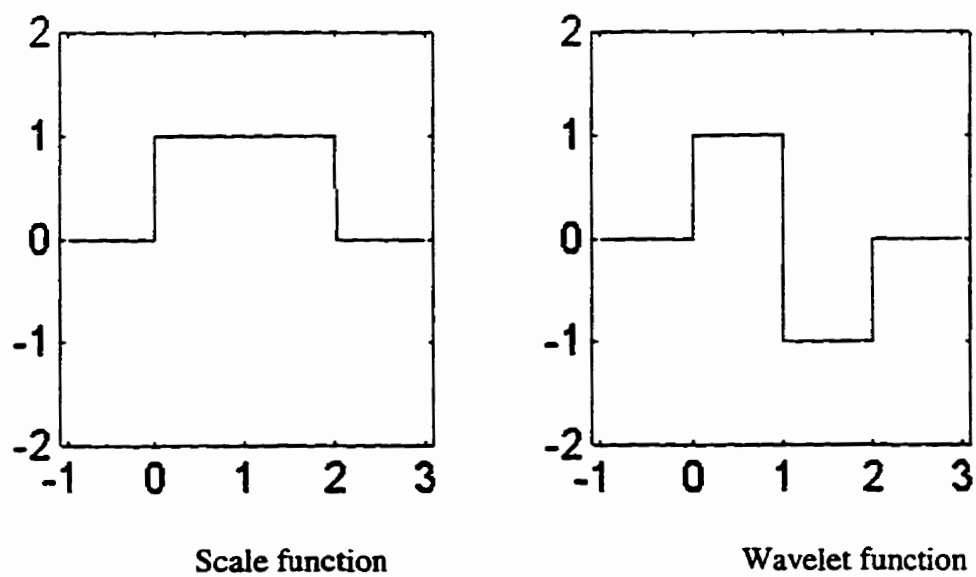
Figure 3.3 shows some examples of scaling functions and wavelet functions corresponding to different multiresolution analyses.



(a) Meyer wavelet



(b) Battle-Lemarie wavelet



(c) Haar wavelet

Figure 3.3 Three examples of orthonormal wavelets (Daubechies, 1992)

It can be shown that the Meyer wavelets are in  $C^\infty$ , infinitely supported, symmetric, and decay faster than any inverse polynomial, while the Battle-Lemarie wavelets which are spline functions and can be chosen as  $C^k$  ( $N \geq k+1$ ,  $N$  is the degree of the B-spline) have also infinite support and symmetry with exponential decay.

The above multiresolution analysis with an integer dilation factor 2 can be extended to one with integer dilation factors larger than 2 (Daubechies, 1992; Cohen and Daubechies, 1993). A multiresolution analysis for an integer dilation factor  $n$  is defined in exactly the same way as for dilation 2 except that Property 3) is replaced by  $f(x) \in V_i \Leftrightarrow f(nx) \in V_{i+1}$ . It is also possible to define a multiresolution with a non-integer dilation factor. However, the dilation factor must be rational (Auscher, 1989) and construction of such a multiresolution analysis is different from that with integer dilation (Daubechies, 1992). Since scaling functions and wavelet functions for multiresolution analysis with integer dilation factor larger than 2 or non-integer dilation factor are not available, only multiresolution analysis with dilation 2 will be in this dissertation. This is currently a limitation of working with wavelets. However, non-dyadic multiresolution analysis could be used as soon as scaling functions and wavelet functions for multiresolution analysis with integer dilation factor larger than 2 or non-integer dilation factor are available.

### **3.2.2 Two-Dimensional Multiresolution Analysis**

Multiresolution analysis in the 1D case can be readily extended to the 2D case. A two

dimensional multiresolution analysis can be defined as a sequence of subspaces  $\{ V_i, i \in Z \}$  of the 2D square-integrable function space  $L^2(\mathbb{R}^2)$  which have the following properties:

- 1)  $V_i \subset V_{i+1}, i \in Z;$
- 2)  $\bigcap_{i \in Z} V_i = \{0\}$  and  $\bigcup_{i \in Z} V_i = L^2(\mathbb{R}^2);$
- 3)  $f(x, y) \in V_i \Leftrightarrow f(2x, 2y) \in V_{i+1};$
- 4)  $f(x, y) \in V_0 \Leftrightarrow f(x-n, y-m) \in V_0, n, m \in Z;$
- 5)  $\exists \phi(x, y) \in V_0$  such that  $\{\phi(x-n, y-m), n, m \in Z\}$  is an orthonormal basis of  $V_0$ .

Only one method of constructing an orthonormal basis for  $L^2(\mathbb{R}^2)$  will be described here, although there are other methods available( Daubechies 1992; Wickerhauser 1994). The method consists of the tensor product of two one-dimensional multiresolution analyses. Tensor product of two one-dimensional function spaces  $V$  and  $W$  is defined as follows:

$$V \otimes W = \{F(x, y) = f(x)g(y) \mid f(x) \in V, g(y) \in W\}. \quad (3.9)$$

So the two-dimensional multiresolution analysis  $\{ V_i, i \in Z \}$  using the tensor product can be defined as

$$V_i = V_i \otimes V_i. \quad (3.10)$$

Since  $\{ \phi(x-n), n \in \mathbb{Z} \}$  forms the basis of the space  $V_0$ , the product functions set  $\{ \phi(x-n), y-m) = \phi(x-n)\phi(y-m), n, m \in \mathbb{Z} \}$  forms an orthonormal basis for  $V_0 = V_0 \otimes V_0$ . As in the one-dimensional case, for each  $i \in \mathbb{Z}$ ,  $V_{i+1}$  can be represented as the direct sum of  $V_i$  and the orthogonal complement space  $W_i$  of  $V_i$  in  $V_{i+1}$ , i.e.  $V_{i+1} = V_i \cup W_i$ . On the other hand,  $V_{i+1}$  can be written as:

$$\begin{aligned} V_{i+1} &= V_{i+1} \otimes V_{i+1} = (V_i \oplus W_i) \otimes (V_i \oplus W_i) \\ &= (V_i \otimes V_i) \oplus [(V_i \otimes W_i) \oplus (W_i \otimes V_i) \oplus (W_i \otimes W_i)]. \end{aligned} \quad (3.11)$$

Therefore,

$$W_i = (V_i \otimes W_i) \oplus (W_i \otimes V_i) \oplus (W_i \otimes W_i). \quad (3.12)$$

It follows that  $W_i$  consists of three tensor products of one-dimensional function spaces, i.e.  $W_{i,1} = V_i \otimes W_i$ ,  $W_{i,2} = W_i \otimes V_i$  and  $W_{i,3} = W_i \otimes W_i$ . This leads to the following three wavelet functions corresponding to these three spaces:

$$\psi_1(x, y) = \phi(x)\psi(y), \quad (3.13a)$$

$$\psi_2(x, y) = \psi(x)\phi(y), \quad (3.13b)$$

$$\psi_3(x, y) = \psi(x)\psi(y). \quad (3.13c)$$

### 3.3 COMPACTLY SUPPORTED ORTHONORMAL WAVELETS

The wavelet bases given in Figure 3.3 are infinitely supported functions except for the Haar wavelet basis. Since data are often collected within a limited area, it might be useful if the wavelet basis could be defined in a finite region in this case. To construct a compactly supported wavelet basis, the scaling function must have a compact support, i.e. will vanish outside a finite interval, say  $[0, N-1]$ , here  $N$  is a positive integer. It can be shown that it is sufficient to construct a scale function with only finitely many coefficients  $h(n)$ ,  $n = 0, 1, \dots, N-1$ , in equation (3.4) which satisfies the following three conditions (Williams and Ameratunga, 1994):

- (i) In order to uniquely define the scale function, the area under the scale function is normalized, i.e.

$$\int_{-\infty}^{\infty} \phi(x) dx = 1, \quad (3.14)$$

which leads to the following condition on the filter coefficients:

$$\sum_{n=0}^{N-1} h(n) = \sqrt{2}. \quad (3.15)$$

- (ii) For the scale function to be orthogonal to its integer translates, the filter coefficients must satisfy the additional requirement that

$$\int_{-\infty}^{\infty} \phi(x)\phi(x+k)dx = \delta_{0,k}, \quad (3.16)$$

This yields the condition

$$\sum_{n=0}^{N-1} h(n)h(n+2k) = \delta_{0,k}, \quad (3.17)$$

where  $\delta_{0,k}$  is the delta function, i.e.

$$\delta_{0,k} = \begin{cases} 1, & k = 0 \\ 0, & k \neq 0 \end{cases}.$$

(iii) Equations (3.15) and (3.17) are insufficient to determine a unique set of filter coefficients. In a  $N$  coefficient system, they yield a total of  $N/2 + 1$  equations. Another  $N/2 - 1$  equations are therefore required for a unique solution. One way to achieve this is to require the scale function to be able to represent polynomial of order up to, but not greater than  $N/2$ . Enforcing this requirement leads to the compactly supported wavelets developed by Daubechies (1988). This requirement means that for any polynomial  $f(x)$  with order not greater than  $N/2$ , the following conditions must be met:

$$\int_{-\infty}^{\infty} f(x)\psi(x)dx \equiv 0, \quad (3.18)$$

which is equivalent to the following  $N/2$  equations:

$$\int_{-\infty}^{\infty} \psi(x)x^k dx = 0, \quad k=0,1,\dots,N/2-1. \quad (3.19)$$

Thus the first  $N/2$  moments of the wavelet function must be zero. The constraints of equation (3.19) on the filter coefficients are

$$\sum_{n=0}^{N-1} (-1)^n h(n)n^k = 0, \quad k=0,1,\dots,N/2-1. \quad (3.20)$$

To demonstrate how the above requirements can be used to construct the filter coefficients  $h(n)$ ,  $N$  is chosen as 4. From Equations (3.15), (3.17) and (3.20), one can easily obtain the following equations:

$$\begin{aligned} h(0) + h(1) + h(2) + h(3) &= 2, \\ h^2(0) + h^2(1) + h^2(2) + h^2(3) &= 2, \\ h(0) - h(1) + h(2) - h(3) &= 0, \\ -h(1) + 2h(2) - 3h(3) &= 0. \end{aligned} \quad (3.21)$$

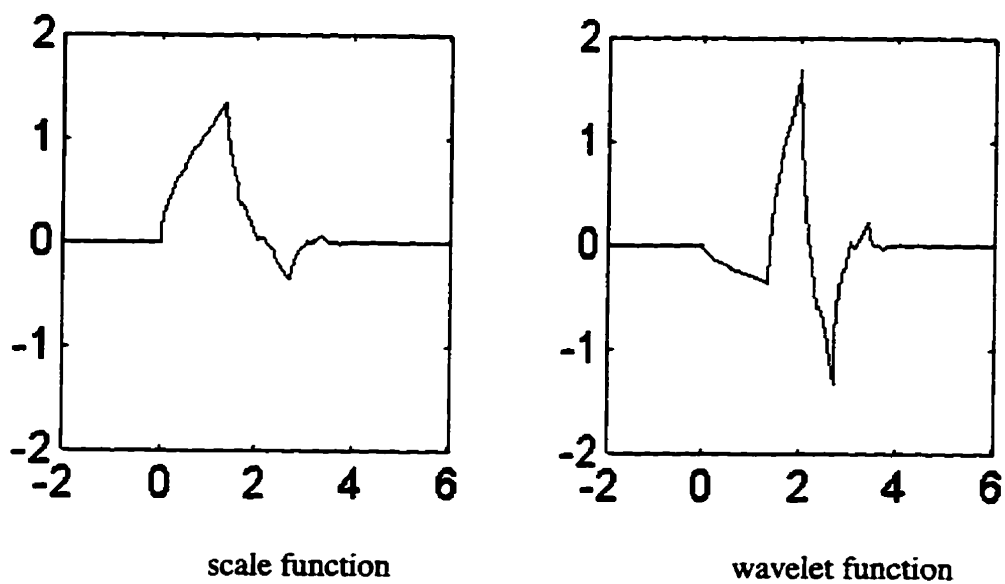
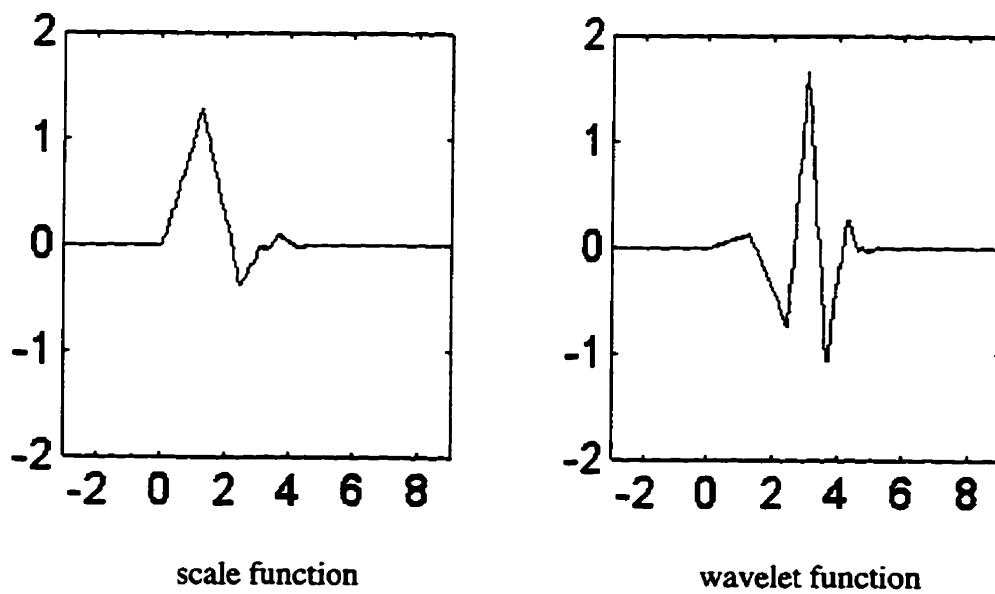
The solution of Equation (3.21) is

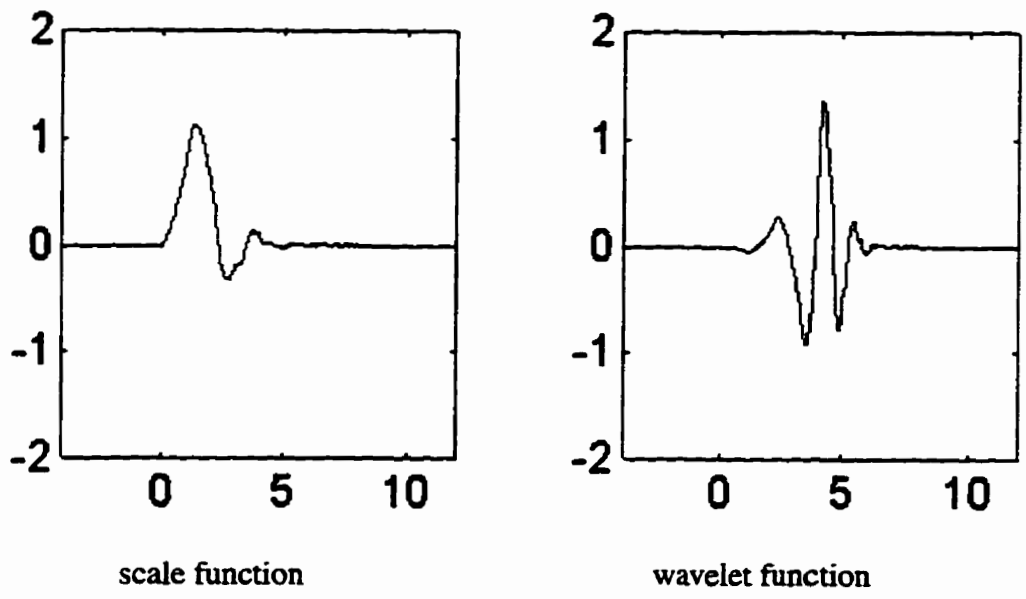
$$\begin{aligned} h(0) &= \frac{1 + \sqrt{3}}{4} = 0.4829613, \\ h(1) &= \frac{3 + \sqrt{3}}{4} = 0.8365163, \\ h(2) &= \frac{3 - \sqrt{3}}{4} = 0.2241438, \\ h(3) &= \frac{1 - \sqrt{3}}{4} = -0.1294095. \end{aligned} \quad (3.22)$$

Table 3.1 gives the filter coefficients  $h(n)$  (FIR) for four compactly supported wavelets with  $N = 4, 6, 8$  and  $10$  obtained in this way. Figure 3.4 shows the corresponding compactly supported scaling functions and wavelet functions. The figure shows clearly that they become more regular as  $N$  increases.

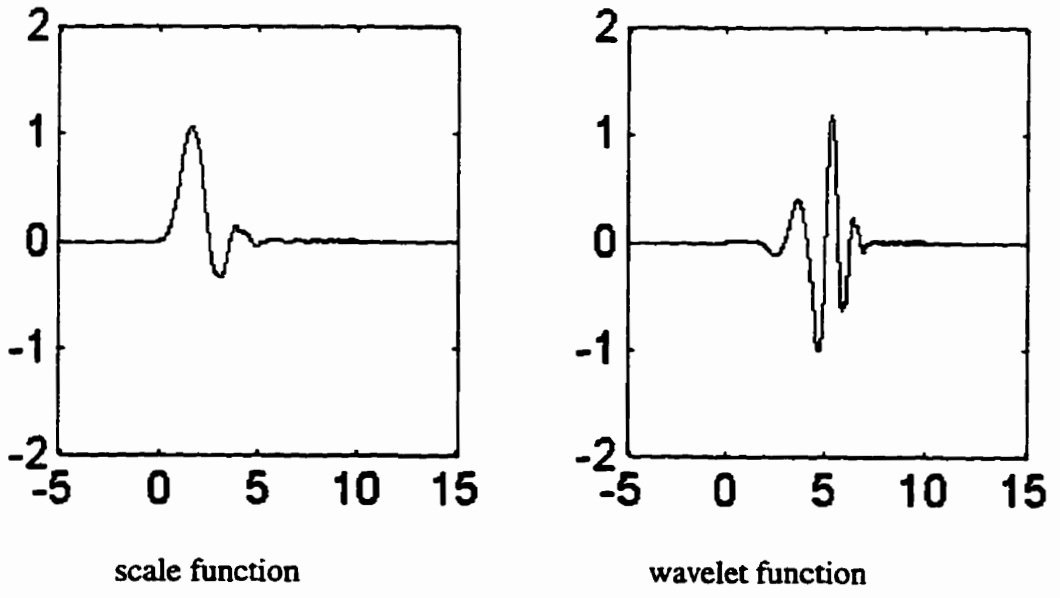
N	n	$h(n)$
4	0	0.4829613
	1	0.8365163
	2	0.2241438
	3	-0.1294095
6	0	0.3326705
	1	0.8068915
	2	0.4598775
	3	-0.1350110
	4	-0.0854412
8	5	0.0355226
	0	0.2303778
	1	0.7178465
	2	0.6388076
	3	-0.0279887
	4	-0.1370348
	5	0.0304413
6	0.0328380	
10	7	-0.0105974
	0	0.1601023
	1	0.6038292
	2	0.7243085
	3	0.1384281
	4	-0.2422948
	5	-0.0322448
	6	-0.0775714
	7	-0.0062414
	8	-0.0125807
9	0.0033357	

Table 3.1 Coefficients  $h(n)$  of the compactly supported wavelets for  $N = 4, 6, 8,$  and  $10$

(a)  $N = 4$ (b)  $N = 6$



(c)  $N = 8$



(d)  $N = 10$

Figure 3.4 Four examples of Daubechies wavelets (Daubechies, 1992)

Figure 3.4 clearly shows that the Daubechies wavelets are compactly supported with width  $N-1$  and are asymmetric. Their smoothness increases with  $N$ , and they have  $N/2$  vanishing moments. It is also worthwhile to mention that the Haar wavelet can be viewed as the first order of the Daubechies wavelets. A more detailed discussion can be found in Daubechies (1988 and 1992).

### **3.4 DISCRETE WAVELET TRANSFORMS USING ORTHONORMAL WAVELETS**

Based on multiresolution analysis, the fast discrete wavelet transform was proposed by Mallat (1989b). It is a 'tree algorithm' or 'pyramid algorithm' that makes discrete wavelet transforms fast and simple. It does for the discrete wavelet transform what the FFT does for the discrete Fourier transform. The algorithm is fully recursive (Strange, 1989). It was further improved by Beylkin et al. (1991).

#### **3.4.1 One-Dimensional Discrete Wavelet Transform**

Generally, a 1D discrete wavelet transform algorithm corresponding to a multiresolution analysis can be described as follows: For a given 1D sequence  $\{ f_{i+1}(n), n \in \mathbb{Z} \}$  of a signal  $f(t)$  at resolution level  $i+1$ , the lower resolution signal sequence  $\{ f_i(n), n \in \mathbb{Z} \}$  can be derived by low-pass filtering with a half band low-pass filter having impulse response  $h(n)$  ( in this dissertation larger  $i$  corresponds to higher resolution or scale and smaller  $i$  corresponds to lower resolution or scale ). At the same time, the added detail  $d_i(n)$ , also

called wavelet coefficients, can be computed by using a high-pass filter with impulse  $g(n)$ , i.e.

$$f_i(n) = \sum_k h(k - 2n)f_{i+1}(k) , \quad (3.23a)$$

$$d_i(n) = \sum_k g(k - 2n)f_{i+1}(k) , \quad (3.23b)$$

or

$$f_i = Hf_{i+1}, \quad (3.24a)$$

$$d_i = Gf_{i+1}. \quad (3.24b)$$

This process is referred to as the decomposition of the signal. The same decomposition procedure can be applied to a lower resolution signal until the lowest resolution of interest is reached.

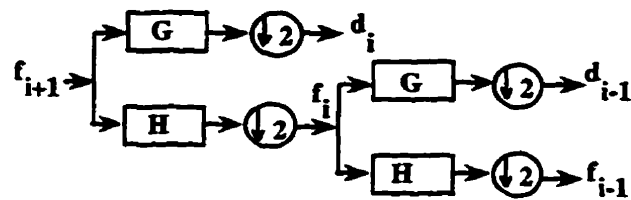
Reversing this process, the synthesis form of the wavelet transform is obtained in which finer and finer representation via a coarse -to -fine scale recursion is achieved, i.e.

$$f_{i+1}(n) = \sum_k h(n - 2k)f_i(k) + \sum_k g(n - 2k)d_i(k), \quad (3.25a)$$

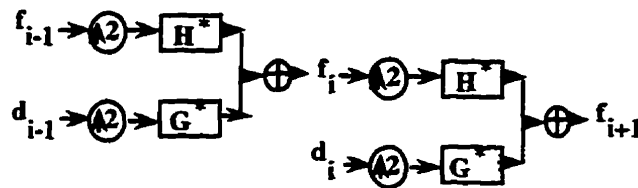
or

$$f_{i+1} = H^*f_i + G^*d_i , \quad (3.25b)$$

This process is also referred to as the reconstruction of the signal. Figures 3.5 illustrates the decomposition and reconstruction process in a block diagram.



(a) Decomposition



(b) Reconstruction

Figure 3.5 Decomposition and Reconstruction of 1D signal

To help understand the above decomposition and reconstruction procedure, let us examine a simple example of decomposition and reconstruction with a sequence  $\{ x_1, x_2, x_3, x_4, x_5, x_6, x_7, x_8 \}$  using Haar filter coefficients  $h(0) = 0.7071$ ,  $h(1) = 0.7071$ ,  $g(0) = 0.7071$ , and  $g(1) = -0.7071$ . In this case, the low-pass filter and high-pass filter are

$$L : \{ x_1, x_2, x_3, x_4, x_5, x_6, x_7, x_8 \} \rightarrow \{ a(x_1 + x_2), a(x_3 + x_4), a(x_5 + x_6), a(x_7 + x_8) \}$$

and

$$G: \{ x_1, x_2, x_3, x_4, x_5, x_6, x_7, x_8 \} \rightarrow \{ a(x_1 - x_2), a(x_3 - x_4), a(x_5 - x_6), a(x_7 - x_8) \},$$

respectively, here  $a = 0.7071$ .

Using (3.24), the above operations can be written as

$$\begin{bmatrix} a & a & 0 & 0 & 0 & 0 & 0 & 0 \\ 0 & 0 & a & a & 0 & 0 & 0 & 0 \\ 0 & 0 & 0 & 0 & a & a & 0 & 0 \\ 0 & 0 & 0 & 0 & 0 & 0 & a & a \end{bmatrix} \begin{bmatrix} x_1 \\ x_2 \\ x_3 \\ x_4 \\ x_5 \\ x_6 \\ x_7 \\ x_8 \end{bmatrix} = \begin{bmatrix} a(x_1 + x_2) \\ a(x_3 + x_4) \\ a(x_5 + x_6) \\ a(x_7 + x_8) \end{bmatrix}$$

(3.26a)

and

$$\begin{bmatrix} a & -a & 0 & 0 & 0 & 0 & 0 & 0 \\ 0 & 0 & a & -a & 0 & 0 & 0 & 0 \\ 0 & 0 & 0 & 0 & a & -a & 0 & 0 \\ 0 & 0 & 0 & 0 & 0 & 0 & a & -a \end{bmatrix} \begin{bmatrix} x_1 \\ x_2 \\ x_3 \\ x_4 \\ x_5 \\ x_6 \\ x_7 \\ x_8 \end{bmatrix} = \begin{bmatrix} a(x_1 - x_2) \\ a(x_3 - x_4) \\ a(x_5 - x_6) \\ a(x_7 - x_8) \end{bmatrix}$$

(3.26b)

It is also easy to verify that

$$\begin{bmatrix} a & 0 & 0 & 0 \\ a & 0 & 0 & 0 \\ 0 & a & 0 & 0 \\ 0 & a & 0 & 0 \\ 0 & 0 & a & 0 \\ 0 & 0 & a & 0 \\ 0 & 0 & 0 & a \\ 0 & 0 & 0 & a \end{bmatrix} \begin{bmatrix} a(x_1 + x_2) \\ a(x_3 + x_4) \\ a(x_5 + x_6) \\ a(x_7 + x_8) \end{bmatrix} + \begin{bmatrix} a & 0 & 0 & 0 \\ -a & 0 & 0 & 0 \\ 0 & a & 0 & 0 \\ 0 & -a & 0 & 0 \\ 0 & 0 & a & 0 \\ 0 & 0 & -a & 0 \\ 0 & 0 & 0 & a \\ 0 & 0 & 0 & -a \end{bmatrix} \begin{bmatrix} a(x_1 + x_2) \\ a(x_3 + x_4) \\ a(x_5 + x_6) \\ a(x_7 + x_8) \end{bmatrix} = \begin{bmatrix} x_1 \\ x_2 \\ x_3 \\ x_4 \\ x_5 \\ x_6 \\ x_7 \\ x_8 \end{bmatrix} \quad (3.27)$$

### 3.4.2 Two-Dimensional Discrete Wavelet Transforms

The 1D discrete wavelet transforms can be extended to 2D discrete wavelet transforms using the tensor product concepts described in Section 3.3.2. In this case, the decomposition and reconstruction of a 2D signal take the following form:

$$f_i(n, m) = \sum_{k,l} h(k-2n)h(l-2m)f_{i+1}(k, l), \quad (3.28a)$$

$$d_{i,1}(n, m) = \sum_{k,l} g(k-2n)h(l-2m)f_{i+1}(k, l), \quad (3.28b)$$

$$d_{i,2}(n, m) = \sum_{k,l} h(k-2n)g(l-2m)f_{i+1}(k, l), \quad (3.28c)$$

$$f_{i,3}(n, m) = \sum_{k,l} g(k-2n)g(l-2m)f_{i+1}(k, l), \quad (3.28d)$$

or

$$f_i = (H \otimes H) f_{i+1}, \quad (3.29a)$$

$$d_{i,1} = (G \otimes H) f_{i+1}, \quad (3.29b)$$

$$d_{i,2} = (H \otimes G) f_{i+1}, \quad (3.29c)$$

$$d_{i,3} = (G \otimes G) f_{i+1}, \quad (3.29d)$$

and

$$\begin{aligned} f_{i+1}(n, m) = & \sum_{k,l} h(k-2n)h(l-2m)f_i(k, l) + \sum_{k,l} g(k-2n)h(l-2m)d_{i,1}(k, l) \\ & + \sum_{k,l} h(k-2n)g(l-2m)d_{i,2}(k, l) + \sum_{k,l} g(k-2n)g(l-2m)d_{i,3}(k, l), \end{aligned} \quad (3.30)$$

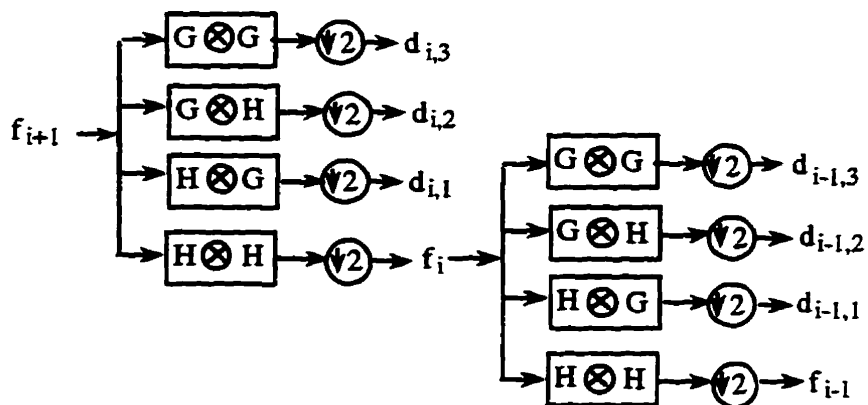
or

$$f_{i+1} = (H^* \otimes H^*) f_i + (G^* \otimes H^*) d_{i,1} + (H^* \otimes G^*) d_{i,2} + (G^* \otimes G^*) d_{i,3} \quad (3.31)$$

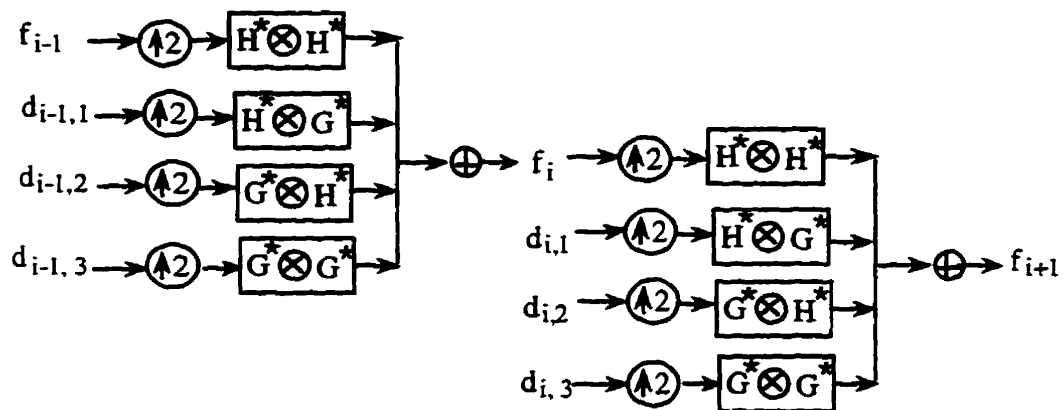
where  $f_i$ ,  $d_{i,1}$ ,  $d_{i,2}$  and  $d_{i,3}$  represent vectors formed by stacking the rows of matrices from 2D signals.

Figures 3.6 illustrates the 2D decomposition and reconstruction in a block diagram ( with only two levels shown).

If the signal  $f_{i+1}$  consists of an  $N \times N$  array, then each of the arrays  $f_i$ ,  $d_{i,1}$ ,  $d_{i,2}$  and  $d_{i,3}$  consists of  $N/2 \times N/2$  elements. Therefore the 2D discrete wavelet transform are often displayed graphically as in Figure 3.7. Figure 3.8 displays Lena image in the form of Figure 3.7. before and after a discrete wavelet transform.



(a) 2D decomposition



(b) 2D reconstruction

Figure 3.6 Decomposition and Reconstruction of 2D signal

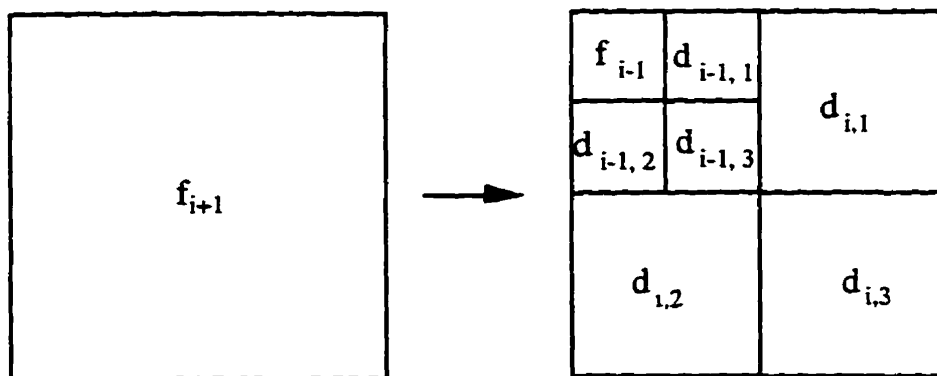


Figure 3.7 The visualization of the 2D discrete wavelet transform



(a) Original Lena image



(b) Decomposition of Lena image

Figure 3.8 Lena image before and after a wavelet transform

One of the attractive features of wavelet transforms for the analysis of signals is that they cannot only be computed recursively in scale, from fine to coarse, but also be completely reconstructed from coarse to fine scale. Therefore, different scales can be related to each other. Such a feature is very useful for the development in this dissertation, since the discrete wavelet transform provides a tool for effectively linking different resolution levels.

### **3.5 CHOICE OF WAVELETS**

From the previous discussion, it is clear that the application of wavelets for signal analysis is influenced by the choice of wavelets. There is no universal criterion for choosing a wavelet basis since the choice of wavelets depends on the objectives of each application. For example, in signal coding applications, the objective is efficient compression of a given signal such as sound or images. In this case, the optimal choice of a wavelet basis from a library orthonormal bases such as orthogonal wavelet-packets is given by the entropy criterion (Coifman and Wickerhauser, 1992; Mayer, 1993; Wickerhauser, 1994). The idea is to choose an orthonormal wavelet basis relative to which the given signal has the lowest information cost.

In gravity field applications, the objective is to link a signal at different resolutions. This means that it should be able to obtain the signal at coarse resolution within a low frequency band from the signal at fine resolution through a lowpass filter corresponding to a scaling function. In other words, it should be able to extract the detailed information

in a high frequency band of the fine-resolution signal using a highpass filter corresponding to a wavelet function. Therefore, the criterion for an optimal choice is that the wavelet function is as close as possible to that of the ideal half-band highpass filter.

The frequency response of the ideal half-band highpass filter is

$$H(\omega) = \begin{cases} 1 & |\omega| > \frac{\pi}{2} \\ 0 & \text{otherwise} \end{cases}, \quad (3.32)$$

as shown in Figure 3.9.

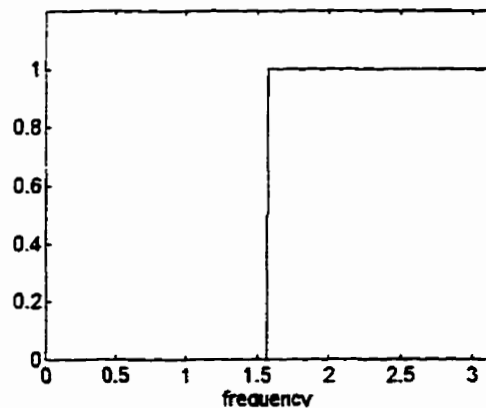


Figure 3.9 The ideal half-band highpass response

In the following, the choice of an wavelet basis from a library of Daubechies compactly supported wavelets will be discussed. To know which Daubechies wavelet should be chosen, one should know which Daubechies wavelet function will be the closest to the ideal half-band highpass filter, or equivalently, which Daubechies scale function will be the closest to the ideal half-band lowpass filter,

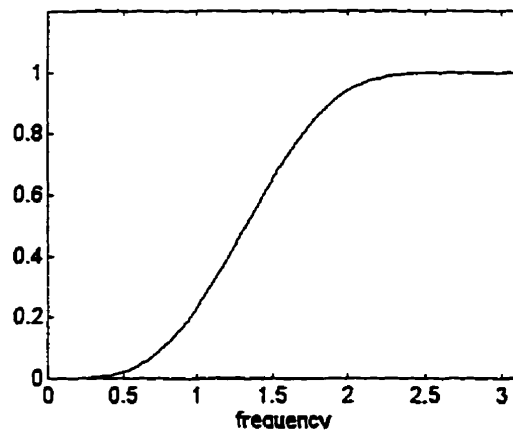
Since the first  $N/2$  moments of the Daubechies wavelet function  $\psi(x)$  are zero for a given  $N$ , as can be seen from Equation (3.19), the following equation can be obtained

$$\Psi^{(k)}(0) = 0, \quad k = 0, 1, \dots, N/2 - 1, \quad (3.33)$$

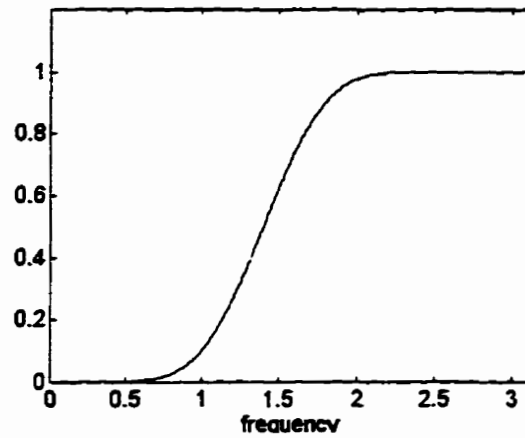
where  $\Psi$  is Fourier transform of the wavelet function. Using the Taylor expansion and Equation (3.33) leads to

$$\Psi(\omega) = \sum_{k=0}^{N/2-1} \frac{1}{k!} \Psi^{(k)}(0) \omega^k + o(\omega^{N/2}) = o(\omega^{N/2}), \quad (3.34)$$

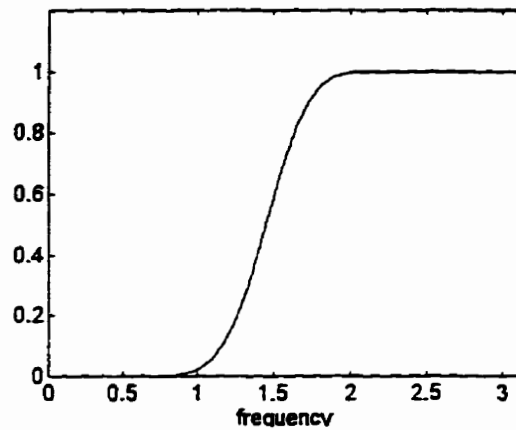
Equation (3.34) indicates that  $\Psi(\omega)$  is close to zero within a certain frequency interval  $[0, \delta_N]$  and  $\delta_N$  will increase with the increase of  $N$ . Therefore the wavelet function will be closer to the ideal half-band highpass filter with larger  $N$ . Figure 3.10 shows the frequency responses of different FIR highpass filters corresponding to Daubechies wavelets of different  $N$ .



(a) Daubechies wavelet  $N = 8$



(b) Daubechies wavelet  $N = 16$



(c) Daubechies wavelet  $N = 32$

Figure 3.10 Frequency response of different Daubechies wavelet FIR filters

From Figure 3.10, it is easy to see that the frequency response of Daubechies wavelets is closer to the ideal half-band highpass filter with increasing  $N$ . Therefore, the higher the order of Daubechies wavelets, the better the choice of the wavelet for gravity field approximation.

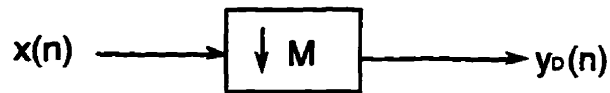
### 3.6 MULTIRATE SYSTEMS

As mentioned before, a current limitation of using discrete wavelet transforms based on multiresolution analysis is that only a dyadic tree structure can be implemented. This means that sampling rate conversion between two different resolution levels can only be done by a factor of 2. For the non-dyadic cases, sampling rate conversion cannot be realized by using the discrete wavelet transforms at this time. In this case, a multirate system can be used to solve this problem. Multirate systems have been widely used e.g. in communication, speech processing, image compression, antenna systems, adaptive signal processing, and numerical solution of differential equations ( e.g. Khan, 1980; Crochiere and Rabiner, 1981; Vaidynathan, 1990 and 1993; Liu, 1994; Fliege, 1994; Ratzlaff, 1995). Multirate signal processing is a technique of using different sampling rates within a system to achieve computational efficiencies that are impossible to obtain with a system that operates on a single fixed sampling rate.

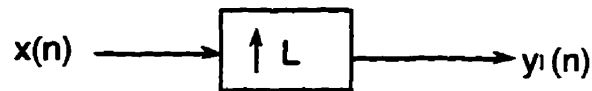
#### 3.6.1 Fundamentals of Multirate Systems

The basic building blocks in a multirate digital signal processing system are decimators and interpolators. Figure 3.11 shows a block diagram of these building blocks. The decimator is characterized by the input-output relation

$$y_D(n) = x(Mn), \quad (3.35)$$



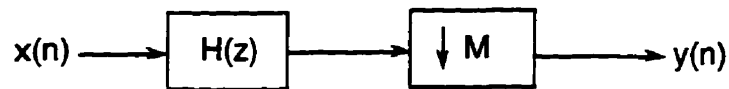
(a) M-fold decimator



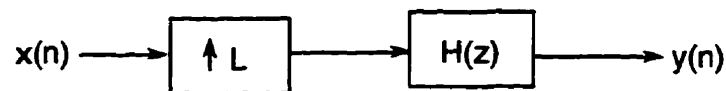
(b) L-fold interpolator

Figure 3.11 Multirate system building blocks

Equation (3.35) means that decimation by a factor of  $M$  is achieved by keeping every  $M$ th samples of an incoming signal. However, to avoid aliasing of frequencies above the passband into the passband requires lowpass filtering ( decimation filter ) the incoming signal prior to decimation, as shown in Figure 3.12a.



(a) Decimation filter



(b) Interpolation filter

Figure 3.12 Decimation and interpolation filters

The interpolator, on the other hand, is described by the following input-output relation

$$y_I(n) = \begin{cases} x\left(\frac{n}{L}\right) & \text{if } n \text{ is a multiple of } L \\ 0 & \text{otherwise} \end{cases} \quad (3.36)$$

That is, the output is obtained by inserting  $L-1$  zero values between adjacent samples of  $x(n)$ . However, to prevent amplitude and phase distortion in the frequency band above the lowpass cutoff frequency, a second filter called interpolation filter is required on the final output sequence, as illustrated in Figure 5.12b.

Decimation and interpolation filters can be described using the following input-output relation in the time domain

$$y(n) = \sum_{k=-\infty}^{\infty} x(k)h(nM - k), \quad M - \text{fold decimation filters} \quad (3.37a)$$

$$y(n) = \sum_{k=-\infty}^{\infty} x(k)h(n - kL), \quad L - \text{fold interpolation filters} \quad (3.37b)$$

or, in matrix form,

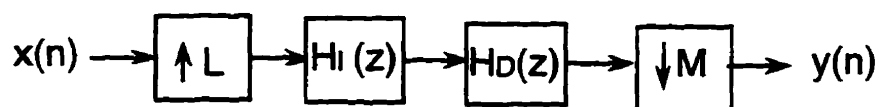
$$y = H_D x, \quad M - \text{fold decimation filters} \quad (3.38a)$$

$$y = H_I x, \quad L - \text{fold interpolation filters} \quad (3.38b)$$

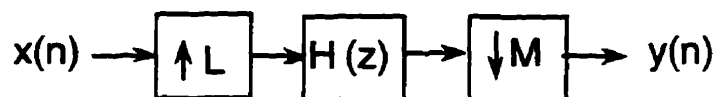
The above decimation and interpolation procedures only allow the change of sampling rate by interger number. For sampling rate conversion by a nonintergral (rational) number

$M/L$ , these two procedures can be combined. This is done by first increasing the sampling rate by  $L$  using an interpolation filter and then decreasing it by  $M$  using a decimation filter, as shown in Figure 5.13. The input-output relation in this case can be written as

$$y(n) = \sum_{k=-\infty}^{\infty} x(k)h(nM - kL). \quad (3.39)$$



(a) Cascade of an interpolation filter and decimation filter



(a) General structure

Figure 3.13 Sampling rate conversion by a rational number

### 3.6.2 Polyphase Structure

An efficient implementation of decimation and interpolation filters can be done using polyphase decomposition. To introduce polyphase decomposition, one starts with the following transfer function representing a digital filter:

$$H(z) = \sum_{n=-\infty}^{\infty} h(n)z^{-n}. \quad (3.40)$$

Set

$$E_0(z) = \sum_{n=-\infty}^{\infty} h(2n)z^{-n} \quad (3.41a)$$

$$E_1(z) = \sum_{n=-\infty}^{\infty} h(2n+1)z^{-n}, \quad (3.41b)$$

Equation (3.40) can then be written as

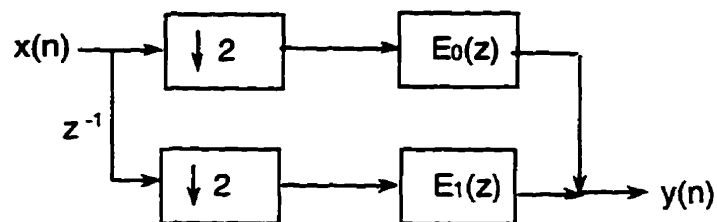
$$H(z) = E_0(z^2) + z^{-1}E_1(z^2). \quad (3.42)$$

Basically, Equation (3.42) regroups the impulse response  $h(n)$  into even numbered samples  $h(2n)$  and odd numbered samples  $h(2n+1)$ . Equation (3.42) is called Type 1 polyphase decomposition ( $M=2$ ). Equation (3.42) can also be written in another form, i.e.

$$H(z) = z^{-1}R_0(z^2) + R_1(z^2). \quad (3.43)$$

where  $R_0(z) = E_1(z)$  and  $R_1(z) = E_0(z)$ . Equation (3.43) is called Type 2 polyphase decomposition. Equations (3.42) and (3.43) can be easily extended to the case of  $M > 2$ .

With the help of polyphase decomposition, a decimation filter and an interpolation filter can be implemented in a polyphase form, as shown in Figure 3.14.



(a) Decimation filter

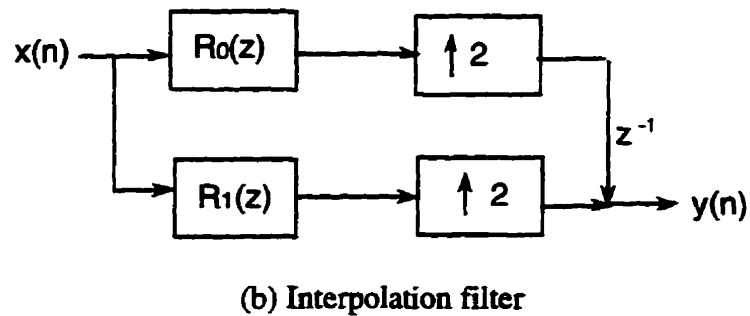


Figure 3.14 Decimation and interpolation filter in a polyphase form

A discussion on the efficiency of using the polyphase form for decimation and interpolation can be found in Vaidyanathan (1993).

### 3.6.3 Window Technique for the Design of a Multirate Lowpass FIR Filter

There are different methods available to design a multirate lowpass FIR filter (e.g. Crochiere and Rabiner, 1981; Vaidyanathan, 1993; Fliege, 1994 ). One straightforward approach used in this dissertation is the windowing technique, in which the filter design  $h(n)$  can be obtained as

$$h(n) = \frac{\sin\left(\frac{\pi n}{M}\right)}{\pi n} w(n), \quad (3.44)$$

where  $w(n)$  is a finite-duration sequence called the window function. One commonly used type of windows is Kaiser window, which will be used to design a multirate lowpass FIR filter in Section 5.5. The Kaiser window is given by (Vaidyanathan, 1993 )

$$w(n) = \begin{cases} \frac{I_0\left(b\sqrt{1-(n/0.5N)^2}\right)}{I_0(b)} & , -\frac{N}{2} \leq n \leq \frac{N}{2} \\ 0 & \text{otherwise} \end{cases} \quad (3.45)$$

where  $I_0(x)$  is the modified zeroth-order Bessel function. The parameter  $\beta$  can be found using the following formula

$$b = \begin{cases} 0.1102(A_s - 8.7) & \text{if } A_s > 50 \\ 0.5842(A_s - 21)^{0.4} + 0.07886(A_s - 21) & \text{if } 21 < A_s < 50 \\ 0 & \text{if } A_s < 21 \end{cases} \quad (3.46)$$

$A_s$  is the minimum stopband attenuation. The filter order  $N$  is estimated from

$$N = \frac{A_s - 7.95}{14.36\Delta f} \quad (3.47)$$

for given parameters  $A_s$  and  $\Delta f$  (Normalized transition bandwidth).

### 3.6.4 Two Dimensional Decimation and Interpolation Filters

The basic concepts of decimator and interpolator can be extended to the 2D case. However, decimation and interpolation of a 2D signal are fundamentally more complicated because there are many ways to choose the sampling geometry. The simplest

method is rectangular sampling, which can be viewed as a direct extension from the 1D case.

The decimator and interpolator using rectangular sampling is characterized by the following input-output relations

$$y_D(n_0, n_1) = x(M_0 n_0, M_1 n_1), \quad (3.48a)$$

and

$$y_I(n_0, n_1) = \begin{cases} x\left(\frac{n_0}{L_0}, \frac{n_1}{L_1}\right) & \text{if } n_0 \text{ and } n_1 \text{ are multiples of } L_0 \text{ and } L_1, \text{ respectively} \\ 0 & \text{otherwise} \end{cases} \quad (3.48b)$$

Similar to the 1D case, a 2D decimation filter and an 2D interpolation filter should be used to avoid aliasing, amplitude and phase distortion. For rectangular sampling, a separable 2D filter coefficients  $h_2(n_0, n_1)$  can be obtained from 1D filter coefficients  $h(n)$  as follows:

$$h_2(n_0, n_1) = h(n_0)h(n_1) \quad (3.49)$$

In this case, 2D decimation and interpolation filters can be described using the following input-output relation in time domain

$$y(n, m) = \sum_{k, l=-\infty}^{\infty} x(k, l)h(nM - k)h(mM - l), \quad M - \text{fold decimation filters} \quad (3.50a)$$

$$y(n, m) = \sum_{k, l=-\infty}^{\infty} x(k, l)h(n - kL)h(m - lL), \quad L - \text{fold interpolation filters} \quad (3.50b)$$

or, in matrix form,

$$y = (H_D \otimes H_D)x, \quad M - \text{fold decimation filters} \quad (3.51a)$$

$$y = (H_I \otimes H_I)x, \quad L - \text{fold interpolation filters} \quad (3.51b)$$

A detailed discussion on 2D filter design can be found in Vaidyanathan (1993).

### 3.6.5 Multirate Filter Banks

A filter bank decomposes the signal spectrum in a number of directly adjacent frequency banks and reconstructs the signal spectrum by using lowpass, bandpass, and highpass filters. Decomposition is performed by an analysis filter bank and reconstruction by a synthesis filter bank. An analysis bank is a set of analysis filters which splits signals into  $M$  subband signals, while a synthesis bank consists of  $M$  synthesis filters which combine  $M$  signals ( usually an analysis filter bank ) into a reconstructed signal. Figure 3.15 shows a diagram of an analysis filter bank and a synthesis filter bank. If the analysis filters is followed by decimators, the analysis filter bank is the decimated analysis filter bank. To reconstruct the signal from the output of the decimated analysis filter bank, interpolation is needed before using the synthesis filter bank. This type of filter banks is a multirate filter bank. The basis structure of such a filter bank is illustrated in Figure 3.16.

The reconstructed signal using the multirate filter bank may differ from the original signal for three reasons: aliasing, amplitude distortion and phase distortion. To eliminate some or all of these distortions, different types of multirate filter banks, e.g. maximally decimated filter banks, paraunitary perfect reconstruction filter banks, and linear phase perfect reconstruction quadrature mirror filter banks, etc., have been proposed. A detailed discussions on these filter banks can be found in Vaidyanathan (1993).

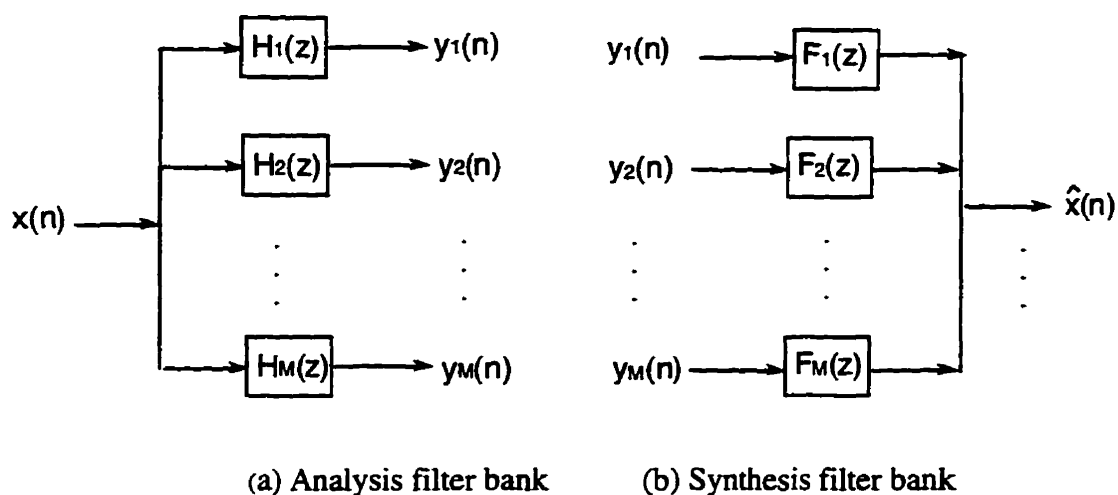
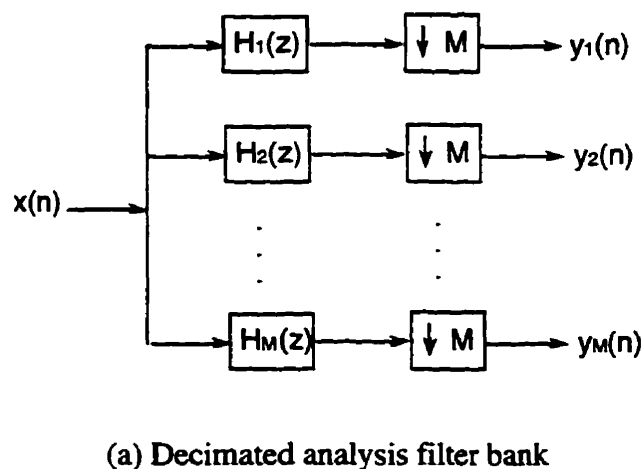
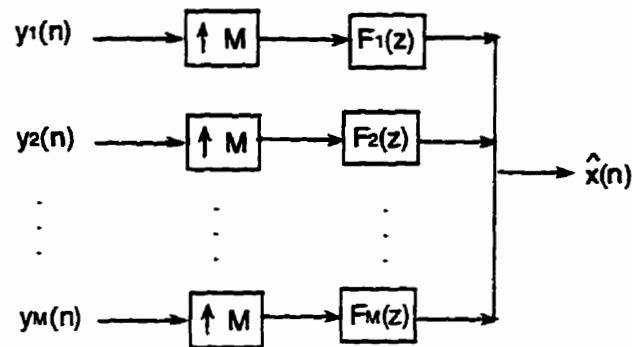


Figure 3.15. Analysis and synthesis filter bank





(b) Interpolated synthesis filter bank

Figure 3.16 Multirate filter bank

In the following, only dyadic tree structured filter banks will be briefly reviewed, and the relationship between the filter bank and dyadic wavelets will be pointed out.

In a tree structure, a signal is split into two subbands, lowpass half-band and highpass half-band. By successively splitting the low frequency output signal into two subbands, a dyadic tree structured analysis filter bank is obtained. The cutoff frequencies are related to each other by a factor of two and spaced in octaves, as shown in Figure 3.17. This is called octave analysis filter bank. Figure 3.18(a) shows a diagram of such an analysis filter for the two level trees. This octave analysis filter bank is equivalent to the filter bank shown in Figure 3.18(b). This corresponds to a three channel with unequal decimation rate.

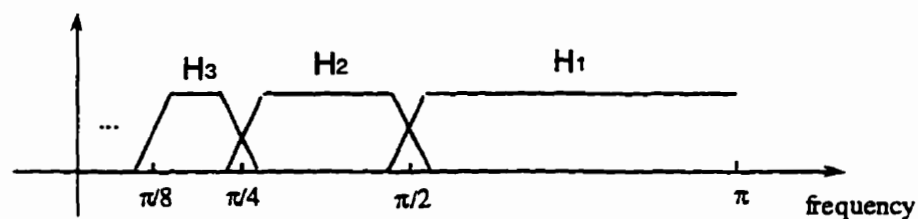
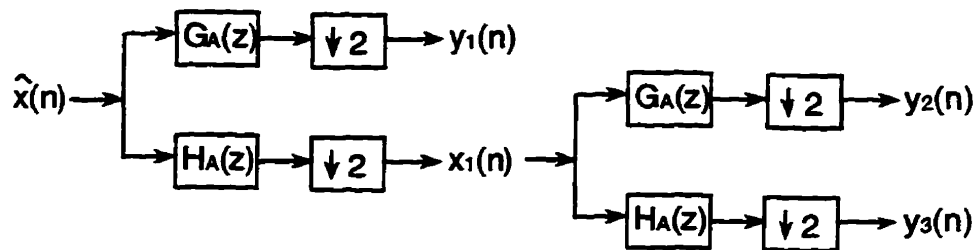
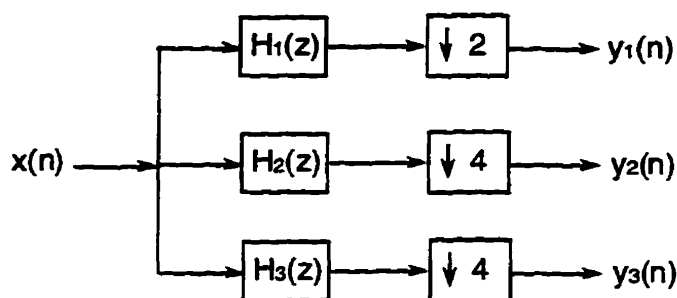


Figure 3.17 Frequency response of an octave analysis filter bank



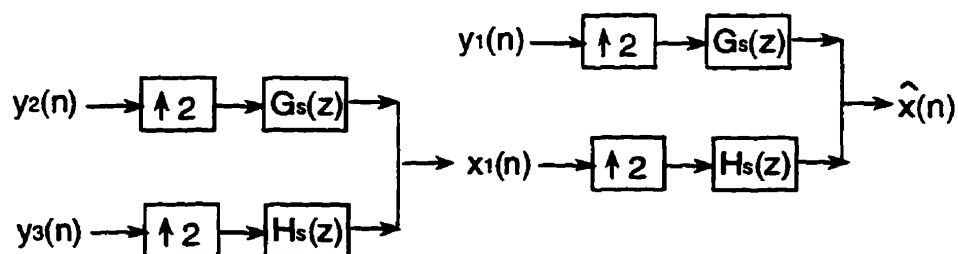
(a) Tree-structured analysis filter bank



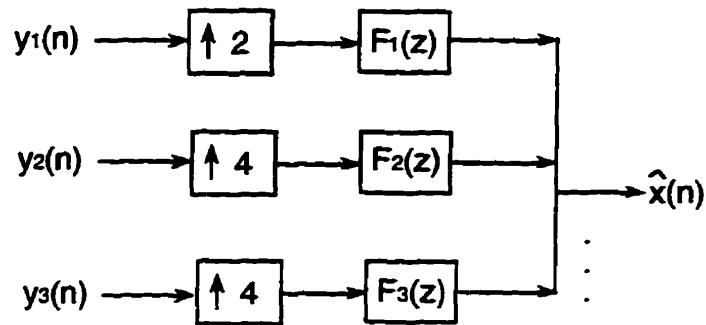
(b) Analysis filter bank with unequal decimation rate

Figure 3.18 Octave analysis filter bank

Similarly, an octave synthesis filter bank can be obtained by successively recombining the low frequency and high frequency output signals from the octave analysis filter at the same level of the tree. Figure 3.19 shows a diagram of such a synthesis filter and its equivalent system for the two level trees.



(a) tree-structured synthesis filter



(b) Synthesis filter bank with unequal interpolation

Figure 3.19 Octave synthesis filter bank

When going through an octave analysis filter bank and an octave synthesis filter bank, an output signal is obtained. If the output signal is exactly the same as the input signal, the octave filter bank is a perfectly reconstructed filter bank.

From the above introduction to the octave filter banks, it is easy to see that the wavelet decomposition and reconstruction of a signal by using a dyadic multiresolution analysis can be viewed as a special octave filter bank, which has the properties of perfect reconstruction and orthogonality. Therefore a discrete wavelet transform can be considered as a multirate filter bank. References are made to Vaidyanthan (1993) and Fliege (1994) for detailed discussions on the relationship between multirate filter banks and wavelet transforms.

## **CHAPTER 4**

### **SOLUTIONS TO THE MULTIREOLUTION APPROXIMATION PROBLEM FOR GRAVITY FIELD MODELING**

In this chapter, solutions to the multiresolution approximation problem for gravity field modeling formulated in Section 2.6 will be presented. More specifically, a general methodology of combining different methods for solving the multiresolution approximation problem is presented. Both signal domain and measurement domain approaches are considered. Two signal domain approaches, fine-to-coarse estimation and coarse-to-fine estimation, is derived by the combination of wavelet transforms and least-squares collocation. A measurement domain approach is also proposed using a multirate system and a MISO system. The proposed signal domain algorithms is then compared to stepwise least-squares collocation taking into account mathematical models, assumptions, optimality criteria and solutions.

#### **4.1 A GENERAL METHODOLOGY**

After introducing the multiresolution approximation problem in Section 2.6 , the next step is to find solutions to solve the problem. First, the currently available approaches in gravity field approximation will be examined. The purpose of this is to see if there is any possibility to solve the problems using the methods available. The solution of the problems must address the resolution problem ( due to different resolution of

measurements and signals ), the observable problem ( due to different type of observables), the attenuation problem ( due to the attenuation effect of signals at different altitudes ), and the noise problem ( due to different characteristics of measurement noise from different procedures and different technologies ). Three methods described in Chapter 2, i.e. the integral approach, the least-squares collocation approach and the MISO approach, will be examined here.

The integral method can be used to solve the observable problem and the attenuation problem since the gravity field signal can be determined from measurements, the type and the altitude of which can be different from that of the signal. However, it cannot solve the resolution problem and the noise problem due to the fact that the integral method does not allow the input of measurements at two or more different resolution scales and doesn't take measurement noise into account at all. The least-squares collocation method can solve the observable problem, the attenuation problem, and the noise problem because it allows not only inputs of measurements of different types and at different altitudes and output of different signals but also considers the noise statistics of the measurements. It cannot solve, however, the resolution problem. The reason, as mentioned before, is that the correlation between resolution levels cannot be handled by least-squares collocation. The MISO method is quite similar to least-squares collocation in the sense that it also allows not only inputs of measurements of different types and at different altitudes and output of different signals but also considers the noise statistics of the measurements. It, therefore, can also be used to solve the observable problem, the attenuation problem, and

the noise problem. However, it cannot solve the resolution problem because it requires that all measurement inputs have the same sampling rate. This is not the case when measurements are given at different resolution scales.

From the above discussion, one can see that none of the three methods can solve the resolution problem. That means none of them can solve the multiresolution approximation problem. Therefore other methods are needed. Two methods, which can be used to solve the resolution problem, are multirate systems and wavelet transforms. This is because different resolutions can be linked through either a multirate system or a wavelet transform. They, however, cannot solve the observable problem, the attenuation problem, and the noise problem. This is due to the fact that they can only handle signals of same type and don't consider noise characteristics. Therefore, a multirate system or a wavelet transform cannot solve the multiresolution approximation problem alone.

The capabilities of the above methods for solving the multiresolution approximation problem are summarized Table 4.1.

Table 4.1 clearly indicates that to solve the multiresolution approximation problem, the combination of two different methods is necessary. Therefore, the following discussion will emphasize a general methodology of combining different methods for solving the multiresolution approximation problem. Specific algorithms will then be proposed in the next two sections.

Method	Resolution problem	Observable problem	Attenuation problem	Noise problem
Integral formulas	No	Yes	Yes	No
LSC	No	Yes	Yes	Yes
MISO	No	Yes	Yes	Yes
Multirate systems	Yes	No	No	No
Wavelet transforms	Yes	No	No	No

Table 4.1 Capabilities of different methods for solving multiresolution problems

Possible solutions to the multiresolution approximation problem can be classified as

- (i) Signal domain approaches
- (ii) Measurement domain approaches

These two approaches will be discussed separately.

#### 4.2.1 Signal Domain Approaches

In signal domain approaches, the transition from one resolution level to the next is done in signal domain. That means that decomposition and reconstruction are performed on signals. These approaches can be categorized as:

- (i) Fine-to-coarse estimation schemes: the estimation is done from the finest scale to the coarsest scale, followed by sweeping from the coarsest scale to the finest scale.
- (ii) Coarse-to-fine estimation schemes: the estimation is done from the coarsest scale to the finest scale, followed by sweeping from the finest scale to the coarsest scale.

A fine-to-coarse estimation scheme starts with the estimation of a signal at finest scale using the finest-scale measurements only. Possible estimation schemes at this stage are, e.g. least-squares collocation and integral formulas. If least-squares collocation is used, the minimum criterion will be the minimum principle (2.31) in Chapter 2. If an integral formula is used, no minimum criterion will be available. Instead, an estimation error will be computed by error propagation. The second step will be downsampling of the estimate of the signal at finest scale. This can be done by using, e.g. a discrete wavelet transform or a multirate analysis filter bank. The error of the estimated signal at coarse scale due to the downsampling procedure will be calculated by error propagation. The third step will then be to update this coarse-scale estimate using measurements at this resolution scale. This can be done by using, e.g. least-squares collocations or the double-input single-output system or the frequency-domain least-squares adjustment, in which the estimated signal at coarse-scale is taken as measurement. If least-squares collocation is employed, the minimum criterion will be of the same form as Equation (2.31). If a double-input single-output system is used, the minimum criterion will be of the same form as Equation (2.46). The minimum criterion for the frequency-domain least-squares adjustment can be

found in Sideris (1996). The second and third steps will be repeated until the coarsest scale has been reached. The final step is to obtain estimated signals at each scale by sweeping from the coarsest scale to the finest scale. This step can be done by using, e.g. the corresponding inverse discrete wavelet transform or a multirate synthesis filter bank. The estimation errors are again computed by error propagation.

The procedure for a coarse-to-fine estimation scheme is very similar to that for the fine-to-coarse estimation scheme except that the coarse-to-fine estimation scheme starts with the coarsest scale.

The block diagrams in Figures 4.1 and 4.2 illustrate the fine-to-coarse and the coarse-to-fine coarse estimation procedure described above.

The above two estimation procedures will be detailed in the next section where specific algorithms based on discrete wavelet transforms and least-squares collocation are discussed.

#### **4.2.2 Measurement Domain Approaches**

In measurement domain approaches, the transition from one resolution level to the next is done in the measurement domain. This means that upsampling and downsampling are performed at the measurement level.

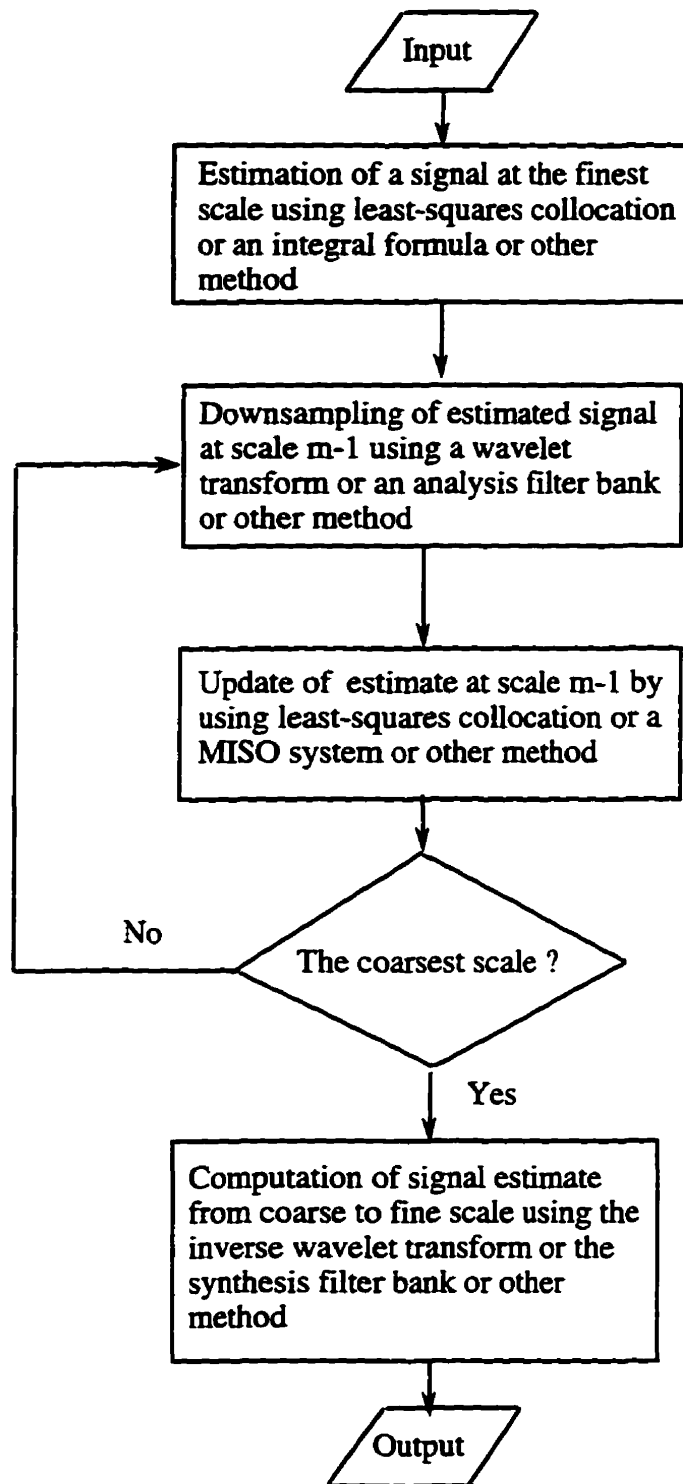


Figure 4.1 Block diagram for a fine-to-coarse estimation procedure

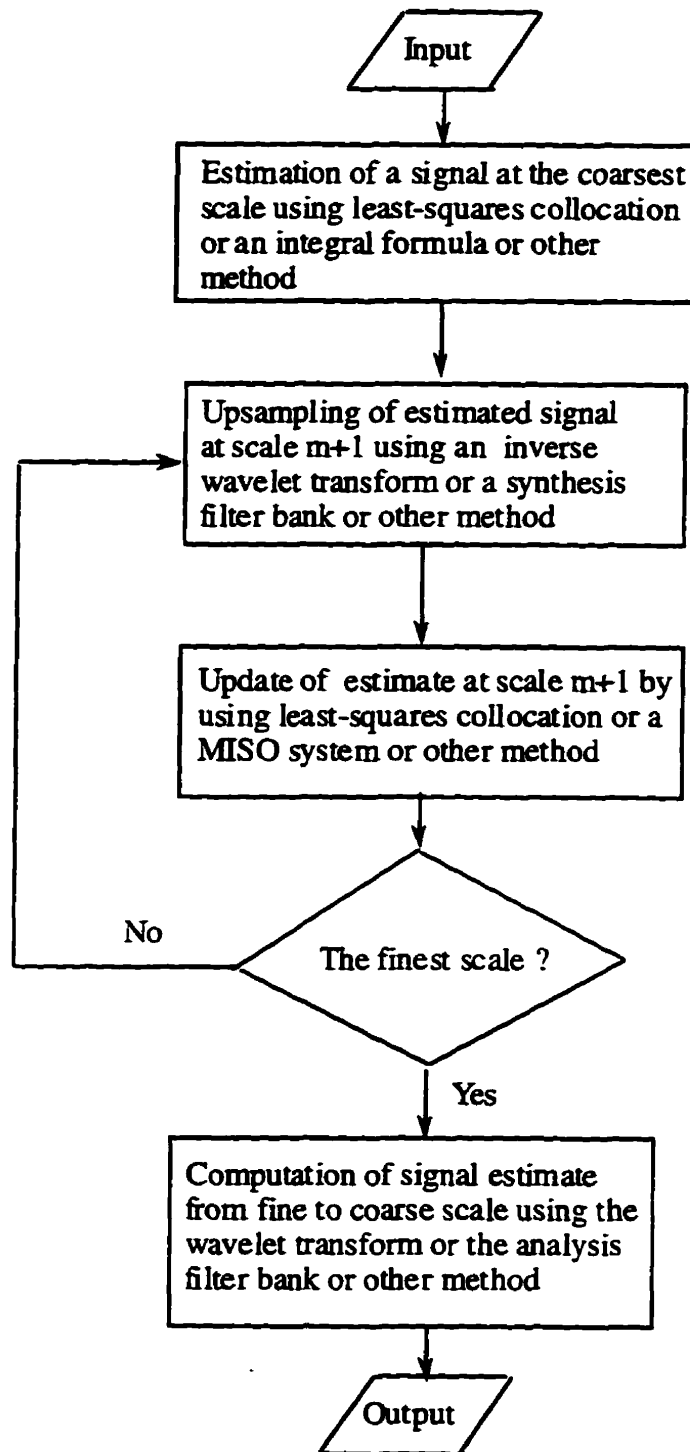


Figure 4.2 Block diagram for a coarse-to-fine estimation procedure

A measurement domain approach consists the following two major steps:

**Step 1:** Downsampling and upsampling of the measurements at different resolutions to a given resolution.

**Step 2:** Estimation of the signal at the given resolution by combining all measurements at this scale.

For a given resolution scale  $m$ , the measurements at resolution scales  $i > m$  will be downsampled and the measurements at resolution scales  $i < m$  will be upsampled to the resolution level  $m$ . This can be done by using, e.g., a discrete wavelet transform or a multirate system. The errors of the downsampled and upsampled measurements will be computed by error propagation.

Estimation at a specific scale uses the original measurements, the downsampled measurements, and the upsampled measurements. The estimation of the signal at this scale can be done by using, e.g. least-squares collocation or a multiple-input single-output system or the frequency-domain least-squares adjustment. The minimum criterion for this estimation will be of the same form as that in signal domain approaches whether least-squares collocation or a multiple-input single-output system or the frequency-domain least-squares adjustment is used.

The above two steps will be repeated for each resolution scale starting either from the

finest scale or the coarsest scale.

A measurement domain approach procedure is shown in Figure 4.3.

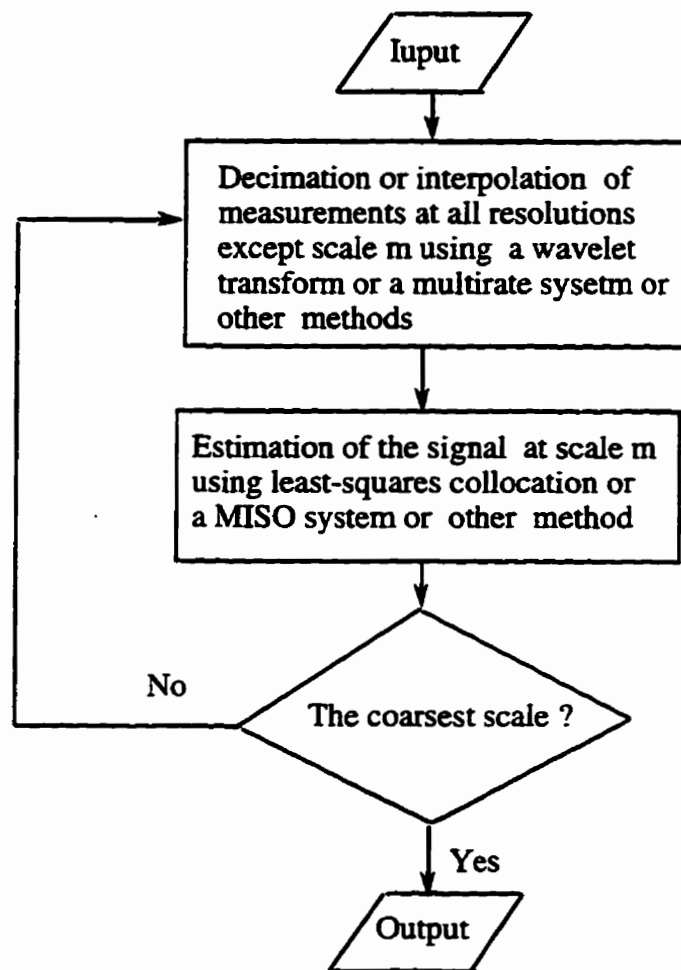


Figure 4.3 Block diagram for a measurement domain approach

From the above discussion on both signal domain and measurement domain approaches, it can be seen that both methods use the same information from measurements at multiple resolution scales but different implementations. In signal domain approaches, different

resolution levels are linked at the signal levels. However, they are linked at the measurement level in measurement domain approaches. Measurement domain approaches have the advantage that they are more flexible than signal domain approaches because they allow to estimate different signals at different resolutions from multiresolution measurements and signals domain approaches only allow to estimate same signals at different resolutions. Also, if a signal is needed only at one resolution level between the finest and the coarsest scales, the use of measurement domain approaches will be more efficient since no sweep either from the finest to the coarsest scale or from the coarsest to-the finest scale is needed.

Table 4.2 lists some possible approaches to solve the multiresolution approximation problem by combining the different methods mentioned above.

Domain	Method I	Method II	Method III	Method IV
Signal or measurement	Least-squares collocation plus a wavelet transform	A MISO system plus a multirate system	Least-squares collocation plus a multirate system	A MISO system plus a wavelet transform

Table 4.2 Combination of different methods for solving the multiresolution problem

## **4.2 SIGNAL DOMAIN APPROACHES COMBINING WAVELET TRANSFORMS AND LEAST-SQUARES COLLOCATION**

In this section, two specific estimation schemes in the signal domain ( fine-to-coarse and coarse-to-fine) will be discussed separately using a discrete wavelet transform and least-squares collocation. All procedures will be given for the 2D case since the proposed framework will be applied to gravity field modeling.

### **4.2.1 A Fine-to-Coarse Estimation Scheme**

To begin, some notations will be defined.  $x(m)$  denotes the estimate of  $x$  at scale  $m$  based on all measurements with resolution higher or equal to  $m$ .  $x(m+)$  denotes the estimate of  $x$  at scale  $m$  based on all measurements with resolution higher than  $m$ . Similar notations are used for other quantities.  $x_f(m)$  denotes the fused estimate of  $x$  at scale  $m$  based on all available measurements.

The fine-to-coarse estimation procedure starts with an upward or fine-to-coarse sweep, which propagates the measurement information, level by level, from the fine scale to the coarse scale, followed by a downward or coarse-to-fine sweep that propagates the measurement information downward. The fine-to-coarse sweep consists of a downsampling step from fine scale to coarse scale and a measurement update step, while

the coarse-to-fine sweep consists of a fusion step from coarse scale to fine scale. The upward and downward sweep steps are as follows:

### **Upward sweep or fine-to-coarse sweep**

There are three essential steps to this procedure:

- 1) Estimation of  $x(M)$  and the corresponding error covariance matrix at the finest scale.
- 2) Estimation of  $x((m-1)+)$  from  $x(m)$ .
- 3) Measurement update at scale  $m-1$ :

They will now be discussed one by one. The upward sweep starts with the estimation of  $x(m)$  and the corresponding error covariance matrices at the finest scale  $M$ . The mathematical model for estimating  $x(M)$  is

$$y_M = L_M(x(M)) + v_M = t_M + v_M, \quad (4.14)$$

where  $y_M$  is the measurement vector at the finest scale  $M$ , and  $L_M$  is the linear functional relating the finest scale measurements to the signal  $x(M)$ . The first and second moments of which are assumed to be known, i.e.

$$E(x(M)) = 0, \quad (4.15a)$$

$$E(x(M)x(M)^T) = C_{xx}(M). \quad (4.15b)$$

$v_M$  is the measurements noise vector at the finest scale, the first and second moments of which are assumed to be known, i.e.

$$E(v_M) = 0, \quad (4.16a)$$

$$E(v_M v_M^T) = C_{vv}(M). \quad (4.16b)$$

Equation (4.14) indicates that the measurements at the finest scale are involved in the estimation of  $x(M)$  at this stage.

The estimation of  $x(M)$  can be done using least-squares collocation solution (2.32) based on the minimum principle (2.31) in Chapter 2, i.e.

$$x(M) = C_{xt}(M)(C_{tt}(M) + C_{vv}(M))^{-1} y_M \quad (4.17)$$

with error covariance

$$C_\varepsilon(M) = C_{xx}(M) - C_{xt}(M)(C_{tt}(M) + C_{vv}(M))^{-1} C_{tx}(M), \quad (4.18)$$

where  $C_{tt}(M)$ ,  $C_{vv}(M)$  and  $C_{xx}(M)$  are the covariance matrix of  $t_M$ ,  $v_M$  and  $x(M)$ , respectively,  $C_{xt}(M)$  is the covariance matrix between  $x$  and  $t$  at the finest scale  $M$ , and  $C_\varepsilon(M)$  is the error covariance of estimate  $x(M)$ . Readers who are not familiar with the theory of collocation are referred to Moritz (1980) and Krakiwsky (1990) for details.

Since the objective of multiresolution approximation is to estimate a signal at multiple scales, the next step will be the prediction of the next coarse-scale signal using the information in Step 1). One way of doing this is to use a discrete wavelet transform because it provides a tool for linking a signal at two different scales together. One assumption made here is that a signal at different resolution can be represented using base functions in a multiresolution analysis. In this dissertation, the discrete wavelet transforms using orthonormal wavelets described in Section 3.4.2 will be used.

Suppose that  $x(m)$  and the corresponding error covariance matrixes  $C_{\varepsilon}(m)$  have been computed. The prediction  $x((m-1)+)$  can be done using the discrete wavelet transform (3.29a) described in Chapter 3, i.e.

$$x((m-1)+) = (H \otimes H) x(m) \quad (4.19)$$

with error covariance

$$C_{\varepsilon}((m-1)+) = (H \otimes H) C_{\varepsilon}(m) (H \otimes H)^T. \quad (4.20)$$

Equation (4.19) can be written as

$$x((m-1)+) = P_m x(m), \quad (4.21)$$

where,  $P_m = H \otimes H$  is the orthogonal projection operator from  $V_m$  to  $V_{m-1}$  in the multiresolution analysis:

$$P_m: V_m \rightarrow V_{m-1} . \quad (4.22)$$

Therefore Equation (4.18) can be interpreted geometrically as an orthogonal projection of  $x(m) \in V_m$  onto  $V_{m-1}$  by  $x((m-1)+) = P_m x(m)$ .

At the same time, the details added can also be computed using formulas (3.29b)-(3.29d), i.e.

$$d_1((m-1)+) = (G \otimes H) x(m), \quad (4.23a)$$

$$d_2((m-1)+) = (H \otimes G) x(m), \quad (4.23b)$$

$$d_3((m-1)+) = (G \otimes G) x(m). \quad (4.23c)$$

with error covariance matrix

$$C_{\varepsilon d_{m,1}} = (G \otimes H) C_{\varepsilon}(m) (G \otimes H)^T, \quad (4.24a)$$

$$C_{\varepsilon d_{m,2}} = (H \otimes G) C_{\varepsilon}(m) (H \otimes G)^T, \quad (4.24b)$$

$$C_{\varepsilon d_{m,3}} = (G \otimes G) C_{\varepsilon}(m) (G \otimes G)^T, \quad (4.24c)$$

where  $C_{\varepsilon d_{m,1}}$ ,  $C_{\varepsilon d_{m,2}}$  and  $C_{\varepsilon d_{m,3}}$  are the error covariance matrices of  $d_{m,1}$ ,  $d_{m,2}$  and  $d_{m,3}$ , respectively.

Equations (4.23) and (4.24) will be used in Step 2. Similarly, Equations (4.23a) to (4.23c) can also be interpreted geometrically as orthogonal projections of  $x^{(m)} \in V_m$  onto  $W_{m-1,1}$ ,  $W_{m-1,2}$  and  $W_{m-1,3}$ , respectively, in the multiresolution analysis.

The  $x^{((m-1)+)}$  from Step 2) can then be updated if the measurements at scale  $m-1$  are available. To this, the following mathematical models are used:

$$y_{(m-1)+} = x^{(m-1)} + \varepsilon_{(m-1)+}, \quad (4.25a)$$

$$y_{m-1} = L_{m-1}(x^{(m-1)}) + v_{m-1} = t_{m-1} + v_{m-1}, \quad (4.25b)$$

where,  $y_{(m-1)+} = x^{((m-1)+)}$ ,  $\varepsilon_{(m-1)+}$  is the prediction error of  $x^{((m-1)+)}$  from scale  $m$  to  $m-1$ ,  $y_{m-1}$  is the measurement vector at the finest scale  $m-1$ , and  $L_{m-1}$  is the linear functional relating measurements at scale  $m-1$  to the signal  $x^{(m-1)}$ .  $v_{m-1}$  is the measurements noise vector at scale  $m-1$ , the first and second moments of which are assumed to be known, i.e.

$$E(v_{m-1}) = 0, \quad (4.26a)$$

$$E(v_{m-1} v_m^T) = C_{vv}(m-1). \quad (4.26b)$$

Equation (4.25a) means that  $x((m-1)+)$  will be used as measurement in the measurement update step.

The following minimum principle is used for the estimation of  $x(m-1)$ :

$$x(m-1)^T C_x^{-1}(m-1)x(m-1) + \begin{bmatrix} \varepsilon_{m-1} \\ v_{m-1} \end{bmatrix}^T \begin{bmatrix} C_\varepsilon((m-1)) & C_{\varepsilon v}(m-1) \\ C_{v\varepsilon}(m-1) & C_{vv}(m-1) \end{bmatrix}^{-1} \begin{bmatrix} \varepsilon_{m-1} \\ v_{m-1} \end{bmatrix}$$

= **minimum**.

(4.27)

Since the measurement noise between different scales is assumed to be uncorrelated, it is easy to prove that  $\varepsilon_{(m-1)+}$  and  $v_{m-1}$  are also uncorrelated, i.e.  $C_{\varepsilon v}(m-1) = C_{v\varepsilon}(m-1) = 0$ .

Therefore, the minimum principle (4.27) can be written as

$$x(m-1)^T C_x^{-1}(m-1)x(m-1) + v_{m-1}^T C_{vv}^{-1}(m-1)v_{m-1} + \varepsilon_{m-1}^T C_\varepsilon^{-1}((m-1)+)\varepsilon_{m-1}$$

= **minimum**.

(4.28)

The following solution to Equation (4.25) can be derived based on the minimum criterion (4.28):

$$x(m-1) = A_{m-1}x((m-1)+) + K_{m-1}(y_{m-1} - B_{m-1}x((m-1)+)),$$

$$C_{x_{m-1}} = C_{xx}((m-1)+1) + C_\varepsilon((m-1)+1),$$

$$\begin{aligned}
A_{m-1} &= C_{xx}((m-1)+)C_{x_{m-1}}^{-1}, \\
K_{m-1} &= C_{m-1}\bar{C}_{m-1}^{-1}, \\
C_{m-1} &= C_{xt}((m-1)+) + C_{xt}((m-1)+)C_{x_{m-1}}^{-1}C_{xt}^T((m-1)+), \\
\bar{C}_{m-1} &= C_{tt}((m-1)+) + C_{vv}(m) + C_{xt}^T((m-1)+)C_{x_{m-1}}^{-1}C_{xt}((m-1)+), \\
B_{m-1} &= C_{xt}^T((m-1)+)C_{x_{m-1}}^{-1}, \\
C_{\varepsilon}((m-1)) &= C_{xx}((m-1)+) - C_{xx}((m-1)+)C_{x_{m-1}}^{-1}C_{xx}((m-1)+) \\
&\quad + \bar{C}_{x_{m-1}t_{m-1}}C_t^{-1}((m-1)+)\bar{C}_{x_{m-1}t_{m-1}}^{-T}, \\
\bar{C}_{x_{m-1}t_{m-1}} &= C_{x_{m-1}t_{m-1}} - C_{x_{m-1}x_{m-1}}C_{x_{m-1}}^{-1}C_{x_{m-1}t_{m-1}}.
\end{aligned}
\tag{4.29}$$

The derivation of (4.29) is the same as that of stepwise collocation in Moritz (1980) except that the downsampled signal is used as measurement. For a detailed comparison see Section 4.3. The above prediction and update procedures are repeated until the lowest scale 0 is reached. Steps 2) and 3) provide the mechanism for combining data from two different resolution levels for estimating the signal.

### **Downward sweep or coarse-to-fine sweep**

At the coarsest scale 0, the estimate of the signal based on all multiresolution data is obtained. However, it is necessary to reverse the procedure, i.e. to make a downward

sweep, if the estimates of the signal at other scales based on all available information are needed. The estimated signals at the coarsest scale provide the initialization of the downward sweep, which proceeds recursively. Assume that the estimate  $x_f(m)$  at a finer scale has been computed with the initialization at the finest scale. The estimates  $x_f(m+1)$  can be calculated by using the inverse discrete wavelet transform (3.31) in Chapter 3, i.e.

$$\begin{aligned} x_f(m+1) = & (H^* \otimes H^*) x_o(m) + (G^* \otimes H^*) d_{m,1} \\ & + (H^* \otimes G^*) d_{m,2} + (G^* \otimes G^*) d_{m,3} \\ (m = & 0, 1, 2, \dots, M). \end{aligned} \quad (4.30)$$

with the error covariance matrix

$$\begin{aligned} C_{\varepsilon_f}(m+1) = & (H^* \otimes H^*) C_{\varepsilon}(m) (H^* \otimes H^*)^T + (G^* \otimes H^*) C_{\varepsilon_{d_{m,1}}} (G^* \otimes H^*)^T \\ & + (H^* \otimes G^*) C_{\varepsilon_{d_{m,2}}} (H^* \otimes G^*)^T + (G^* \otimes G^*) C_{\varepsilon_{d_{m,3}}} (G^* \otimes G^*)^T. \end{aligned} \quad (4.31)$$

The downward sweep provides the mechanism for obtaining estimates at each and can be viewed as the synthesis of the signal at different scales in the multiresolution analysis.

#### 4.3.2 A Coarse-to-Fine Estimation Scheme

In the following, a coarse-to-fine estimation scheme for the solution of the multiresolution approximation problem will be described.

In this scheme,  $x(m^-)$  denotes the estimate of  $x$  at scale  $m$  based on all measurements with resolution lower than  $m$ . Similar notations are used for other quantities.  $x_f(m)$  denotes the optimal estimate of  $x$  at scale  $m$  based on all available measurements. Mathematical models and assumptions made will be the same as in the fine-to-coarse estimation scheme.

The coarse-to-fine estimation procedure starts with a downward or coarse-to-fine sweep, which propagates the measurement information, level by level, from the coarsest scale to the finest scale, followed by an upward or fine-to-coarse sweep that propagates measurement information upward. The coarse-to-fine sweep consists of a prediction or interpolation from coarse-scale to fine-scale and a measurement update step, while the fine-to-coarse sweep consists of a downsizing resolution step from the finest scale to the coarsest. The downward and upward sweep steps are detailed as follows:

#### **Downward sweep or coarse-to-fine sweep**

There are three essential steps to this procedure:

- 1) Estimation of  $x(0)$  and the corresponding error covariance matrix at the coarsest scale.
- 2): Estimation of  $x((m+1)^-)$  from  $x(m)$ .
- 3) Measurement update at scale  $m+1$ .

They will be now discussed in detail. The downward sweep starts with the estimation of  $x(0)$  and the corresponding error covariance matrix at the coarsest scale. The estimation of  $x(0)$  can be done using the least-squares collocation solution (2.32) based on the minimum principle (2.31) in Chapter 2, i.e.

$$x(0) = C_{xt}(0)(C_{tt}(0) + C_{vv}(0))^{-1} y_0 \quad (4.32a)$$

with error covariance

$$C_{\varepsilon}(0) = C_{xx}(0) - C_{xt}(0)(C_{tt}(0) + C_{vv}(0))^{-1} C_{tx}(0), \quad (4.32b)$$

where  $C_{tt}(0)$ ,  $C_{vv}(0)$  and  $C_{xx}(0)$  are the covariance matrix of  $t_0$ ,  $v_0$  and  $x(0)$ , respectively,  $C_{xt}(0)$  is the covariance matrix between  $x$  and  $t$  at the coarsest scale  $0$ , and  $C_{\varepsilon}(0)$  is the error covariance of estimate  $x(0)$ . Similarly as before, the integral method might also be employed if the type of measurements at the coarsest scale is the same, e.g., the geoidal height measurements derived from satellite altimetry.

Suppose that  $x(m)$  and the corresponding error covariance matrixes  $C_{\varepsilon}(m)$  have been computed, the updated estimates of the signal  $x(m)$  are then predicted down to the next finer scale according to the inverse wavelet transform (3.31) described in Chapter 3, i.e.

$$\begin{aligned}
x((m+1)-) &= (H^* \otimes H^*) x(m) + (G^* \otimes H^*) d_{m,1} \\
&+ (H^* \otimes G^*) d_{m,2} + (G^* \otimes G^*) d_{m,3}
\end{aligned} \tag{4.33a}$$

with the error covariance matrix

$$\begin{aligned}
C_{\varepsilon}((m+1)-) &= (H^* \otimes H^*)^T C_{\varepsilon}(m) (H^* \otimes H^*) + (G^* \otimes H^*)^T C_{\varepsilon d_{m,1}} (G^* \otimes H^*) \\
&+ (H^* \otimes G^*)^T C_{\varepsilon d_{m,2}} (H^* \otimes G^*) + (G^* \otimes G^*)^T C_{\varepsilon d_{m,3}} (G^* \otimes G^*).
\end{aligned} \tag{4.33b}$$

where  $d_{m,1}$ ,  $d_{m,2}$  and  $d_{m,3}$  are set to 0 due to the fact that detailed information is not available at this point.  $C_{\varepsilon d_{m,1}}$ ,  $C_{\varepsilon d_{m,2}}$  and  $C_{\varepsilon d_{m,3}}$  are the error covariance matrices of  $d_{m,1}$ ,  $d_{m,2}$  and  $d_{m,3}$ , the elements of diagonals of which are set to be larger enough since there is no any information regarding  $d_{m,1}$ ,  $d_{m,2}$  and  $d_{m,3}$ .

The  $x((m+1)-)$  from Step 2 can then be updated if the measurements at scale  $m+1$  are available. To this, the following mathematical models are used:

$$y_{(m+1)-} = x(m+1) + \varepsilon_{(m+1)-}, \tag{4.34a}$$

$$y_{m+1} = L_{m+1}(x(m+1)) + v_{m+1} = t_{m+1} + v_{m+1}, \tag{4.34b}$$

where,  $y_{(m+1)-} = x((m+1)-)$ ,  $\varepsilon_{(m+1)-}$  is the prediction error of  $x((m-1)+)$  from scale  $m$  to  $m+1$ ,  $y_{m+1}$  is the measurement vector at scale  $m+1$ , and  $L_{m+1}$  is the linear functional

relating measurements at scale  $m+1$  to the signal  $x(m+1)$ .  $v_{m+1}$  is the measurements noise vector at scale  $m+1$ , the first and second moments of which are assumed to be known, i.e.

$$E(v_{m-1}) = 0, \quad (4.35a)$$

$$E(v_{m-1} v_m^T) = C_{vv}(m-1). \quad (4.35b)$$

The following minimum principle for estimating  $x(m+1)$  is used:

$$\begin{aligned} & x(m+1)^T C_x^{-1}(m+1)x(m+1) + v_{m-1}^T C_{vv}^{-1}(m+1)v_{m-1} + \varepsilon_{m+1}^T C_\varepsilon^{-1}((m+1)-)\varepsilon_{m+1} \\ & = \text{minimum}. \end{aligned} \quad (4.36)$$

The following solution to Equation (4.34) can be derived based on the minimum criterion (4.26):

$$x(m+1) = A_{m+1}x((m+1)-) + K_{m+1}(y_{m+1} - B_{m+1}x((m+1)-)),$$

$$C_{x_{m+1}} = C_{xx}((m+1)-) + C_\varepsilon((m+1)-),$$

$$B_{m+1} = C_{xx}((m+1)-)C_{x_{m+1}}^{-1},$$

$$K_{m+1} = C_{m+1} \bar{C}_{m+1}^{-1},$$

$$C_{m+1} = C_{xt}((m+1)-) + C_{xt}((m+1)-)C_{x_{m+1}}^{-1} C_{xt}^T((m+1)-),$$

$$\bar{C}_{m+1} = C_{tt}((m+1)+) + C_{vv}(m) + C_{xt}^T((m+1)-)C_{x_{m-1}}^{-1}C_{xt}((m+1)-),$$

$$A_{m+1} = C_{xt}^T((m+1)-)C_{x_{m+1}}^{-1},$$

$$C_{\varepsilon}(m+1) = C_{xx}((m+1)-) - C_{xx}((m+1)-)C_{x_{m+1}}^{-1}C_{xx}((m+1)-) +$$

$$\bar{C}_{x_{m+1}t_{m+1}} C_t^{-1}((m+1)-) \bar{C}_{x_{m+1}t_{m+1}}^{-T},$$

$$\bar{C}_{x_{m+1}t_{m+1}} = C_{x_{m+1}t_{m+1}} - C_{x_{m+1}x_{m+1}} C_{x_{m+1}}^{-1} C_{x_{m+1}t_{m+1}}.$$

(4.37)

The above update and prediction procedures are repeated until the finest scale  $M$  is reached.

### Upward sweep or fine-to-coarse sweep

At the finest scale, the estimate of the signal based on all multiresolution data is obtained. However, it is necessary to reverse the procedure, i.e. do an upward sweep, if the estimates of the signals at coarser scales based on all multiresolution data available are needed. The estimated signals at the finest scale provide the initialization of the upward sweep. This step also proceeds recursively. Assume that the estimate  $x_f(m)$  at a finer scale has been computed with the initialization at the finest scale. The estimates  $x_f(m-1)$  can be calculated using the wavelet transform (3.29a) in Chapter 3:

$$x((m-1)+) = (H^* \otimes H^*) x(m) \quad (4.38a)$$

with the error covariance

$$C_{\varepsilon_0}((m-1)+) = (H^* \otimes H^*)^T C_{\varepsilon_0}(m) (H^* \otimes H^*). \quad (438b)$$

Equation (4.38) provide the formulas for estimating the signal and the corresponding error covariance matrix at the coarse scales.

From the above derivations, it can be seen that both fine-to-coarse estimation and coarse-to-fine estimation use the same information from data at multiple scales. The major difference between them is the way they are implemented. When a signal is only required at the coarsest scale, the use of the fine-to-coarse estimation scheme is more efficient since there is no need to perform the coarse-to-fine sweep. On the other hand, if a signal is only required at the finest scale, the use of the coarse-to-fine scheme is more efficient since there is no need to perform the fine-to-coarse sweep.

The main advantage of these approaches is that they allow not only solutions of the problem at multiple resolutions but also the fusion of measurements at multiple resolutions, which will be demonstrated in Chapter 5.

### **4.3 A MEASUREMENT DOMAIN APPROACH COMBINING A MULTIRATE SYSTEM AND A MISO SYSTEM**

In this section, a specific algorithm for measurement domain approach is proposed using a multirate system and a MISO system.

To simplify the discussion, the derivation will be done for signals and measurements at two different resolutions assuming that the sampling rate difference between them is 2. A similar procedure can be applied to other cases. The assumption in this section is that both the input signals and their errors are stochastic variables with known power spectral densities.

The measurement domain approach combining a multirate system and a MISO system consists of the following two steps:

- 1) Decimation ( or interpolation ) of measurements at fine scale ( or coarse scale ) by a factor 2 using a multirate system.
- 2) Estimation of the signal at coarse scale ( or fine scale ) using the double-input single-output system based on measurements at coarse scale ( or fine scale ) and decimated ( or interpolated ) measurements

These two steps will now be discussed in detail. The measurement domain approach starts with decimation of the fine-scale measurements  $y_1$  by using a decimation filter (3.51a), i.e.

$$y_{D0} = H_D y_1, \quad (4.39a)$$

where  $H_D$  is the 2D decimation filter coefficients matrix and  $y_{D0}$  is the decimated output. At the same time, the error covariance matrix after decimation can be computed by standard error propagation procedures by assuming that the covariance matrices of noise in  $y_1$  is known, i.e.

$$C_{v_{D0}v_{D0}} = H_D C_{v_1v_1} H_D^T, \quad (4.39b)$$

where  $C_{v_1v_1}$  and  $C_{v_{D0}v_{D0}}$  are the covariance matrices of noise in  $y_1$  and  $y_{D0}$ , respectively. In the frequency domain, Equation (4.39) takes the following form

$$Y_{D0}(\omega) = \frac{1}{2} [H_D(\frac{\omega}{2}) Y_1(\frac{\omega}{2}) + H_D(\frac{\omega}{2} - \pi) Y_1(\frac{\omega}{2} - \pi)], \quad (4.40a)$$

and

$$P_{v_{y_{D0}}}(\omega) = \frac{1}{4} [ |H_D(\frac{\omega}{2})|^2 P_{v_{y_1}}(\frac{\omega}{2}) + |H_D(\frac{\omega}{2} - \pi)|^2 P_{v_{y_1}}(\frac{\omega}{2})(\frac{\omega}{2} - \pi) ], \quad (4.40b)$$

where  $\omega = [u, v]$  is the 2D circular frequency.  $H_D(\omega)$  is the frequency response of the 2D decimation filter.  $Y_1$  is the Fourier transform of  $y_1$ .  $Y_{D0}$  is the frequency representation of  $y_{D0}$ .  $P_{vy_1}(\omega)$  and  $P_{vy_{D0}}(\omega)$  are the power spectral densities of noise in  $y_1$  and  $y_{D0}$ , respectively. The derivation of Equation (4.40a) can be found in e.g. (Crochiere and Rabiner, 1981). The second term in Equation (4.40a) is due to the aliasing effect. If the decimation filter  $H_D(\omega)$  is close to the ideal half band lowpass filter, the second term in Equation (4.40a) can be neglected. In this case, Equation (4.40) can be simplified, i.e.

$$Y_{D0}(\omega) = \frac{1}{2} H_D\left(\frac{\omega}{2}\right) Y_1\left(\frac{\omega}{2}\right), \quad (4.41a)$$

and

$$P_{vy_{D0}}(\omega) = \frac{1}{4} |H_D\left(\frac{\omega}{2}\right)|^2 P_{vy_1}\left(\frac{\omega}{2}\right). \quad (4.41b)$$

After finishing the above measurement decimation procedure, the next step will be the estimation of the signal at coarse scale based on the coarse-scale measurements  $y_0$  and the decimated measurements  $y_{D0}$ . This can be done by using the double-input single-output system, in which the coarse-scale measurements  $y_0$  and the decimated measurements  $y_{D0}$  are the two inputs and the signal to be estimated at coarse scale is the output. The mathematical model to be used in this case is

$$X_0(\omega) = H_1(\omega)Y_0(\omega) + H_2(\omega)Y_{D0}(\omega) + E_0(\omega), \quad (4.42)$$

where  $H_1(\omega)$  and  $H_2(\omega)$  are the frequency responses to be estimated, and  $E_0(\omega)$  is the noise of the estimated signal at coarse scale expressed in frequency domain. To determine  $H_1(\omega)$  and  $H_2(\omega)$ , the following minimum criterion

$$|P_{e_{x_0}}(\omega)| = |X_0(\omega) - H_1(\omega)Y_0(\omega) + H_2(\omega)Y_{D0}(\omega)|^2 = \text{minimum} \quad (4.43)$$

is used, where  $P_{e_{x_0}}(\omega)$  is the power spectral density of the output noise. Therefore, the following estimate of the signal  $x_0$  at coarse scale in the frequency domain and the corresponding error power spectral density can be obtained using Equations (2.48) and (2.49) in Section 2.5, i.e.

$$\hat{X}_0(\omega) = \hat{H}_1(\omega)Y_0(\omega) + \hat{H}_2(\omega)Y_{D0}(\omega), \quad (4.44a)$$

$$P_{e_{\hat{x}_0}} = P_{x_0} - |\hat{H}_1(\omega)|^2 P_{y_0} - 2\hat{H}_1^*(\omega)\hat{H}_2(\omega)P_{y_0y_{D0}} - |\hat{H}_2(\omega)|^2 P_{y_{D0}}, \quad (4.44b)$$

where

$$\hat{H}_1(\omega) = \frac{P_{x_0y_0}(\omega)}{P_{y_0}(\omega)} \frac{1}{1 + \frac{P_{vy_0}(\omega)P_{y_{D0}}(\omega) + P_{vy_{D0}}(\omega)}{P_{y_0}(\omega)P_{vy_{D0}}(\omega)}}, \quad (4.45a)$$

$$\hat{H}_2(\omega) = \frac{P_{x_0 y_{D0}}(\omega)}{P_{y_{D0}}(\omega)} \frac{1}{1 + \frac{P_{v_{yD0}}(\omega) P_{y_0}(\omega) + P_{v_{y_0}}(\omega)}{P_{y_{D0}}(\omega) P_{v_{y_0}}(\omega)}}, \quad (4.45b)$$

where  $P_x$  is the power spectral density of  $x$ .  $P_{xy}$  is the cross-spectral density of  $x$  and  $y$ .

After  $\hat{X}_0(\omega)$  and  $P_{e_{\hat{x}_0}}$  have been computed, the estimates of the signal and the corresponding error covariance matrix at coarse scale can be obtained by using the inverse FFT method.

Similarly, interpolated measurements at fine scale from the coarse-scale measurements  $y_0$  can be obtained by using an interpolation filter (3.51b), i.e.

$$y_{II} = H_I y_0, \quad (4.46a)$$

where  $H_I$  is the 2D interpolation filter coefficients matrix and  $y_{II}$  is the interpolated measurements. At the same time, the error covariance matrix due to interpolation can be computed by the error propagation assuming the covariance matrices of noise in  $y_0$  is known, i.e.

$$C_{v_{II}v_{II}} = H_D C_{v_0v_0} H_D^T, \quad (4.46b)$$

where  $C_{v_0v_0}$  and  $C_{v_{II}v_{II}}$  are the covariance matrices of noise in  $y_0$  and  $y_{II}$ .

Equation (4.46) can also be written in the frequency domain (Crochiere and Rabiner, 1981), i.e.

$$Y_{II}(\omega) = H_I(\omega) Y_0(2\omega), \quad (4.47a)$$

and

$$P_{vy_{II}}(\omega) = |H_I(\omega)|^2 P_{vy_0}(2\omega), \quad (4.47b)$$

where  $H_I(\omega)$  is the frequency response of the 2D interpolation filter.  $Y_0(\omega)$  is the Fourier transform of  $y_0$ .  $Y_{II}(\omega)$  is the frequency representation of  $y_{II}$ .  $P_{vy_0}(\omega)$  and  $P_{vy_{II}}(\omega)$  are the power spectral densities of the noise in  $y_0$  and  $y_{II}$ , respectively.

After finishing the above measurement interpolation procedure, the next step is the estimation of the signal at fine scale based on fine-scale measurements  $y_1$  and the interpolated measurements  $y_{II}$ . This can also be done by using the double-input single-output system, in which the fine-scale measurements  $y_1$  and the interpolated measurements  $y_{II}$  are the two inputs and the signal to be estimated at fine scale is the output. The mathematical model and the minimum criterion used in this case is the same as Equations (4.42) and (4.43), respectively, except that two inputs are  $y_1$  and  $y_{II}$  not  $y_0$  and  $y_{D0}$ . Therefore, formulas similar to Equations (4.44) and (4.45) can be obtained for

estimating the signal  $x_1$  at fine scale in frequency domain and the corresponding error power spectral density, i.e.

$$\hat{X}_1(\omega) = \hat{H}_1(\omega)Y_1(\omega) + \hat{H}_2(\omega)Y_{II}(\omega), \quad (4.48a)$$

$$P_{v_{\hat{x}_1}} = P_{x_1} - |\hat{H}_1(\omega)|^2 P_{y_1} - 2\hat{H}_1^*(\omega)\hat{H}_2(\omega)P_{y_1 y_{II}} - |\hat{H}_2(\omega)|^2 P_{y_{II}}, \quad (4.48b)$$

where

$$\hat{H}_1(\omega) = \frac{P_{x_1 y_1}(\omega)}{P_{y_1}(\omega)} \frac{1}{1 + \frac{P_{v_{y_1}}(\omega) P_{y_{II}}(\omega) + P_{v_{y_{II}}}(\omega)}{P_{y_1}(\omega) P_{v_{y_{II}}}(\omega)}}, \quad (4.49a)$$

$$\hat{H}_2(\omega) = \frac{P_{x_1 y_{II}}(\omega)}{P_{y_{II}}(\omega)} \frac{1}{1 + \frac{P_{v_{y_{II}}}(\omega) P_{y_1}(\omega) + P_{v_{y_1}}(\omega)}{P_{y_{II}}(\omega) P_{v_{y_1}}(\omega)}}. \quad (4.49b)$$

After  $\hat{X}_1(\omega)$  and  $P_{v_{\hat{x}_1}}$  have been computed, the estimates of the signal and the corresponding error covariance matrix at fine scale can be obtained by using the inverse FFT method.

#### 4.4 COMPARISONS BETWEEN THE PROPOSED ALGORITHMS AND STEPWISE LEAST-SQUARES COLLOCATION

In this section, the similarities and differences between the algorithms described in the previous section and stepwise least-squares collocation (LSC) will be analyzed by

examining the assumptions, the mathematical models, the minimum criteria and the solutions of both methods. The advantages and disadvantages of the proposed method when compared to stepwise LSC for solving multiresolution approximation problems will then be addressed. This will similarly apply to structural similarities between proposed algorithms and those of Kalman filtering, which for the purpose of this discussion can be viewed as a form of stepwise least-squares collocation (Moritz, 1980).

To make the comparisons more clear, only measurements at two resolution levels and estimates of a signal at these two scales will be used. Also, only the fine-to-coarse estimation scheme will be compared to stepwise LSC. For analysis in other cases, the same procedure can be followed.

Table 4.3 summarizes the assumptions, the mathematical models, the minimum criteria and solutions in both methods. The second column lists all assumptions made in both methods. Listed in the third column are the mathematical models used in both methods. The fourth column shows the minimum criteria for both methods. The fifth column gives the solution for each method. The similarities and differences of the two methods will now be discussed column by column.

### **Assumptions**

The assumptions for both methods are quite similar in the sense that both methods assume that the first and second moments of both the signal and measurement noise at

Method	Assumptions	Mathematical Models	Minimum Criteria	Solutions
Stepwise LSC	$E(x(m))=0$ $E(x(m)x(m)^T) = C_{xx}(m)$ $E(v(m))=0$ $E(v(m)v(m)^T) = C_{vv}(m)$ $E(x_m v_m^T) = 0$ $(m = 0, 1)$ $E(v_0 v_1^T) = C_{v_0 v_1}$ $E(x(0)x(1)^T) = C_{x(0)x(1)}$	$y_m = L_m(x(m)) + v_m$ $(m = 0, 1)$	$x = \begin{bmatrix} x(0) \\ x(1) \end{bmatrix}$ $v = \begin{bmatrix} v_0 \\ v_1 \end{bmatrix}$ $C_x = \begin{bmatrix} C_{xx}(0) & C_{x_0 x_1} \\ C_{xx}^T & C_{xx}(1) \end{bmatrix}$ $C_v = \begin{bmatrix} C_{v_0 v_1} & C_{v_0 v_1} \\ C_{v_0 v_1}^T & C_{v_0 v_1}(1) \end{bmatrix}$ $x^T C_x^{-1} x + v^T C_v^{-1} v = \min$	$x(1) = C_{x1}(1)(C_{u}(1) + C_{vv}(1))^{-1} y_1$ $x(0) = C_{x1}(0)(C_{u}(1) + C_{vv}(1))^{-1} y_1$ $x_f(0) = x(0) + K_1(y_0 - A_1 y_1)$ $x_f(1) = x(1) + K_2(y_0 - A_1 y_1)$
Fine-to-coarse estimation	$E(x(m))=0$ $E(x(m)x(m)^T) = C_{xx}(m)$ $E(v(m))=0$ $E(v_m v_m^T) = C_{vv}(m)$ $E(x_m v_m^T) = 0$ $(m = 0, 1)$ $E(v_0 v_1^T) = 0$ Signal at different resolutions can be represented using a multiresolution analysis	$y_m = L_m(x(m)) + v_m$ $(m = 0, 1)$ $x(0) = (H \otimes H)x(1)$ $d_{i,1}(0) = (H \otimes G)x(1)$ $d_{i,2}(0) = (G \otimes H)x(1)$ $d_{i,3}(0) = (G \otimes G)x(1)$ $x(1) = (H^* \otimes H^*)x(0) + (H^* \otimes G^*)d_{i,1}(0) + (G^* \otimes H^*)d_{i,2}(0) + (G^* \otimes G^*)d_{i,3}(0)$	$x(1)^T C_{xx}^{-1}(1)x(1) + v_1^T C_{vv}^{-1}(1)v_1 = \min$ $x(0)^T C_x^{-1}(0)x(0) + v_0^T C_{vv}^{-1}(0)v_0 + \epsilon_0^T C_{\epsilon}^{-1}(0+\epsilon_0) = \min$	$x(1) = C_{x1}(1)(C_{u}(1) + C_{vv}(1))^{-1} y_1$ $x(0+) = (H \otimes H)x(1)$ $x(0) = A_0 x(0+) + K_0(y_0 - B_0 x(0+))$ $x_f(0) = x(0)$ $x_f(1) = (H^* \otimes H^*)x_f(0) + (H^* \otimes G^*)d_{i,1}(0) + (G^* \otimes H^*)d_{i,2}(0) + (G^* \otimes G^*)d_{i,3}(0)$ $d_{i,1}(0) = (H \otimes G)x(1)$ $d_{i,2}(0) = (G \otimes H)x(1)$ $d_{i,3}(0) = (G \otimes G)x(1)$

Table 4.3 Summaries of the fine-to-coarse estimation scheme and the stepwise LSC

two different resolutions are known. It is assumed that there is no correlation between the signal and measurement noise. The correlation between measurement noise at two different resolution is also assumed to be known. In the proposed method, measurement noise at two different resolution is assumed to be uncorrelated. This assumption is usually valid since the measurements at two different resolutions are obtained from different sources or different technologies.

In spite of these similarities, there is a fundamental difference in the assumptions. It is the way in which the signal at two different resolutions is linked. In stepwise LSC, the signal at two different resolution is linked through the correlation of the signals and measurements at two different resolutions. Therefore the cross-covariance matrices  $C_{x(0)y1}$ ,  $C_{x(1)y0}$  and  $C_{y0y1}$  have to be known. These matrices are usually calculated by an analytical covariance function. Since this covariance function is only a function of distance between two points, theoretically it cannot be used to compute the correlation between signals with different resolution. In the proposed method, the signal at two different resolution is treated in a different way. Instead of considering the correlation between the signal at the different resolution, the signal at each resolution scale  $m$  is assumed to be a function belonging to the function space  $V_m$  in a multiresolution analysis. This means that the signal at each resolution can be represented by using the base functions corresponding to this multiresolution analysis. In this way, the signal at two different resolutions can be related through the wavelet transform which corresponds

to this multiresolution analysis. Therefore the computation of the cross-covariance matrices  $C_{x(0)y1}$ ,  $C_{x(1)y0}$  and  $C_{y0y1}$  is not necessary.

### **Mathematical Models**

The mathematical model used in both methods is almost the same, except for the difference in linking the estimates at two different scales. This is due to the assumptions made in each case.

### **Minimum Criteria**

The minimum criteria used in both method are also quite similar in structure, i.e. both methods use the quadratic forms. However the meaning is different.

In stepwise LSC, only one quadratic form is used for the minimization through the whole stepwise LSC procedure. The estimates of the signal at two different resolutions from stepwise LSC are therefore optimal if the auto-covariance and cross-covariance matrices of the signal and measurement noise in the quadratic form can be correctly computed. This is usually not the case. Covariance models are derived from empirical data and are simply estimates. In addition, the cross-covariance matrix of the signal at two different resolutions cannot be correctly calculated. The optimality of the solution in this case is not valid.

In the proposed method, two quadratic forms are used. Each minimum criterion is only valid at its resolution level. For example, the minimum principle

$$\mathbf{x}(1)^T \mathbf{C}_{\mathbf{x}\mathbf{x}}^{-1}(1)\mathbf{x}(1) + \mathbf{v}_1^T \mathbf{C}_{\mathbf{v}\mathbf{v}}^{-1}(1)\mathbf{v}_1 = \text{minimum}$$

is only applicable to the fine-scale measurement. Therefore these two criteria can be considered as local minimization criteria when compared to that of stepwise least-squares collocation. In the fine-to-coarse estimation scheme, the improvement of the coarse estimate is achieved by optimally combining the coarse-scale measurement and the predicted estimate from the fine-scale, while the improvement on the fine-scale estimate is obtained through the coarse-to-fine sweep procedure by using the inverse wavelet transform. The improved estimate at the coarse-scale will contribute to improvement of the fine-scale estimate in the low frequency part.

### **Solutions**

Some formulas in both methods are either the same or very similar. For example, the formula for estimating  $\mathbf{x}(1)$  is the same in both methods since the least-squares collocation solution is used for both cases. Also, the formula for estimating  $\mathbf{x}_f(0)$  is similar in form.

The major difference between the two solutions is the way in which they connect the signal between resolutions. In stepwise LSC, the link between two resolutions is through the cross-covariance matrices  $C_{12}$ ,  $C_1(0)$ ,  $C_2(0)$ ,  $C_1(1)$  and  $C_2(1)$ , as shown in the formulas for estimating  $x(0)$ ,  $x_f(0)$  and  $x_f(1)$ . However, in the proposed method, it is done by using the wavelet transform, as indicated in the corresponding formulas for estimating  $x(0)$  and  $x_f(1)$ .

As far as computation efficiency is concerned, the proposed method is more efficient than stepwise LSC, as will be explained in the following. Assuming that the total number of measurements  $y_1$  and  $y_2$  is  $2N \times 2N$  and  $N \times N$ , respectively, and the number of estimates of the signal at fine scale and coarse scale is also  $2N \times 2N$  and  $N \times N$ , respectively. Let's compare the number of operations needed to compute  $x(1)$ ,  $x(0)$  ( or  $x(0+)$  ),  $x_f(1)$  and  $x_f(0)$  in the stepwise LSC solution and the proposed solution one by one.

The number of operations for the computation of  $x(1)$  for both methods is the same, as can be seen from the formulas for computing  $x(1)$  in each solution. To calculate  $x(0)$  using the stepwise LSC solution, the number of multiplication and addition operations would be  $N^2 \times (2N)^2$  and  $N^2 \times (2N-1)^2$  assuming  $(C_{tt}(1) + C_{vv}(1))^{-1} y_1$  has been known after computing  $x(1)$ . This is proportional to  $N^4$ . However, the number of multiplication and addition operations to compute  $x(0+)$  using a fast wavelet transform is

only proportional to  $(2N)^2 \times (2N)^2 = 4N^2$  (Beylkin et al, 1991). The number of operations for computing  $x_f(0)$  using stepwise LSC will be much more than that using the proposed approach since the operations on matrices of order  $2N \times 2N$  are needed for the former, while only the operations on matrices of order  $N \times N$  are needed for the latter. This can be seen by comparing (2.36) and (2.38) with (4.29). It is worthwhile to mention that the computation of  $x_f(0)$  in the proposed method can be done by FFT, as indicated in the previous section. But it is impossible to use FFT in stepwise LSC because the sampling rate of the measurements at two different resolutions is different. Therefore, the number of operations for computing  $x_f(0)$  using stepwise LSC will be far more than that using the proposed approach in this case. The number of operations for computing  $x_f(1)$  using stepwise LSC solution will also be much more than in the proposed method since the computation of  $x_f(1)$  in the proposed method is done by an inverse discrete transform, in which the number of operations needed is only proportional to  $2N \times 2N$ .

Therefore the proposed method is more efficient than stepwise LSC solution. Furthermore, the efficiency of the proposed method will increase with the number of resolution levels when compared to that of the stepwise LSC solution. Since the estimates of the signal at multiple resolutions, say 4, are to be calculated from the measurements at multiple resolutions, they have to be updated at each resolution level when using stepwise LSC. This means that the estimate at each resolution level has to be updated four times in this case. However, they are only needed to be estimated twice in the proposed method, no matter how many resolution levels there are.

From the above comparisons between both methods, it can be seen that the main computational advantage of the proposed method over the stepwise LSC method is that it avoids the computation of the cross-covariance matrices of the signals at different resolution levels and provides a more efficient way for solving multiresolution approximation problems. A disadvantage of the proposed methods is that the solution is not globally optimal since it depends on the choice of wavelets. On the other hand, the optimality of stepwise LSC cannot be achieved in practice because of the empirical nature of the covariance function.

## **CHAPTER 5**

### **NUMERICAL RESULTS AND ANALYSIS**

In this chapter, the procedure for generating multiresolution data is described and the software developed for this research is briefly introduced. Two examples are then given on how the general framework developed in Chapter 4 can be applied. The effect of using different wavelets is investigated. A numerical comparison between the wavelet-based signal domain method and the multirate-based measurement domain method is also performed.

#### **5.1 TEST DATA AND SOFTWARE**

##### **5.1.1 Multiresolution Data**

To demonstrate the correctness of the general method and algorithms developed in Chapter 4, multiresolution data are needed. Due to the lack of actual airborne gravity data, the multiresolution data used in the following tests were simulated by using Faye gravity anomaly data with a resolution of  $5' \times 5'$  in the area of British Columbia. This data was obtained from the Geodetic Survey of Canada. The extent of the area is

$$50^\circ \leq \phi \leq 60^\circ,$$
$$250^\circ \leq \lambda \leq 260^\circ.$$

Figure 5.1 shows the 3D plot of the data.

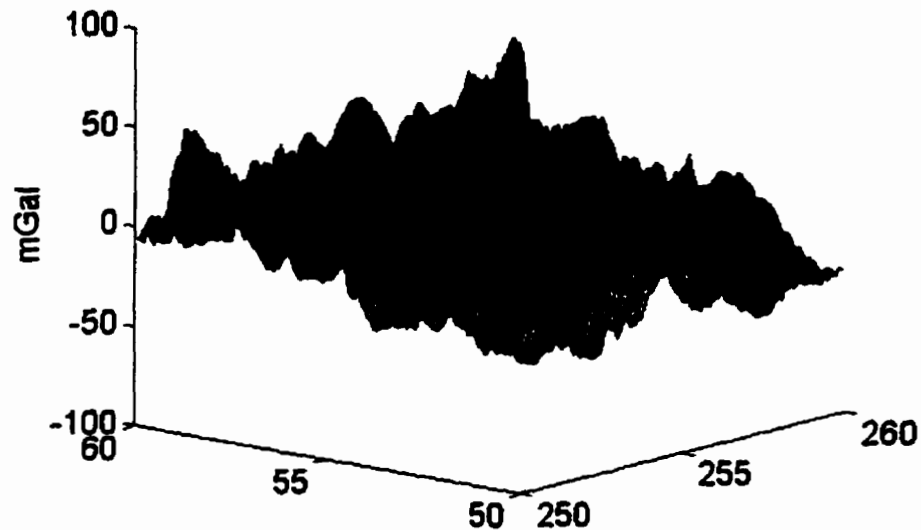


Figure 5.1 3D plot of gravity anomalies

To cover a range of possible applications, data were simulated at two levels and for two functionals of the disturbing gravity potential. Gravity disturbance were used at ground level and at a flying altitude of 1 km above ground. In addition, geoidal heights were also simulated. In the following, a procedure for simulating these data are described, in which planar approximation is adopted:

First,  $5' \times 5'$  grid geoidal height data are computed using the following discrete planar Stokes' formula:

$$N(x, y) = \frac{\Delta x \Delta y}{2\pi\gamma} \sum_{i=1}^M \sum_{j=1}^N \Delta g(x_i, y_j) \frac{1}{\sqrt{(x_i - x)^2 + (y_j - y)^2}}. \quad (5.1)$$

5' × 5' gravity disturbances at flight level  $h$  are calculated by using the following formula:

$$\delta g(x, y, h) = \frac{\Delta x \Delta y}{2\pi} \sum_{i=1}^M \sum_{j=1}^N \Delta g(x_i, y_j) \frac{h}{[(x_i - x)^2 + (y_j - y)^2 + h^2]^{3/2}}. \quad (5.2)$$

These data together with the original 5' × 5' gravity anomaly data are used as the true fine-scale data. The noise of airborne gravity disturbance caused by the INS and GPS sensors can be represented by the following error power spectral density model:

$$S_{\varepsilon\varepsilon} = S_{\varepsilon_{\text{INS}}} + S_{s_{\text{GPS}}}, \quad (5.3)$$

where,  $S_{\varepsilon_{\text{INS}}}$  is the INS error power spectral density and  $S_{s_{\text{GPS}}}$  is the GPS error power spectral density.

The error power spectral density model for INS used in this dissertation has been taken from Schwarz et al (1994), i.e.

$$S_{\varepsilon\varepsilon} = \frac{2\beta_a}{\omega^2 + \beta_a^2} \sigma_a^2 + Q_a, \quad (5.4)$$

where  $\sigma_a^2$  is the variance of vertical accelerometer noise,  $Q_a$  is the PSD of the white noise variance, and  $\beta_a$  is the correlation length.

The power spectral density of the error model for GPS has been proposed by Wei and Schwarz (1994), i.e.

$$S_{\epsilon_{GPS}} = \omega^4 \frac{2\beta_c}{\omega^2 + \beta_c^2} \sigma_c^2 + Q_w, \quad (5.5)$$

where  $\sigma_c^2$  is the variance of the colored noise,  $\beta_c$  is the correlation length of the noise, and  $Q_w$  is the PSD of the white noise variance. The noise generated by the models (5.4) and (5.5) is added to the simulated airborne gravity disturbance data to simulate the fine-scale measurements.

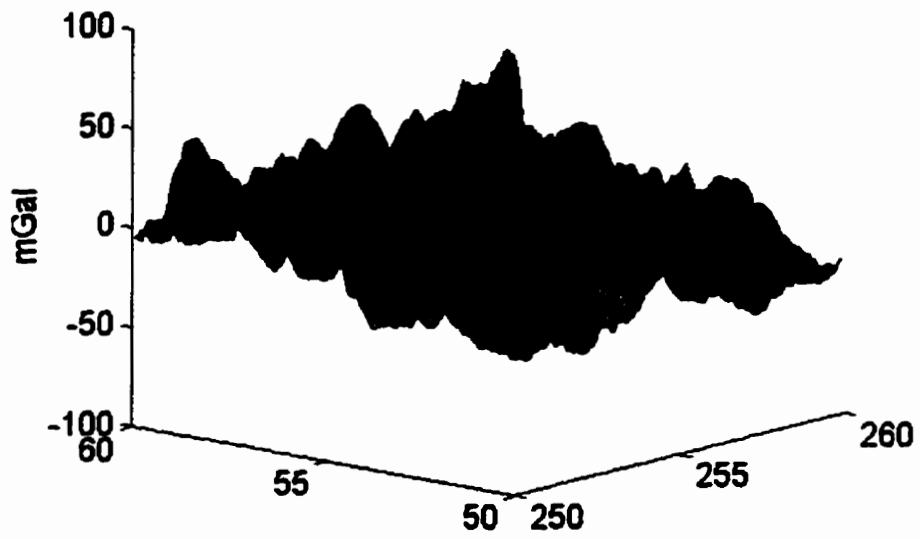
Second, a wavelet transform is applied to the true fine-scale data, to generate the  $10' \times 10'$  true coarse-scale data. White noise is added to the geoidal height and terrestrial gravity disturbance to simulate the coarse-scale measurements. Although a white noise error model oversimplifies the actual situation, empirical noise models are not readily available for this case.

Figures 5.2(a), 5.3(a), and 5.4(a) show the fine-scale airborne gravity disturbance at 1000 m flight height, coarse-scale geoidal height at ground level and coarse-scale terrestrial gravity disturbance, respectively. Figures 5.2(b), 5.3(b) and 5.4(b) show the corresponding measurements, respectively. Table 5.1 gives the statistics of the measurement noise of the fine-scale airborne gravity disturbances, the coarse-scale geoidal heights and the coarse-scale terrestrial gravity disturbances.

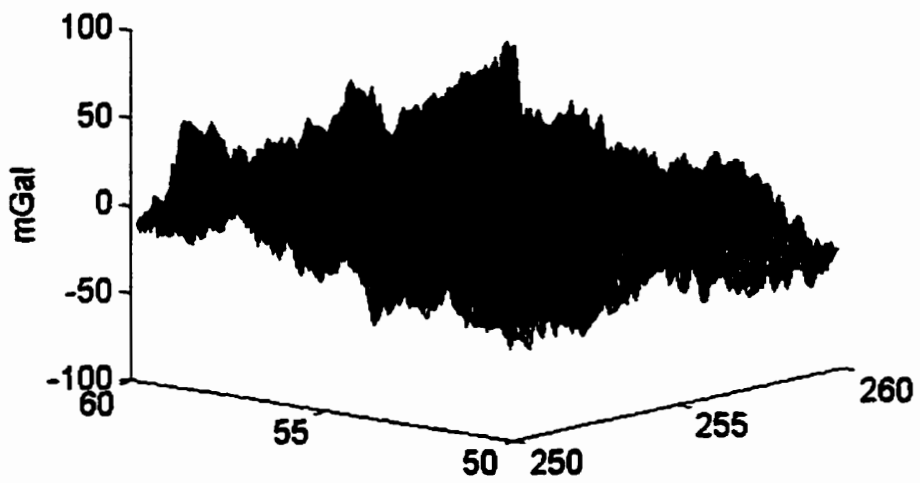
Measurement noise	Max	Min	Mean	Std	RMS	S/N ratio
Fine-scale airborne gravity disturbance (mGal)	18.7	-18.0	0.0	5.0	5.0	3.2
Coarse-scale geoidal height (cm)	35.6	-38.8	0.0	9.9	9.9	13.7
Coarse-scale gravity disturbance (mGal)	10.0	-10.3	0.0	3.0	3.0	5.0

Table 5.1 Statistics of Measurement Noise

Listed in the six columns of Table 5.1 are the maxima, minima, means, standard deviations (Std) and root mean squares (RMS) of the measurement noise, and the signal-to-noise (S/N) ratio. Given in the row headings are airborne gravity disturbance measurements at fine scale, coarse-scale geoidal height measurements and coarse-scale terrestrial gravity disturbance measurements.

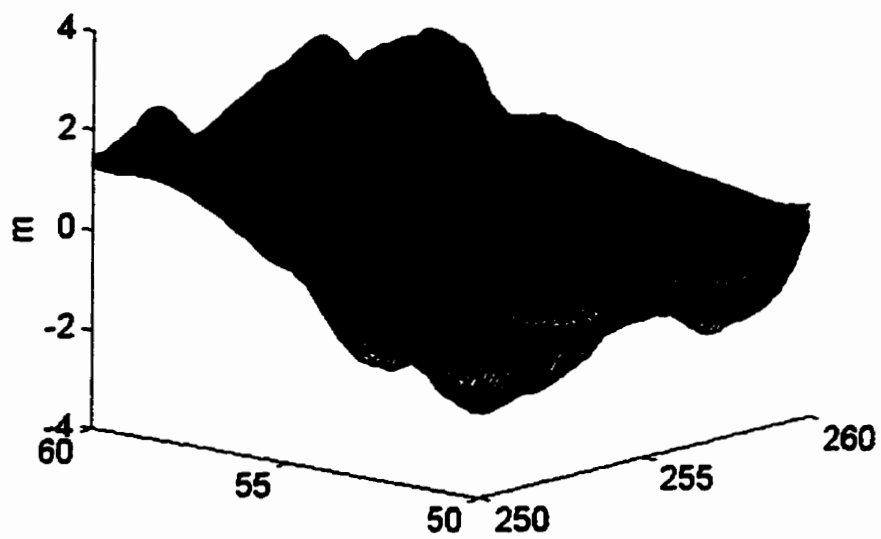


(a) The true fine-scale airborne gravity disturbances

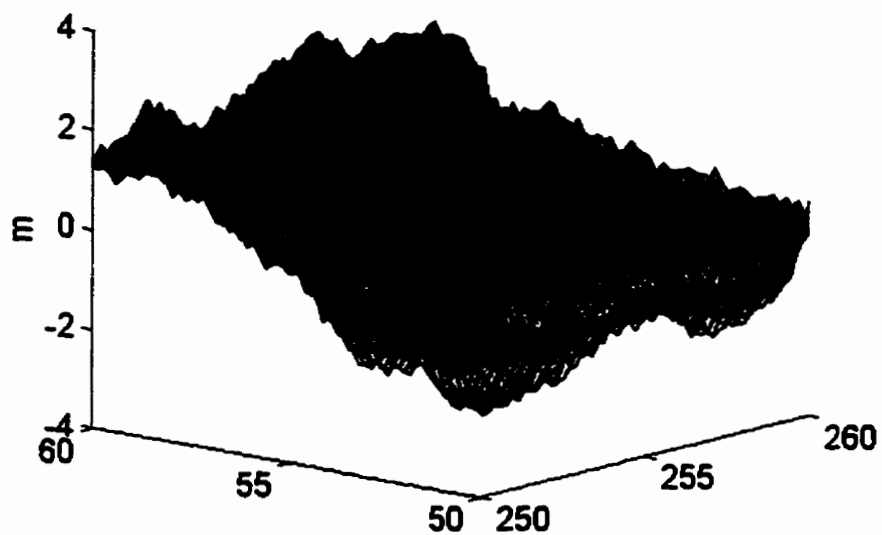


(b) The fine-scale airborne gravity disturbance measurements

Figure 5.2 The fine-scale airborne gravity disturbance

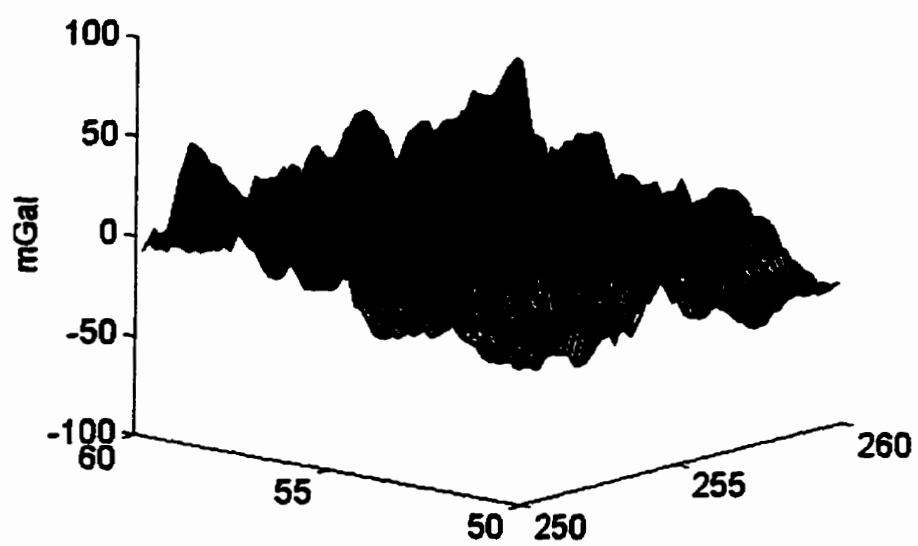


(a) The true coarse-scale geoidal height

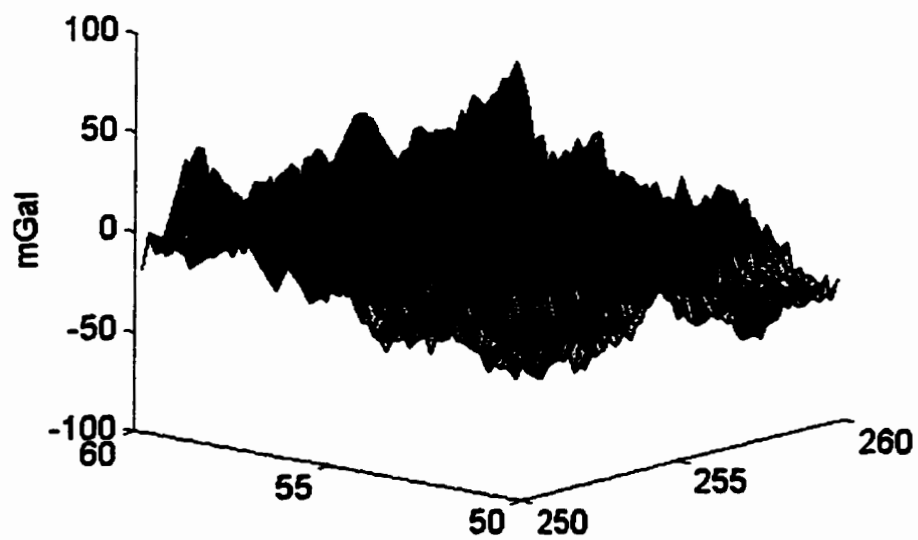


(b) The coarse-scale geoidal height measurements

Figure 5.3 The coarse-scale geoidal height



(a) The true terrestrial coarse-scale gravity anomaly



(b) The coarse-scale terrestrial gravity anomaly measurement

Figure 5.4 The coarse-scale terrestrial gravity anomaly

### 5.1.2 SOFTWARE OVERVIEW

Four main MATLAB programs were developed for this research. The first program is used to generate multiresolution data from gravity anomaly data by using the procedure described in Section 5.1.1. The second and the third programs are implemented to perform the fine-to-coarse estimation and coarse-to-fine estimation schemes for gravity field modeling, which is described in Section 4.2. The fourth program is used to implement a measurement domain approach using a multirate system and a MISO system described in Section 4.3. The output of the first program can be used as an input to the rest of the programs. A simple menu is added to the software to make it user-friendly.

Figure 5.5 shows the basic structure of the programs

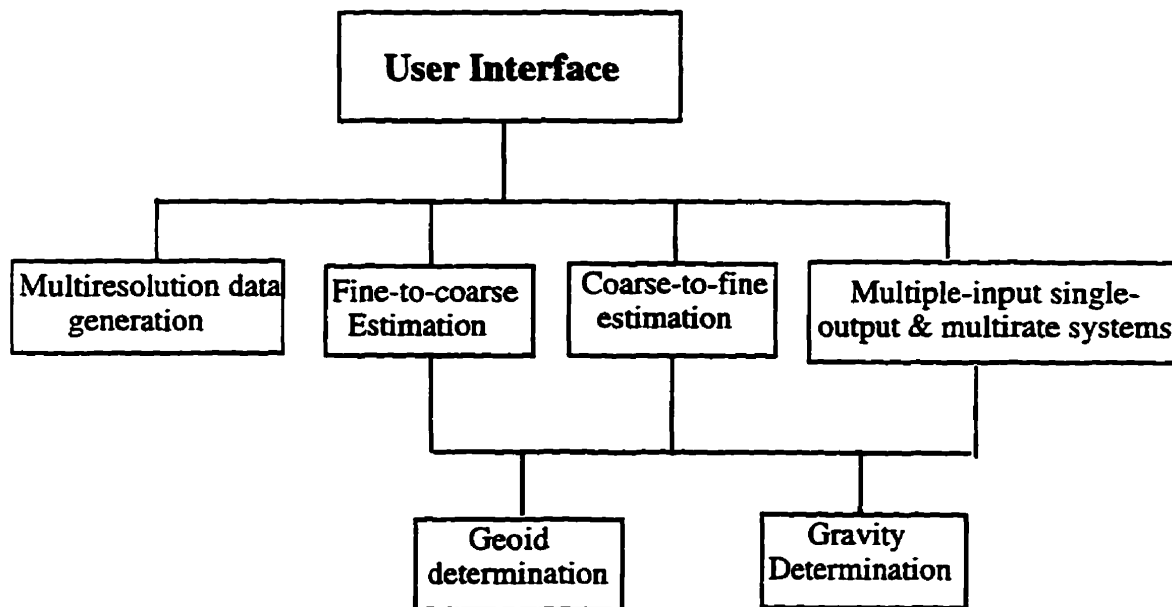


Figure 5.5 Basic structure of the programs

## **5.2 TWO EXAMPLES**

The purpose of the first example is to demonstrate that the proposed framework can be applied to the determination of geoidal heights based on the measurements at two scales, i.e. fine-scale airborne gravity disturbances and coarse-scale geoidal heights. In the second example, fusion of multiresolution measurements is presented using gravity disturbances at two different scales, i.e. fine-scale airborne gravity disturbance and terrestrial coarse-scale gravity disturbances.

Since the purpose of the following two examples is to demonstrate the effectiveness of the proposed framework, only the Haar wavelet is used in the computations. Comparisons using different wavelets will be given in Section 5.3.

### **5.2.1 Geoidal Height Determination from Fine-Scale Airborne Gravity Disturbance Data and Coarse-Scale Geoidal Height Data**

In the first example, measurements at fine scale are the airborne gravity disturbances with a resolution  $5' \times 5'$  and a coverage  $10^\circ \times 10^\circ$ . Measurement noise for the airborne gravity disturbances is assumed to be colored noise, the statistics of which is shown in Table 5.1. At coarse scale, the measurements are geoidal heights with a resolution  $10' \times 10'$  and the same coverage as the airborne gravity disturbances. The measurement noise for the

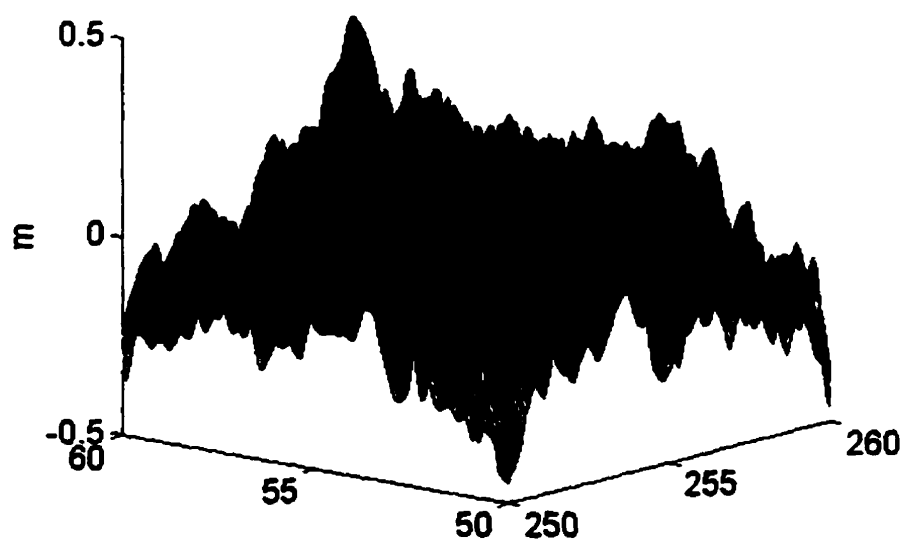
geoidal height is assumed to be white noise with the statistics shown in Table 5.1. The estimates of geoidal heights are computed using the two estimation schemes from the signal domain approach.

In order to evaluate the performance of the method, both internal and external errors before and after data fusion are computed. Internal error covariances are obtained by error propagation, while external error estimates are calculated by differencing the estimates and the true values of the simulated data. The statistics of the external geoidal height and the internal error covariances before and after data fusion are given in Table 5.2. Listed in the six columns are the means, maximums, minimums, standard deviations and variances of the external errors of the geoidal heights, variances of the internal errors of the geoidal height. Given in the first-two rows are the errors of the geoidal height at fine scale and coarse scale using fine-scale measurements only and coarse-scale measurements only, in row three-six the errors of the geoidal height at fine scale and coarse scale using both fine-scale and coarse-scale measurement and two estimation schemes.

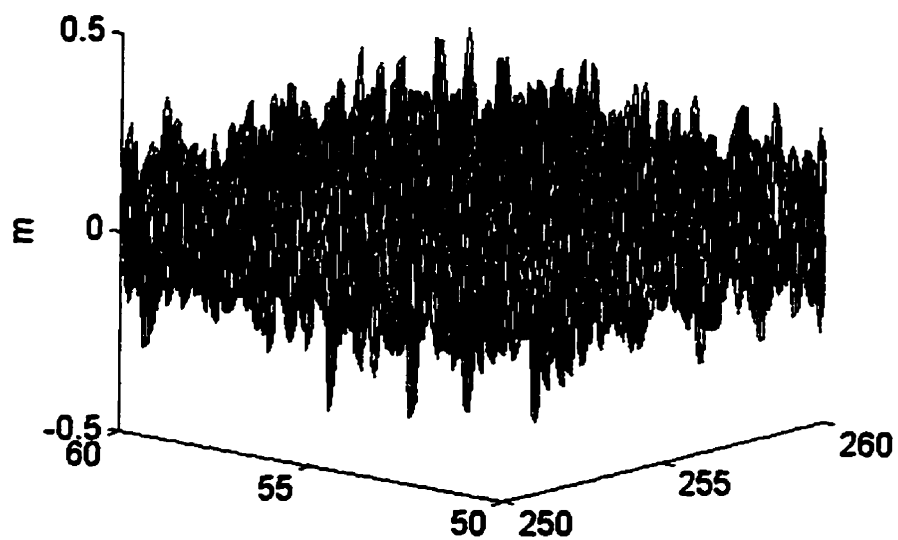
To visualize the estimation errors, the external errors of the geoidal heights at fine scale are also plotted. Figure 5.6a shows the external errors of the initial estimate of geoidal height at the fine scale using the airborne gravity disturbance measurements only and Figure 5.6b and 5.6c show the external errors of the geoidal height at fine-scale combining both fine-scale and coarse-scale measurements and using the two estimation schemes, respectively

Geoidal height errors	External					Internal
	Max (cm)	Min (cm)	Mean (cm)	Std (cm)	Var (cm <sup>2</sup> )	Var (cm <sup>2</sup> )
Error at fine scale (using $\delta g$ only)	51.9	-49.0	0.0	14.0	196.0	192.2
Error at coarse scale (using N only)	35.6	-38.8	0.0	9.9	97.0	97.0
Fused error at fine scale (fine-to-coarse)	36.5	-37.4	0.0	9.9	97.0	95.6
Fused error at coarse scale (fine-to-coarse)	31.6	-31.1	0.0	9.7	94.1	92.6
Fused error at fine scale (coarse-to-fine)	40.8	-47.1	0.0	10.0	100.0	95.8
Fused error at fine scale (coarse-to-fine)	30.4	-31.6	0.0	9.7	94.1	92.4

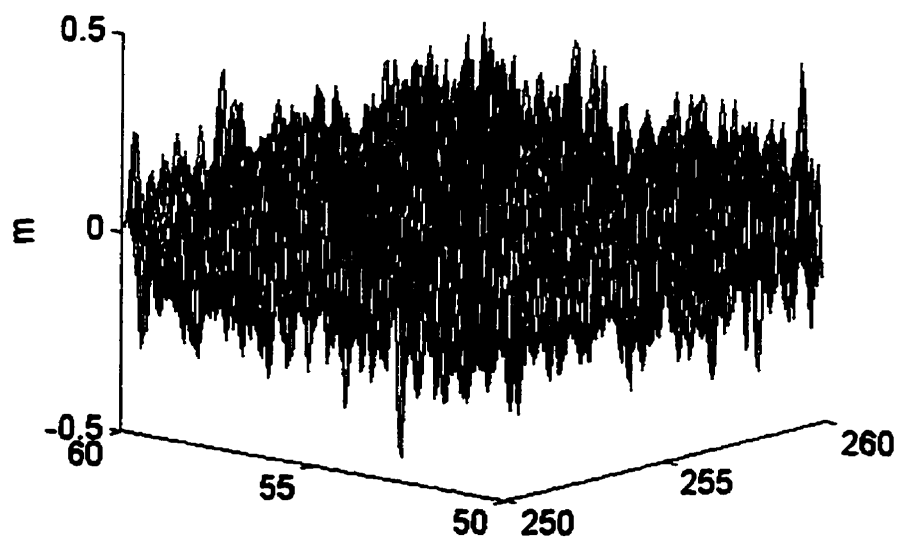
Table 5.2 Statistics of geoidal height estimation before and after data fusion



(a) Before data fusion



(b) After data fusion ( the fine-to-coarse approach)



(c) After data fusion ( the coarse-to-fine approach)

Figure 5.6 The errors of geoidal height at fine-scale before and after data fusion

From Table 5.2 and Figures 5.6, it is easy to see that better results have been achieved after combining the two different measurement sets by the proposed methods. The standard deviation of the error of the geoidal height at fine-scale is reduced by about 4.0 cm as compared to the estimate computed from the airborne data only. This can be seen when the fourth number in the third row is compared to that either in the fifth or the seventh row in Table 5.2. The reason is that highly accurate coarse-scale measurements provide the fine-scale signal estimate with good low frequency information which allows removal or reduction of the error in the low frequency part of the fine-scale estimate, as shown in Figure 5.6a. On the other hand, the geoidal height are not significantly improved. This can be seen by comparing the standard deviation in the sixth or the eighth rows of Table 5.2 to that in the fourth row of Table 5.2. This is due to the fact that the measurement noise of geoidal height at coarse scale is much smaller than the geoidal height error downsampled from the estimate of the geoidal height from airborne measurement at fine scale and the signal-to-noise ratio of the geoidal height at coarse scale is large, 13.7 in this case, as shown in the seventh column of Table 5.1. Therefore, when combining the geoidal height measurements and the downsampled geoidal heights, the error in the geoidal height at coarse scale will be dominated by the error of the coarse scale measurements.

When comparing the results from the fine-to-coarse estimation scheme and the coarse-to-fine estimation scheme, both schemes give nearly the same results. This is due to the fact that both schemes use the same information but different implementation procedures.

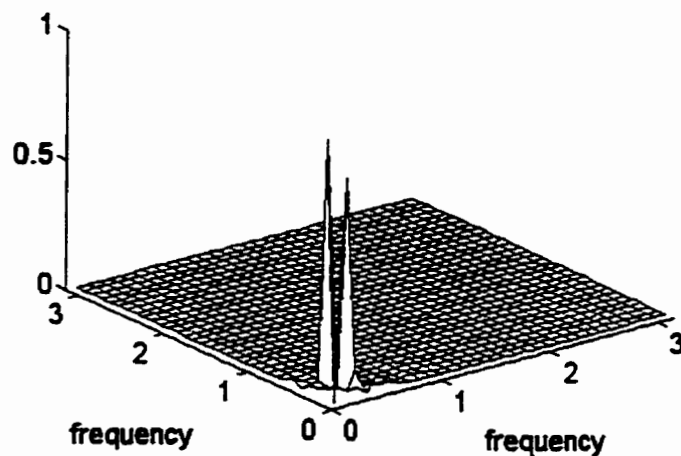
The standard deviation (std) of the external error of the fused geoidal height at fine scale are close to that of the coarse scale geoidal height estimates in this example. This can be explained by the fact that the determination of the geoidal height from the airborne gravity disturbance can be viewed as a filtering process, in which the high frequency noise in the airborne measurements will be reduced. Therefore the major error will be in the low frequency part, as can be seen in Figure 5.6a. On the other hand, since very good geoidal height measurements are available at the coarse scale, corresponding to the low frequency part of the geoidal height, the error of the geoidal height estimate in the low frequency part can be removed.

Form the sixth and seventh columns of Table 5.2, it can seen that both internal and external error variances are very close. This indicates that the proposed approach gives reliable estimations since the results are verified by independent checking.

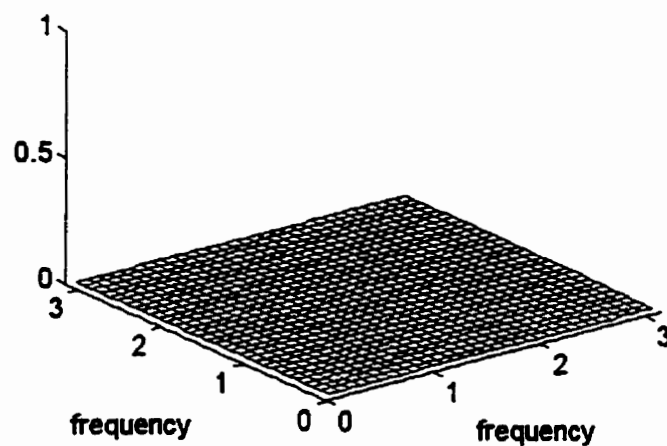
The above analysis is done in the space domain, but the results can also be analyzed in the spectral domain. To do this, the power spectral density of the external geoidal height errors at fine scale before and after data fusion have been computed and plotted in Figure 5.7.

Figure 5.7 clearly indicates that the improvement of the geoidal height signal at fine scale after data fusion is in the low frequency part. This can be explained by the fact that the coarse scale measurements only contribute to the low frequency ( half-band in this case)

information of the signal. Therefore high quality of the coarse scale measurements can improve the geoidal height estimation in the low frequency part.



(a) Before data fusion



(b) After data fusion ( the fine-to-coarse estimation )

Figure 5.7 Normalied power spectral density of the geoidal height errors

before and after data fusion

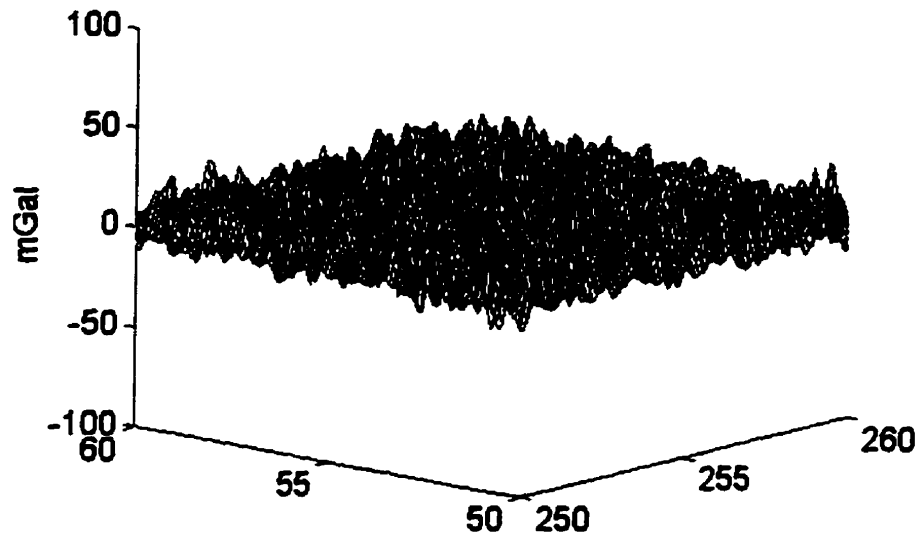
### **5.2.2. Fusion of Fine-Scale Airborne Gravity Disturbances with Coarse-Scale Terrestrial Gravity Disturbances**

In the second example, measurements at fine scale are the airborne gravity disturbances, and the coarse-scale measurements are the terrestrial gravity disturbances with resolution  $5' \times 5'$  and  $10' \times 10'$ , respectively. The coverage for both of them is  $10^\circ \times 10^\circ$ . Measurement noise for the fine-scale gravity disturbances is assumed to be the same colored noise as in the first example. Measurement noise for the coarse-scale gravity disturbances is assumed to be white noise with the statistics shown in Table 5.1. The fusion of these two measurements is done using the two estimation schemes from the signal domain approach.

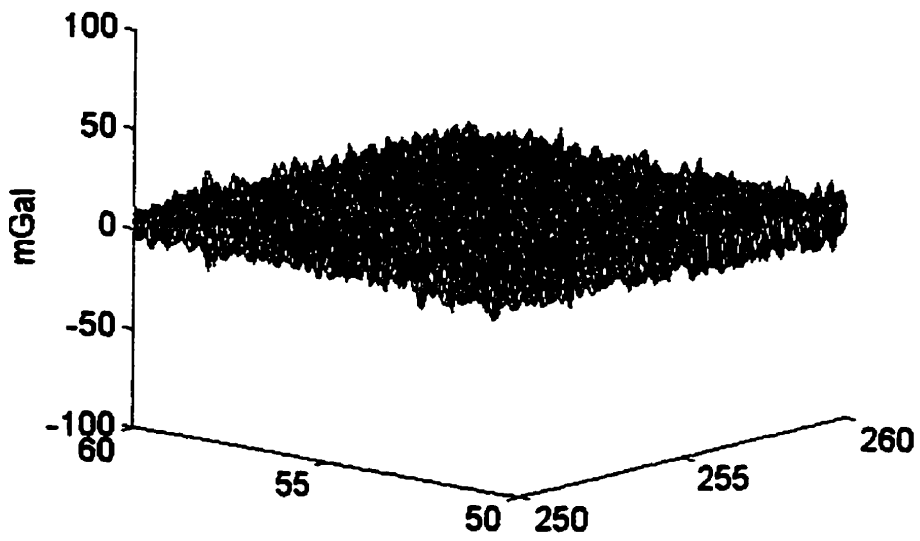
Tables 5.3 summarizes the statistics of the external geoidal height and the internal error covariances before and after data fusion. Listed in the six columns are the means, maximums, minimums, standard deviations and variances of the external errors of the terrestrial gravity disturbance, and the variances of the internal errors of the terrestrial gravity disturbance. Given in the row headings are the errors of the terrestrial gravity disturbance at fine scale and coarse scale using fine-scale measurements only and coarse-scale measurements only ( rows 1 and 2 ), the errors of the terrestrial gravity disturbance at fine scale and coarse scale using both fine-scale and coarse-scale measurement and two estimation schemes ( rows 3 to 6 ). Figure 5.8 shows the errors of the terrestrial gravity disturbance estimates at fine-scale before and after data fusion.

Gravity disturbance errors	External					Internal
	Max (mGal)	Min (mGal)	Mean (mGal)	Std (mGal)	Var (mGal <sup>2</sup> )	Var (mGal <sup>2</sup> )
Error at fine scale (using airborne $\delta g$ only)	30.6	-32.7	0.0	8.1	65.6	63.9
Error at coarse scale (using terrestrial $\delta g$ only)	10.0	-10.3	0.0	3.0	9.0	9.0
Fused error at fine scale ( fine-to-coarse )	19.2	-19.4	0.0	4.6	21.6	20.2
Fused error at coarse scale ( fine-to-coarse )	8.8	-8.7	0.0	2.8	7.8	7.5
Fused error at fine scale (coarse-to-fine)	20.9	-20.2	0.0	4.7	22.9	20.4
Fused error at fine scale (coarse-to-fine)	8.9	-9.0	0.0	2.8	7.8	7.4

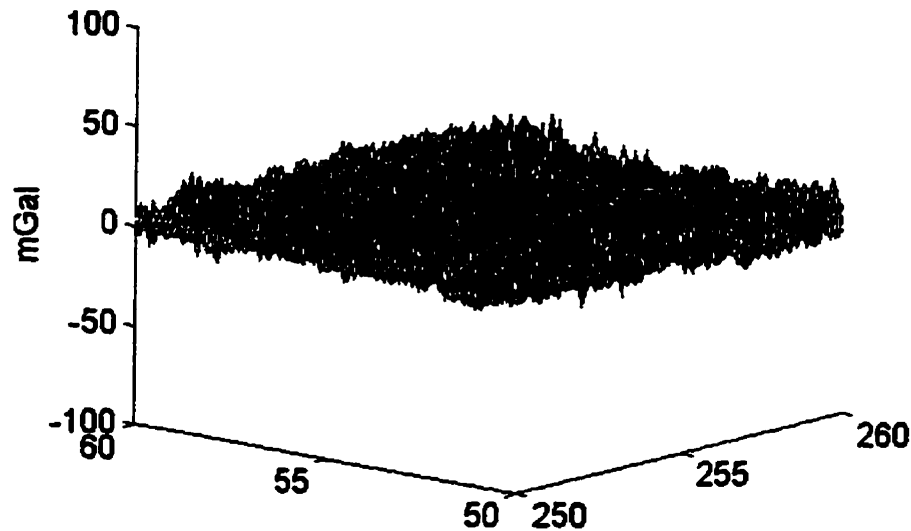
Table 5.3 Statistics for the fusion of airborne gravity disturbances and terrestrial gravity disturbance using the two estimation schemes



(a) Before data fusion



(b) After data fusion ( the fine-to-coarse approach)



(c) After data fusion ( the coarse-to-fine approach)

Figure 5.8 Errors of the terrestrial gravity disturbance estimate at fine-scale  
before and after data fusion

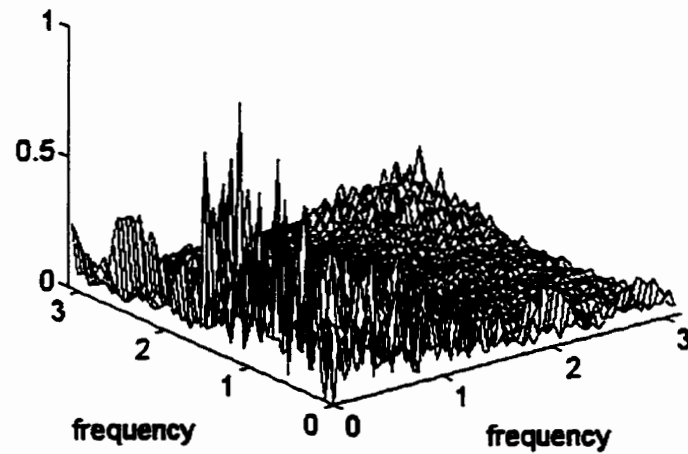
Similar conclusions as in Section 5.2.1 can be drawn from Table 5.3 and Figures 5.8. The standard deviation of the error of the terrestrial gravity disturbances at fine-scale has been reduced by about 3.5 mGal after fusing the two data sets by the proposed schemes, as compared to the estimate computed from airborne data only. This can be seen by comparing the fourth number in the third row with that in the fifth or seventh row in Table 5.3. The accurate coarse-scale measurements improves the fine-scale estimate of the terrestrial gravity disturbance in the low frequency part but not in the high frequency part, as shown in Figure 6.8. The fused terrestrial gravity disturbance estimates at coarse scale also improve. The percentage improvement is about 7 %, when comparing the

standard deviation of the external error after data fusion ( in the sixth or eighth row in Table 5.3) with the standard deviation of the external error before data fusion ( in the fourth row of Table 5.3 ). Internal and external error variances are close indicating the reliability of the terrestrial gravity disturbance estimations. Similar to Section 5.2.1, the results from both schemes are nearly the same. The reason is the same as before.

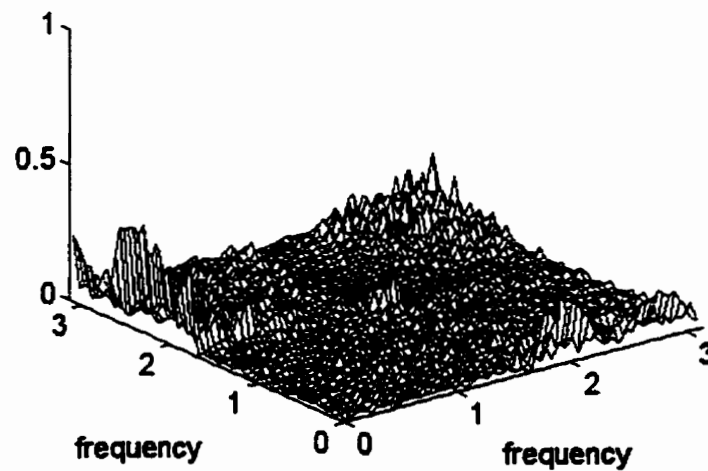
Unlike the results in Section 5.2.1, the standard deviation of the error of the fused gravity disturbance at fine scale are different from the fused terrestrial gravity disturbance at coarse-scale, as can be seen from the fifth and sixth rows or the seventh and eight rows. This can be considered by downward continuation effects. The determination of the terrestrial gravity disturbance from the airborne gravity disturbance measurement is a downward continuation process, in which the noise in the airborne measurements will be amplified. This problem can be partially solved by filtering the airborne data by a low-pass filter before downward continuation (Vassiliou, 1986). As mentioned before, good measurements at coarse-scale can only improve the estimate in the low frequency part. They will have no effect on the noise amplified in high frequency part. That is the reason why the two statistics mentioned above are different.

The power spectral density of the external gravity disturbance errors at fine scale before and after data fusion are plotted in Figure 5.9. From Figure 5.9(a), one can see that a major error source of the terrestrial gravity disturbance before data fusion comes a high frequency part due to the downward continuation process. The low frequency error is

reduced by using high quality coarse-scale measurements, the high frequency error remains, as indicated by Figure 5.9(b).



(a) Before data fusion



(b) After data fusion ( the fine-to-coarse estimation)

Figure 5.9 Normalized power spectral density of the gravity disturbance  
before and after data fusion

### 5.3 EFFECTS OF USING DIFFERENT WAVELETS

To see how different wavelets affect the final results, a numerical test was conducted using four different wavelets, Haar wavelet and three different Daubechies wavelets ( $N=4, 6$  and  $8$ ). The measurements used in the test are fine-scale airborne gravity disturbance and coarse-scale geoidal heights. The estimated signals are the geoidal heights at both fine and coarse scales. The data is the same as that in Section 5.2.1 except that the different wavelets are used. The true coarse-scale geoidal height was simulated in this test by using the Daubechies wavelet  $N=8$ .

Table 5.4 shows the statistics of the external error of the geoidal height estimation using these four wavelets. Figure 5.10 illustrates the errors of the fine-scale geoidal height estimate by combining fine-scale airborne gravity disturbances and coarse-scale geoidal heights using the four different wavelets.

From Table 5.4 and Figure 5.10, it can be seen that different wavelets affect the estimation of geoidal height. Both mean and the standard deviation are affected. The maximum deviation of the mean at the fine scale is 1.7 cm, while that of the standard deviation is 1.3 cm, respectively. The reason is that different wavelets define a different multiresolution analysis, i.e. a different approximation of  $L^2(\mathbb{R})$ . Therefore, if a signal at specific scale cannot be exactly represented by a given wavelet, this will result in representation error. To illustrate this numerically, the errors caused by the inaccuracy

Geoidal height error	Scale	Max (cm)	Min (cm)	Mean (cm)	Std (cm)	RMS (cm)
Haar wavelet	Fine	59.4	-45.7	1.7	11.4	11.5
Daubechies wavelet N=4	Fine	57.2	-45.5	1.2	10.7	10.8
Daubechies wavelet N=6	Fine	49.4	-34.4	0.3	10.2	10.2
Daubechies wavelet N=8	Fine	38.4	-37.4	0.0	10.1	10.1
Haar wavelet	Coarse	31.4	-32.4	0.0	9.8	9.8
Daubechies wavelet N=4	Coarse	30.8	-31.7	0.0	9.7	9.7
Daubechies wavelet N=6	Coarse	31.2	-30.9	0.0	9.7	9.7
Daubechies wavelet N=8	Coarse	30.4	-30.2	0.0	9.7	9.7

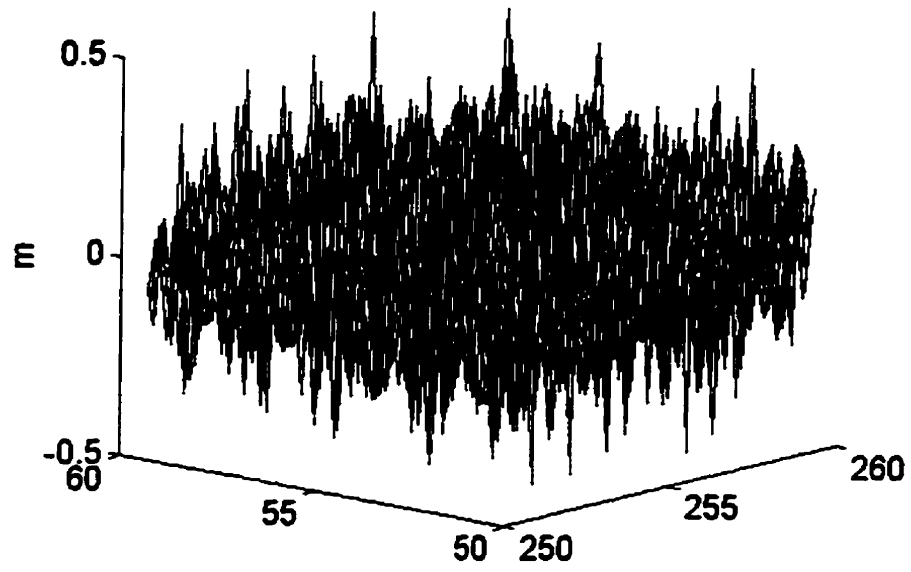
Table 5.4 Statistics of geoidal height error using different wavelets

when the geoidal height signal is transformed from fine scale to coarse scale and coarse to fine scale using these four wavelets have been computed. The errors at coarse-scale are obtained by computing the coarse-scale signal from the fine-scale true signal for a given wavelet and then comparing it to the true value. The errors at fine-scale are obtained by calculating the fine-scale signal from the coarse-scale true signal and the detailed signal components along the horizontal, vertical, and diagonal for a given wavelet. They are then compared to the true value. Table 5.5 summarizes the statistics of these errors.

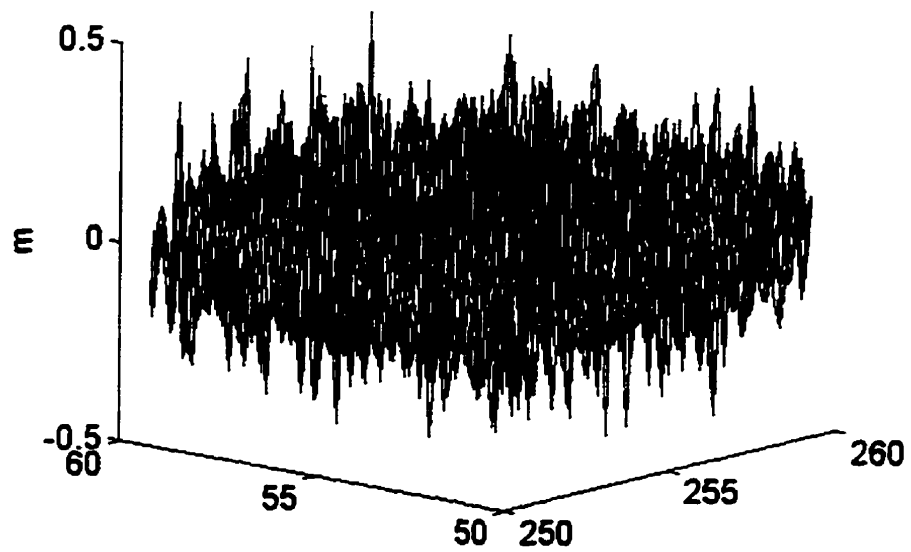
Geoidal height error	Scale	Max (cm)	Min (cm)	Mean (cm)	Std (cm)	RMS (cm)
Haar wavelet	Fine	15.9	-14.2	1.7	4.2	4.5
Daubechies wavelet N=4	Fine	12.1	-8.6	1.2	2.9	3.2
Daubechies wavelet N=6	Fine	4.5	-3.7	0.3	1.1	1.1
Daubechies wavelet N=8	Fine	0.0	0.0	0.0	0.0	0.0
Haar wavelet	Coarse	14.2	-11.6	1.5	4.0	4.3
Daubechies wavelet N=4	Coarse	10.6	-8.1	1.1	2.6	2.8
Daubechies wavelet N=6	Coarse	4.1	-3.3	0.2	1.0	1.0
Daubechies wavelet N=8	Coarse	0.0	0.0	0.0	0.0	0.0

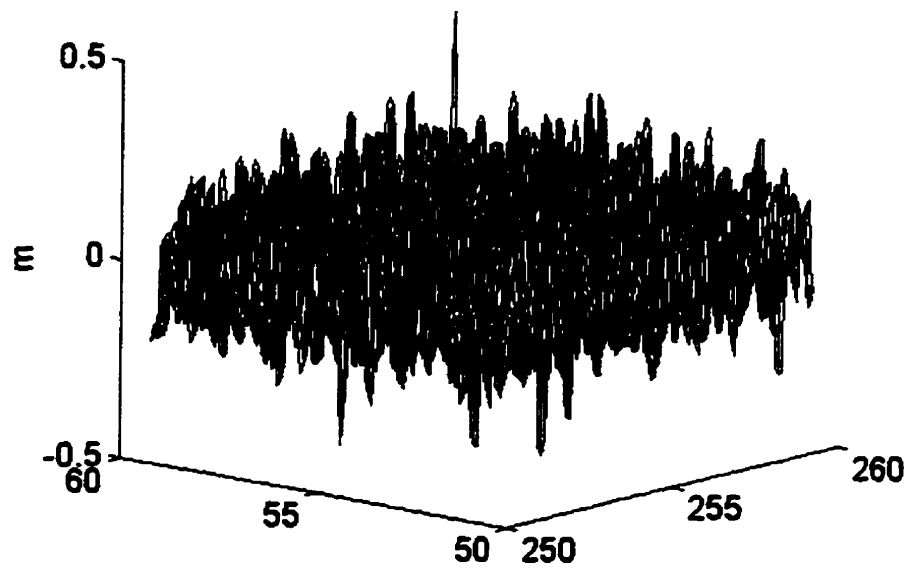
Table 5.5 Geoidal height error due to inaccurate representation using different wavelets

Table 5.5 clearly indicates that a distortion of the geoidal height signal has been introduced due to the inaccurate representation of the signal at both scales when using different wavelets. The maximum errors of the mean and standard deviation are 1.7 cm and 4.2 cm at fine scale, respectively, and 1.5 cm and 4.0 cm at coarse scale, respectively. When the fourth and fifth columns of Table 5.5 are compared to that of Table 5.4, one can see that the estimates at coarse-scale are hardly affected by the error at coarse-scale caused by the inaccurate representation of the geoidal height signal. This is because the error caused by the inaccurate representation is corrected by the high quality coarse-scale measurements when measurement update is performed at coarse scale.

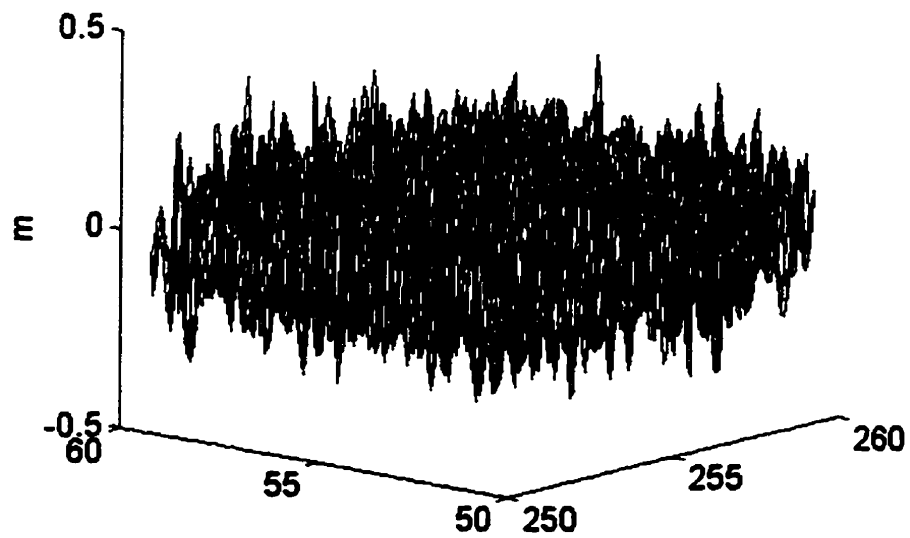


(a) Haar wavelet

(b) Daubechies wavelet  $N=4$



(c) Daubechies wavelet N=6



(d) Daubechies wavelet N=8

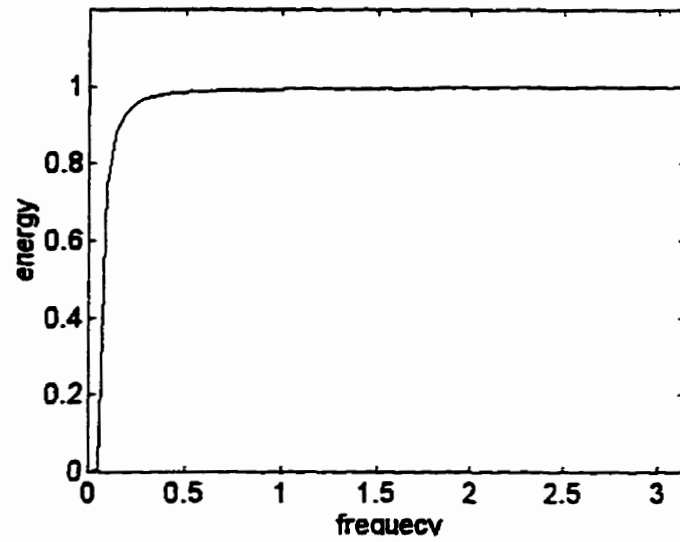
Figure 5.10 External geoidal height errors using different wavelets

#### **5.4 NUMERICAL COMPARISON BETWEEN A SIGNAL DOMAIN APPROACH AND A MEASUREMENT DOMAIN APPROACH**

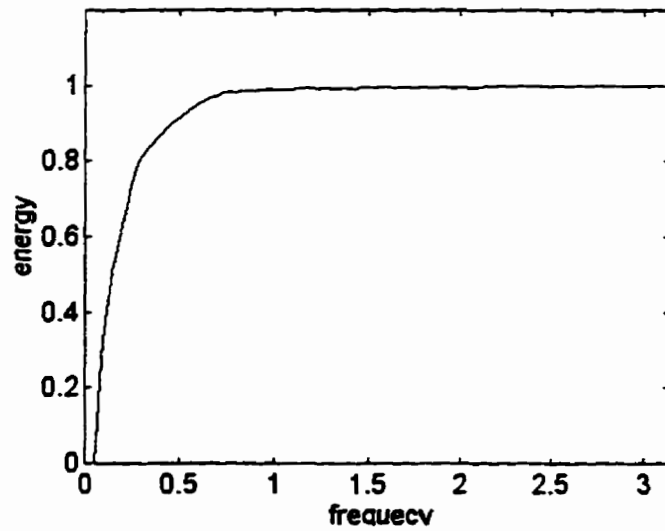
To investigate how different methods affect the estimation of the gravity field signal, a numerical comparison was conducted using a signal domain approach combining a wavelet transform and least-squares collocation (Method I) and a measurement domain approach combining a multirate system and a MISO system (Method II). The effect of different gravity field signal spectra on both approaches will also be investigated. In addition, the effect of resolution differences between the fine scale and the coarse scale for both methods will also be analyzed for both methods.

The measurements used in the comparison are the same as used in Section 5.2 except that a wavelet transform using a Daubechies wavelet ( $N=40$ ) is applied to the true fine-scale data to simulate coarse-scale data. The signals to be estimated are also the same as that in Section 5.2, i.e. geoidal heights and the terrestrial gravity disturbances at both fine and coarse scales. Figure 5.11 shows the relative energy distribution of these two signals, which is obtained in three steps. In the first step the power spectral densities of these two signals are computed. In the next step the power spectral density from zero to the desired frequency is integrated. Lastly, these integrated values are then normalized using the total energy.

The reason of using a Daubechies wavelet  $N=40$  is the following: As can be seen from the relative energy distribution of the geoidal height and the gravity disturbance in



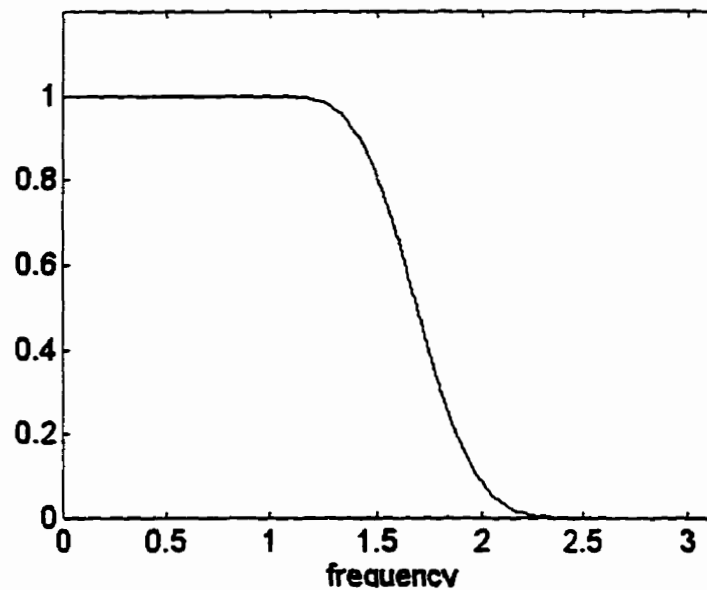
(a) Geoidal height



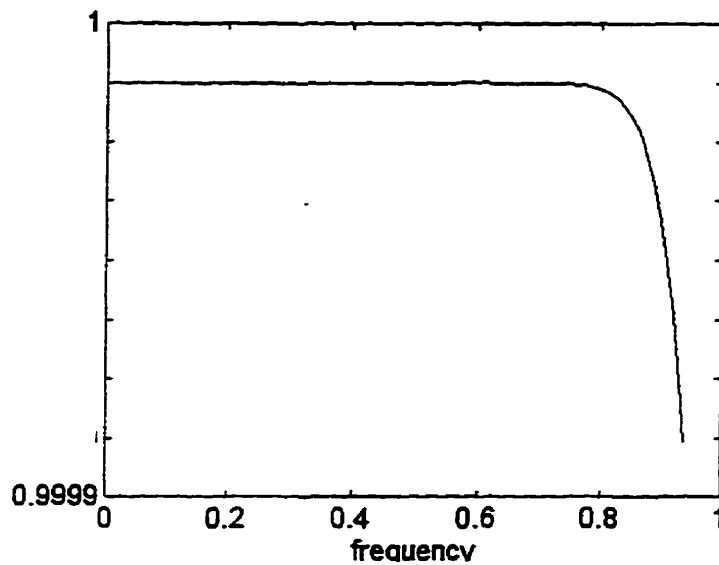
(b) Terrestrial gravity disturbance

Figure 5.11 Relative energy distribution of the geoidal height and the terrestrial gravity disturbance

Figure 5.11, most of the energy of the geoidal height and gravity disturbance signals is in the lower frequency part. %99 of the energy of the geoidal height signal is within the frequency band of about  $[0 \ 0.2\pi]$  and %99 of the energy of the terrestrial gravity disturbances is within the frequency band of about  $[0 \ 0.3\pi]$ . In order to give a reasonable simulation of the coarse-scale signal of these gravity signals, the fine-scale signal in this frequency band should be passed with as little distortion as possible. In other word, the magnitude of the frequency response in this frequency band should be as close 1 as possible when generating coarse-scale data. Figure 5.12 shows the magnitude of the frequency response for the Daubechies (N=40) FIR lowpass filter ( the order of the filter is N=40).



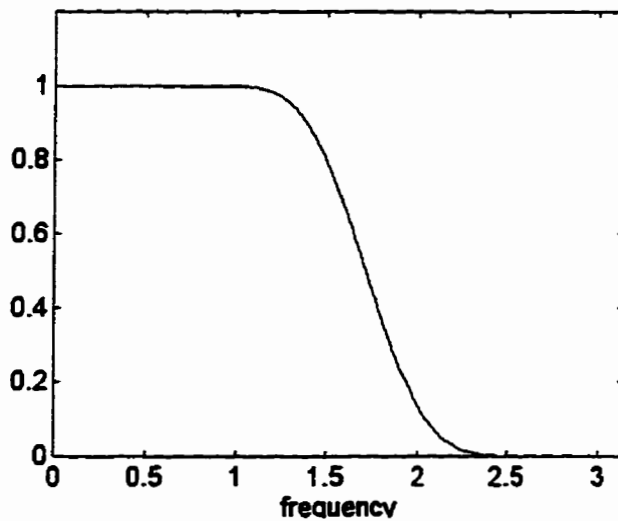
(a)  $[0 \ \pi]$

(b)  $[0 \ 0.3\pi]$ Figure 5.12. Frequency responses of Daubechies lowpass filter (  $N = 40$ )

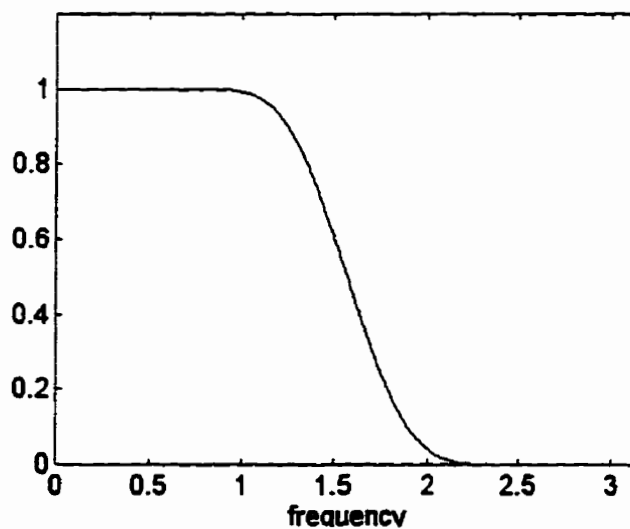
From Figure 5.12, the magnitude of the frequency response is very close to 1 within the  $0.3\pi$  bandwidth. The maximum difference is 0.00006.

The wavelet used in Method I is a Daubechies wavelet ( $N=24$ ). The frequency response of the lowpass filter coefficients corresponding to the Daubechies wavelet  $N=24$  is plotted in Figure 5.13(a).

The multirate system used in Method II is a Kaiser multirate system which is obtained by using a Kaiser window in the window design technique described in Section 3.6.3. The frequency response of the lowpass FIR Kaiser filter ( $N = 24$ ) are shown in Figure 5.13(b).



(a) Daubchies



(b) Kaiser

Figure 5.13 Frequency response of lowpass FIR Daubechies and Kaiser filters ( $N=24$ )

Tables 5.6 summarizes the statistics of the external errors of the geoidal height estimations based on the fine-scale and coarse-scale geoidal height measurements using the two methods. Tables 5.7 summarizes the statistics of the external errors of the

terrestrial gravity disturbance estimation based on the fine-scale airborne gravity disturbance and coarse-scale terrestrial gravity disturbance measurements using the two methods. Listed in the last four columns of both tables are the means and standard deviations of the external errors of the geoidal heights ( or the terrestrial gravity disturbance ) for both methods. Figures 5.14 and 5.15 show the external errors of the geoidal height and the gravity disturbance for the both methods, respectively.

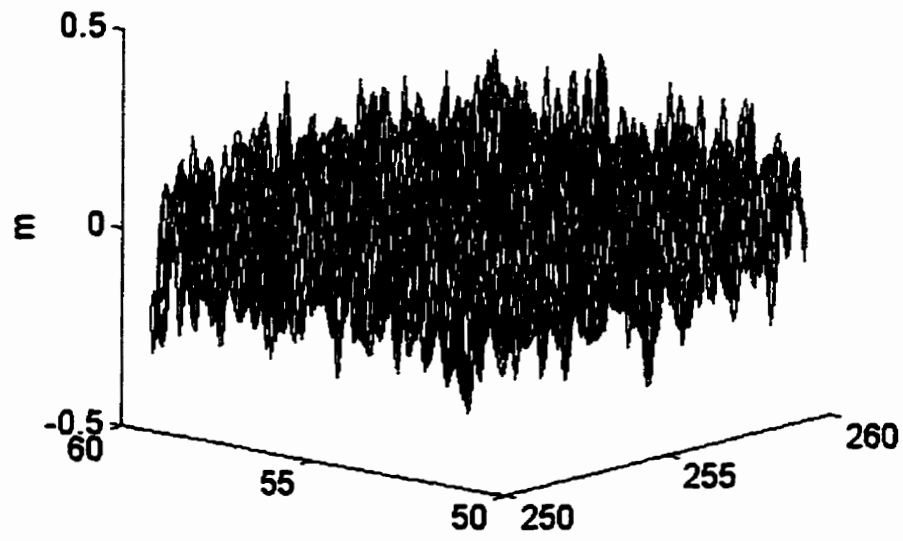
Method		Method I		Method II	
Geoidal height errors	Scale difference	Mean (cm)	Std (cm)	Mean (cm)	Std (cm)
Fine scale	1	0.0	10.1	0.0	10.2
Coarse scale	1	0.0	9.7	0.0	9.7

Table 5.6 The statistics of the geoidal height errors using both methods (I)

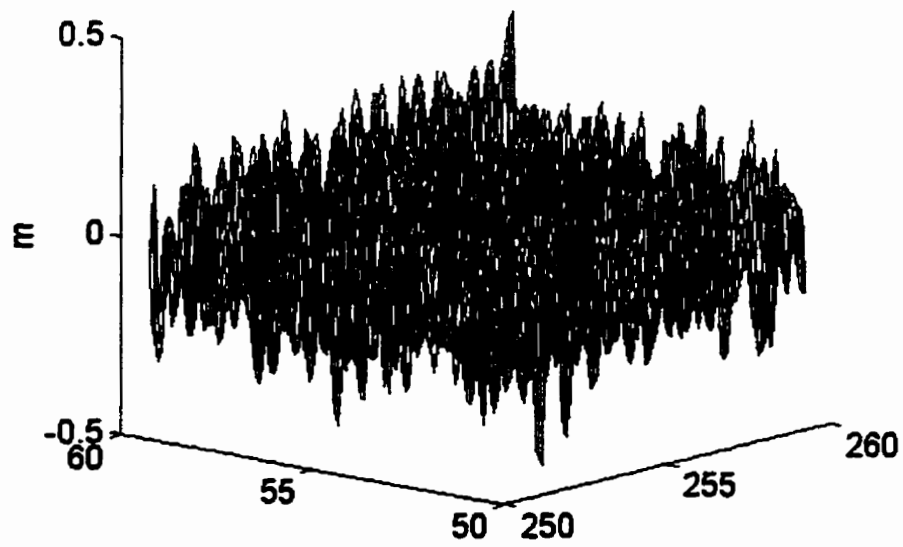
Method		Method I		Method II	
Gravity disturbance errors	Scale difference	Mean (mGal)	Std (mGal)	Mean (mGal)	Std (mGal)
Fine scale	1	0.0	4.8	0.1	4.9
Coarse scale	1	0.0	2.8	0.0	2.8

Table 5.7 The statistics of the terrestrial gravity disturbance errors using both methods (I)

From Tables 5.6 and 5.7 as well as Figures 5.14 and 5.15, it is easy to see that both methods give essentially the same results. There are two reasons for this. First, since the geoidal height and gravity anomaly signals are in the low frequency bandwidth within

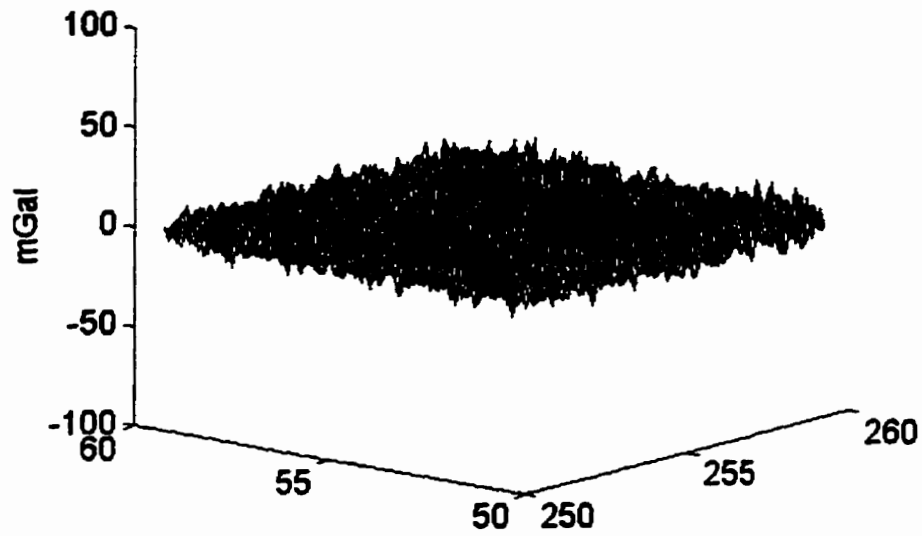


(a) Geoidal height error (Method I)

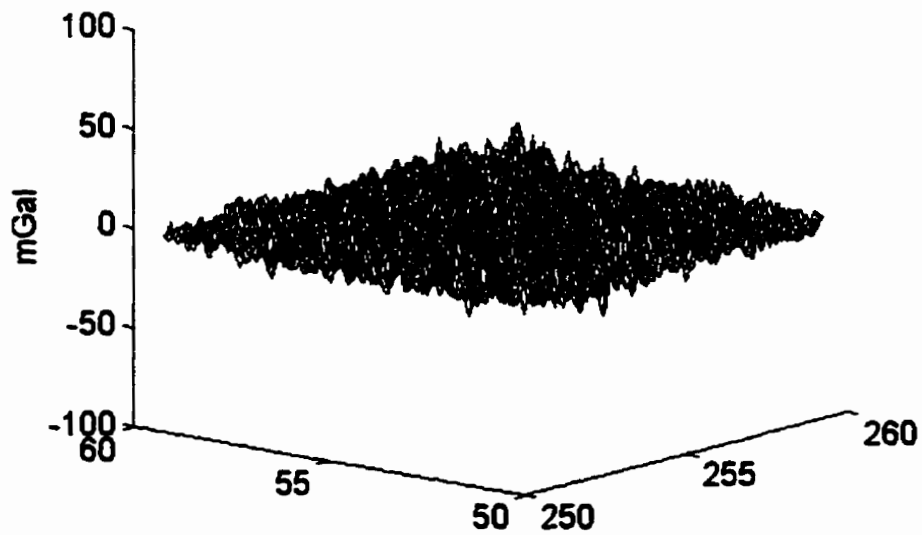


(b) Geoidal height error (Method II)

Figure 5.14 The geoidal height errors using both methods



(a) Terrestrial gravity disturbance error ( Method I )



(b) Terrestrial gravity disturbance error ( Method II )

Figure 5.15 Terrestrial gravity disturbance error using both methods

$0.3\pi$ , the decimation and interpolation of these signals using either the Daubechies or the Kaiser half-band FIR lowpass filter will not cause much distortion of the signals in this part. This can be seen from the spectrum of the Daubechies and the Kaiser FIR filter in Figure 5.13. Second, both methods use the same information, i.e. same measurements at fine and coarse scale; the major difference between them is the way of implementation. The implementation of Method I is in the signal domain, i.e. the transition from one resolution to another is done using a discrete wavelet transform in the signal domain. The implementation of Method II is in the measurement domain i.e. the transition from one resolution to another is done by using a Kaiser lowpass decimation and interpolation in the measurement domain.

To see how the resolution difference at fine scale and coarse scale will affect the estimates of both methods, the geoidal height and the terrestrial gravity disturbance are estimated using measurements at both scales differing by a scale of 2. This means that the sampling rate difference between the fine-scale measurements and the coarse-scale measurements is 4. The estimation results are listed in Tables 5.8 and 5.9.

Method		Method I		Method II	
Geoidal height errors	Scale difference	Mean (cm)	Std (cm)	Mean (cm)	Std (cm)
Fine scale	2	0.1	10.2	0.1	10.3
Coarse scale	2	0.0	9.7	0.0	9.7

Table 5.8 The statistics of the geoidal height errors using both methods (II)

Method		Method I		Method II	
Gravity disturbance errors	Scale difference	Mean (mGal)	Std (mGal)	Mean (mGal)	Std (mGal)
Fine scale	2	1.0	5.8	1.5	7.1
Coarse scale	2	0.0	2.8	0.0	2.9

Table 5.9 The statistics of the terrestrial gravity disturbance errors using both methods  
(II)

When the third and the fourth column of Tables 5.8 are compared to the fifth and the sixth columns in the same table, one sees that the mean and standard deviation of the geoidal height errors are essentially the same. The reason is that decimation and interpolation of the signal or the measurements at a sampling rate of 4 correspond to the cutoff frequency  $\pi/4$  of the lowpass filters. Therefore, the decimation or interpolation using a wavelet transform will not cause much distortion since the cutoff frequency is still beyond the frequency band of the geoidal height signal. Similarly, the effect of the interpolation of the fine-scale geoidal height measurements from the coarse-scale geoidal height measurement will be small for the same reason. However, the decimation of the airborne measurements could affect the estimation of the geoidal height signal at coarse scale. One should remember, however, that the measurements at coarse scale are of high quality, which will eliminate the effect due to the decimation of measurements. This is why both methods give essentially the same results in Table 5.8.

Different results are obtained at fine scale for estimating the terrestrial gravity disturbances using both methods. When comparing the third and the fourth number of the third row in Table 5.9 to the fifth and sixth number of the third row in the same table, the effect of the lowpass filters used for decimation and interpolation can be seen. The cutoff frequency of the lowpass filters is  $\pi/4$  which is in the same range as that of the signal spectrum. Therefore, the gravity disturbance signal is distorted by the aliasing effect due to the non-ideal frequency response of the lowpass filters. In this test, the effect using the Kaiser filter is larger than that using the Daubechies filter. The reason for this is that the Daubechies filter allows the terrestrial signal in the low frequency band pass with less distortion than the Kaiser filter. This can be seen when comparing the frequency responses of two filters in Figure 5.13. This effect shows up in Table 5.10, where the estimates have been obtained by first decimating or interpolating the true fine-scale or coarse-scale signals using either the Daubechies filter (N=24) or the Kaiser filter (N=24), and then comparing them to those of the Daubechies FIR filter (N=40).

Method		Method I		Method II	
Gravity disturbance errors	Scale difference	Mean (mGal)	Std (mGal)	Mean (mGal)	Std (mGal)
Fine scale	2	1.0	2.6	1.5	4.2
Coarse scale	2	0.9	2.4	1.3	3.9

Table 5.10 The gravity disturbance errors due to lowpass filtering

When comparing the coarse-scale results in Table 5.9 between both methods, one can see that the statistics of the terrestrial gravity disturbance error at coarse scale is nearly the same for both methods. This is initially unexpected because the lowpass filters also affect the coarse-scale signal, as is clearly seen from Table 5.10. However, as mentioned before, good measurements at coarse scale eliminate the error caused by lowpass filtering.

It should be mentioned that, although the result of the terrestrial gravity disturbance estimation at fine scale using Method I is better than that using Method II in this test, it does not mean that the wavelet-based approaches are better than multirate-based approaches since estimation results depend on lowpass filters. Also, we could expect that estimation results will also be different with increase of the resolution difference between fine scale and coarse scale, or, equivalently, the sampling rate difference between fine scale and coarse scale. This is because the cutoff frequency of the lowpass filters will be within the range of the signals and the non-ideal lowpass filters will cause aliasing.

From the above comparisons, it can be seen that the results of gravity field signal estimation depend on the signal spectrum, the resolution difference between measurements at both scales, and the choice of the lowpass filter. If the energy of the signals is concentrated in a narrow low frequency bandwidth and the difference of the sampling rates of the measurements at two scales is small, e.g. 2, the results will be essentially the same using either the Daubechies FIR filter or the Kaiser filter. However, the results from both methods will be different when the sampling rate difference between the two scales is increased. This is due to the aliasing effect of the lowpass

filters. In this case, the proper choice of a lowpass filter for both methods is important. In general, Method II is better than Method I when the filter problem is well handled. There are three reasons for that. First, Method II is more flexible than Method I because it does not depend on a dyadic structure. Secondly, Method II is more efficient than Method I if an estimate of a signal is only required at an intermediate scale between the finest scale and the coarsest scale. This is because no sweep either from the finest to the coarsest scale or from the coarsest to the finest scale is needed. Finally, Method II allows estimation of different signals at different resolutions from multiresolution measurements, while Method I only allow to the estimate same signals at different resolutions.

## **CHAPTER 6**

### **CONCLUSIONS AND RECOMMENDATIONS**

The main contribution of this thesis is the development of a framework for multiresolution approximation and the demonstration of its potential for solving multiresolution problems in gravity field approximation.

#### **6.1 CONCLUSIONS**

The following conclusions can be drawn from this dissertation:

- (a) Different classes of multiresolution problems exist in gravity field modeling. They are due to the use of different types of observables, different gravity field attenuation effects with altitude, different sampling rates, and different measurement noise levels. Four classes have been identified and formulated.
- (b) The analysis of the existing gravity field approximation methods shows that they cannot solve the multiresolution problems.
- (c) A general methodology has been formulated which allows to combine different methods for the solution of multiresolution approximation problems. Both signal domain and measurement domain approaches can be used. Two signal domain approaches have been derived by combining a discrete wavelet transform and least-squares collocation as two special tools. A measurement

domain approach has been formulated as an alternative. It combines a multirate system and a MISO system. The main advantage of the proposed framework is that it allows both estimation of signals at multiple scales and fusion of measurements at different scales.

(d) A theoretical comparison between the proposed method and stepwise least-squares collocation (LSC) shows that LSC does not solve the problem of computing the cross-covariance matrices between different resolution levels. Wavelet transforms or multirate systems solve this problem very efficiently, but have the disadvantage that the solution is not globally optimal since it depends on the choice of wavelets or multirate systems.

(e) Numerical results show that the errors of the fused estimates at both fine scale and coarse scale have been reduced compared to those using one-scale data only. The spectral analysis of the results shows that coarse-scale measurements of high quality definitely improve the estimate in the low frequency part.

(f) The numerical results indicate that the two signal domain estimation schemes give essentially the same results for the two examples. However, the choice of different wavelets does affect the estimation of the gravity field signals due to the fact the representation of signals changes with the wavelet base chosen.

(g) The numerical comparison between the signal domain approach (Method I), combining a wavelet transform and least-squares collocation, and the measurement domain approach (Method

II), using a multirate system and a MISO system, shows that the results of the gravity filed signal estimation depend on the signal spectrum, the resolution difference between measurements at both scales, and the choice of the lowpass filter. If the energy of the signal is concentrated in a narrow low frequency bandwidth and the difference of the sampling rates at two scales is small, e.g. 2, the results will be essentially the same using either a Daubechies FIR filter or a Kaiser filter. However, the results from both methods will be different when the sampling rates of the measurements at two scales is increased. This is due to the aliasing effect of the chosen lowpass filters. In this case, the properly choice of a lowpass filter for both methods is important consideration. In general, Method II is better than Method I since Method II is more flexible and moe efficient than Method I.

(h) The use of multirate systems either in signal domain approaches or measurement domain approaches has the advantage that it is not dependent on dyadic structure. It is therefore recommended for applications where the filter problems are well handled.

## 6.2 RECOMMENDATIONS

Although the framework of multiresolution approximation has been established, considerable work remains to be done. The following recommendations for further research are made:

(a) Since the numerical examples in this dissertation are only used to demonstrate the correctness of the proposed framework and of the algorithms developed, only two data types with two

resolution scales have been used. Therefore, tests involving more sophisticated scenarios are needed.

(b) Due to the lack of true multiresolution data, the proposed framework was tested using simulated data generated from actual terrestrial gravity anomaly data. In order to investigate the feasibility of the proposed framework to gravity field approximation in practice, computations with real data should be done.

(c) The current limitation of using wavelet transforms is that only multiresolution analysis with dilation 2 can be used due to the fact that scaling functions and wavelet functions for multiresolution analysis with integer dilation factor larger than 2 or non-integer dilation factor are not available. Therefore, tests are needed using a wavelet transform with integer dilation factor larger than 2 or non-integer dilation factor when scaling functions and wavelet functions for these cases are available.

(e) All numerical examples given in this dissertation are based on planar approximation. For global gravity field modeling, spherical approximation must be used. In this case, the concept of spherical wavelets should be studied. Therefore, multiresolution approximation on the sphere has to be further investigated.

(f) Since the application of the proposed framework depends on the choice of lowpass filters, optimal choice of a lowpass filter for gravity field modeling is an important topic for further research.

(g) The proposed framework can also be extended for solving other multiresolution problems in geomatics engineering. The multiresolution modeling of a digital elevation model (DEM) from fine-scale compact airborne spectrographic images (CASI) system data and coarse-scale satellite images is an example of such an application. This needs to be investigated.

## REFERENCES

- Auscher, P. (1989): *Ondelettes Fractales et Applications*, PhD Thesis, University of Paris IX, Paris, France.
- Beylkin, G., Coifman, R. and Rokhin, V. (1991): *Fast Wavelet Transforms and Numerical Algorithms I*, *Comm. Pure Appl. Math.*, 44, pp. 141-183.
- Cohen, A. and Daubechies, I. (1993): *Orthonormal Bases of Comapctly Supported Wavelets III. Better Frequency Resolution*, *SIAM. Math. Anal.* Vol.24, No.2, pp.520-527.
- Colombo, J. (1991): *The Role of GPS/INS Integration in Mapping the Earth's Gravity Field in 1990's*, *Proceedings of the IAG International symposium 107 - KIS 1990* ( Eds. Schwarz, K.P. and Lachapelle, G. ), pp. 463-475.
- Crochiere, R.E. and Rabiner, L.R. (1981): *Interpolation and Decimation of Digital Signals - A Tutorial Review*, *Proc. of the IEEE*, Vol. 69, pp. 301-331.
- Daubechies, I. (1992): *Ten Lectures on Wavelets*, *CBMS-NSF Regional Conference Series in Applied Mathematics 61*, SIAM, Philadelphia.
- Daubechies, I.(1988): *Orthonormal Bases for Compactly Supported Wavelets*, *Communication on Pure and Applied Mathematics*, Vol. XLI-7, pp. 507-537.
- Fliege, N.J. (1994): *Multirate Digital Signal Processing:Multirate Systems, Filter Bank, Wavelets*, John Wiley & Sons, Chiches, New York, Brisbane, Toronto, Singapore.
- Forsberg, R. and Tscherning, C.C. (1981): *The use of height data gravity field approximation by collocation*, *Journal of Geophysical Research*, 86, pp. 7843-7854.

- Graps, A. (1995): An Introduction to Wavelets, *IEEE Computational Science and Engineering*, Vol.2, No.2, Summer 1995.
- Grossman, A and Morlet, J. (1984): Decomposition of Hardy Function into Square Integral Wavelets of Constant Shape, *SIAM J. Math.Anal.*, 15, pp. 723-736.
- Heiskanen, W.A. and Moritz, H. (1967): *Physical Geodesy*, W.H.Freeman, San Francisco.
- Jordan, S.K. (1972): Self-Consistent Statistical Model for the Gravity Anomaly, Vertical Deflection, and Undulation of the Geoid, *Journal of Geophysical Research*, Vol. 77 No. 20, pp. 3660-3670.
- Khan, R.H. (1980): *The Analysis and Design of Multirate Digital Filters*, PhD Dissertation, Department of Electrical and Computer Engineering, The University of Calgary.
- Krakiwsky, E.J. (1990): *The Method of Least Squares: A Synthesis of Advances*, Lecture Notes, Department of Geomatics Engineering, The University of Calgary.
- Krarup, T.(1969): *A Contribution of Mathematical Foundation of Physical Geodesy*, Meddelelse No.44, Geodatic Institut, Kobenhavn.
- Lerch, F.J., Klosko, S.M., and Patel, G.B. (1982): A Refined Gravity Model From LAGEOS (GEM-L2), *Geophysical Research Letters*, Vol. 9, No. 11.
- Lerch, F.J., Klosko, S.M., Laubscher, R.E. and Wagner, C.A. (1979): Gravity Model Improvement using GEOS-3 (GEM9 and GEM10), *Journal of Geophysical Research*, Vol. 84, No. B8, The GEOS-3 Special Issue.
- Lerch, F.J., Putney, B.H., Wagner, C.A. and Klosko, S.M. (1981): Goddard Earth Models for Oceanographic Applications (GEM10B and GEM10C), *Marine Geodesy*, Vol. 5, No. 2.
- Li, J. (1996): *Detailed Marine Gravity Field Determination by Combination of Heterogeneous Data*, Master Thesis, Department of Geomatics Engineering, The University of Calgary.

- Li, Y. (1993): **Optimized Spectral Geoidal Determination**, UCGE Reports No. 20050, Department of Geomatics Engineering, The University of Calgary.
- Liu, B. (1994): **Design of Multirate Filter Banks**, PhD Dissertation, Department of Electrical and Computer Engineering, The University of Calgary.
- Mallat, S. G.(1989a): **A Theory for Multiresolution Signal Decomposition: the Wavelet Representation**, IEEE Trans. PAMI, 11, pp. 674-693.
- Mallat, S.G. (1989b): **Multiresolution Approximation and Wavelet Orthonormal Bases of  $L^2$** , Trans. Amer. Math. Soc. Vol. 3 -15, pp. 69-88.
- Meyer, Y. (1992): **Wavelets and operators**, Cambridge studies in advanced mathematics 37, Cambridge University Press.
- Meyer, Y. (1990): **Orthonormal Wavelet**, in **Wavelets, Time-Frequency Methods and Phase Space** (eds. Combes, J.M. et al), Springer Verlag.
- Molodensky, M.s., Eremeev, V.F. and Yourkina, M.I. (1962): **Methods for the Study of the Gravity Field of the Earth**, Translated from Russian (1960), Israel Program for Scientific Translations, Jerusalem.
- Moritz, H. (1980): **Advanced Physical Geodesy**, Herbert Wichmann Verlag, Karlsruhe, Abacus Press, Tunbridge Wells, Kent.
- Rapp, R.H. (1981): **The Earth's Gravity Field to Degree and Order 180, Using SEASAT Altimeter and Terrestrial Data**, Report No. 332, Department of Geodetic Science and Surveying, The Ohio State University.

- Rapp, R.H. (1978): A Global  $1^\circ \times 1^\circ$  anomaly field combining Satellite, GEOS-3 altimeter, and terrestrial anomaly data, Report No. 278, Department of Geodetic Science and Surveying, The Ohio State University.
- Rapp, R.H. (1976): Anomalies Recovered from Geos-3 Altimeter Data Using Least Squares Collocation, Paper presented at the Spring Annual Meeting for the American Geophysical Union, April 12-15, 1976, Washington, D.C. .
- Rapp, R.H., Wang, Y.M. and Pavlis, N.K. (1991): The Ohio State 1991 Geopotential and Sea Surface Topography Harmonic Coefficient Models, Report No. 410, Department of Geodetic Science and Surveying, The Ohio State University.
- Reigber, C., Balmino, G, Moynot, B., and Muller, H. (1983a): The GRIM3 Earth Gravity Field Model, Manuscripta Geodeatica, Vol. 8, pp. 93-138.
- Reigber, C., Muller, H., Rizos, C. Bosch, W., and G, Moynot, B. (1983b): An improved GRIM3 Earth Gravity Field Model (GRIM3B), Proceedings of IAG Symposium, Hamberg, FRG, Aug., 1983.
- Ratzlaff, S. (1995): An Optimal Model-Matching Approach to Multirate FIR Filter Bank Design, Master Thesis, Department of Electrical and Computer Engineering, The University of Calgary.
- Rauhut, A.C. (1992): Regularization Methods for the Solution of the Inverse Stokes Problem, UCGE Reports No. 20045, Department of Geomatics Engineering, The University of Calgary.

- Robbins, J.W. (1985): **Least-Squares Collocation Applied to Local Gravimetric Solutions From Satellite Gravity Gradiometry Data**, Report No. 368, Department of Geodetic Science and Surveying, The Ohio State University.
- Sanso, F. (1987): **Talk on the Theoretical Foundations of Physical Geodesy**, IAG Section IV Contributions to Geodetic Theory and Methodology, XIX General Assembly of the IUGG, Vancouver, B.C., Canada, Aug. 9-22, 1987, pp. 1-27.
- Sanso, F. and Tscherning, C.C. (1980): **Notes on Covergence in Collocation Theory**, Boll. di Geod. e Sc. Aff., No.2, pp.221-252.
- Schwarz, K.P. (1984): **Data Types and Their Spectral Properties**, Proceedings of Local Gravity Field Approximation (Schwarz, K.P. ed.), Beijing International Summer School, Beijing, China, Aug. 21 - Sept. 4, 1984, pp. 1-66.
- Schwarz, K.P. and Lachapelle, G.(1980): **Local Characteristics of the Gravity Anomaly Covariance Function**, Bull. Geod. 54, pp. 21 - 36.
- Schwarz, K.P. and Li, Y. (1995): **What can Airborne Gravimetry Contribute to Geoidal Determination?** Proceedings of IAG Symposium G4: Airborne Gravimetry (Eds: Schwarz, K.P., Brozena, J.M. and Hein, G.W.), IUGG General Assembly, Boulder, Colorado, July 2 - 14, 1995, pp. 143-152.
- Schwarz, K.P., Sideris, M.G. and Forsberg, R.(1990): **The Use of FFT Techniques in Physical Geodesy**, Geophysics. J. 100, pp. 485-514.
- Schwarz, K.P. and Wei, M. (1994): **Some Unsolved Problems in Airborne Gravimetry**, Paper presented at the syposium 'Gravity and Geoid', Graz, Austria, September 11-17.
- Sideris, M.G. (1996): **On the Use of Heterogeneous Noise Data in Spectral Gravity Field Modeling Methods**, Journal of Geodesy, 78/8, pp.470-479.

- Sideris, M.G. (1987): **Spectral Methods for the Numerical Solution of the Molodensky's Problem**, UCSE Report 20024, Department of Surveying Engineering, The University of Calgary.
- Sideris, M.G. (1984): **Computation of Gravimetric Terrain Corrections Using Fast Fourier Transform Techniques**, UCSE Report 20007, Department of Surveying Engineering, The University of Calgary.
- Strange, G. (1989): **Wavelets and Dilation Equations: A Brief Introduction**, SIAM Review, Vol.31, No.4, pp. 614-627.
- Tscherning, C.C. (1984): **Local Approximation of the Gravity Potential by Least-Square Collocation** (Schwarz, K.P. ed.), Beijing International Summer School, Beijing, China, Aug. 21 - Sept. 4, 1984, pp. 277-362.
- Tscherning, C.C. (1976): **Covariance Expressions for Second and Lower Order Derivatives of the Anomalous Potential**, Report No. 225, Department of Geodetic Science and Surveying, The Ohio State University.
- Tscherning, C.C. and Rapp, R.H. (1974): **Closed Covariance Expressions for Gravity Anomalies, Geoid Undulation, and Deflections of the Vertical Implied by Anomaly Degree Variance Models**, Report No. 208, Department of Geodetic Science and Surveying, The Ohio State University.
- Vaidyanathan, P.P. (1993): **Multirate Systems and Filter Banks**, Prentice Hall, Englewood Cliffs, New Jersey, 1993.
- Vaidyanathan, P.P. (1993): **Multirate Digital Filters, Filter Banks, Polyphase Networks, and Applications: A Tutorial**, Proc. of the IEEE, Vol. 78, pp. 56-93.

- Vettrli, M. and Herley, C. (1992): **Wavelet and Filter Banks: Theory and Design**, IEEE Trans. Signal Processing, Vol.40, No.9, pp. 2207-2233.
- Wei, M. and Schwarz, K.P. (1994): **An Error Analysis of Airborne Vector Gravimetry**, Proceedings of KIS 94, Banff, Canada, August 30-September 2, 1994, pp. 509 - 520.
- Windheuser, U.(1995): **Spherical Wavelet Transform and Its Discetization**, Paper presented at Workshop of Mathematical Method of Geodesy, Oberwolfach, Germany, October 1-7, 1995.
- Wu, L. (1996): **Spectral Method for Post Processing of Airborne Gravity Data**, Master Thesis, Department of Geomatics Engineering, The University of Calgary.
- Wu, L. and Sideris, M.G. (1995): **Using Multiple Input-Single Output System Relationships in Post Processing of Airborne Gravity Vector Data**, Proceedings of IAG Symposium G4: Airborne Gravimetry (Eds: Schwarz, K.P., Brozena, J.M. and Hein, G.W.), IUGG General Assembly, Boulder, Colorado, July 2 -14, 1995, pp. 87 - 95.
- Williams, J.R and Amaratunga, K (1994): **Introduction to Wavelets in Engineering**, Int. J. Num. Mthds. Eng., Vol. 37, pp. 2365-2388.
- Wickerhauser, M.V. (1994): **Adapted Wavelet Analysis from Theory to Software**, A K Perter, Wellesley, Massachusetts.